The Dissertation Committee for Jennifer Lee Lyon Certifies that this is the approved version of the following dissertation:

Electrochemical Evaluation of Nanocarbons for Biogenic Analyte Detection

Committee:

Keith J. Stevenson, Supervisor

Richard M. Crooks

Jennifer S. Brodbelt

David C. Graham

James D. Burgess

Electrochemical Evaluation of Nanocarbons for Biogenic Analyte Detection

by

Jennifer Lee Lyon, B.S.

Dissertation

Presented to the Faculty of the Graduate School of

The University of Texas at Austin

in Partial Fulfillment

of the Requirements

for the Degree of

Doctor of Philosophy

The University of Texas at Austin

December 2007

Dedication

To my frog, Noogie, and to my best friend

Acknowledgements

Most dissertation acknowledgements open with the doctoral candidate thanking their advisor for "the great opportunity to work in the lab, which has helped my enthusiasm for science grow immensely," or something equally banal and halfhearted. Since Keith and I share a disdain for such trite formalities, I am departing from the traditional order of acknowledgements by thanking my coworkers first: The members of the Stevenson group are a unique group of people that have greatly motivated me. I extend special gratitude to Dr. Ryan Williams, who has spent the past four and a half years doing even less work than I have. I also thank Dr. Ganesh Vijayaraghavan for synthesizing every single carbon nanotube used in the experiments discussed in this dissertation, and for collecting the data in Figure 2.2b.

I was fortunate to be given several opportunities to work collaboratively with other research groups, both at Texas and abroad, and these experiences have definitely aided my development as a scientist (that statement is not halfhearted). I thank Frau Dörthe Eisele and her supervisor, Dr. Jürgen Rabe, for sponsoring my visiting researcher appointment in the Department of Macromolecular Physics at Humboldt University in Berlin. I also extend a big "Vielen Dank, y'all" to Frau Eisele for almost setting a bed on fire and taking some amazing photos in Paris, as well as Herr Constans Weber for translating the German lunch menu into English and printing off hundreds of informative

pages about Die Bahn train rides. I thank my committee member and true “idea man” Dr. Jim Burgess, as well as Dechen Jiang, for a short but memorable visit to Case Western Reserve University in April 2006. I am also indebted to Dr. Ryan Hill, who was my collaborating partner with the Shear group for over two years and is now one of my closest friends. I thank Dr. Jason Shear for providing me with a highly coveted key to his lab. Finally, I thank my out-of-division friends Suvi Simila and Dr. Natalie Barkey for synthetic chemistry advice and for lending me dozens of chemicals and hoards of glassware from the Martin and Sessler labs.

Several people I’ve met while in graduate school have made my time here more enjoyable, and for that they deserve acknowledgement. I’ve appreciated the many lunch un-invites extended to me by Jeff Wilson, Sarah Pierce and Suncerae Smith, my neighbors in the Brodbelt group. Northern Virginia native Myles Gardner, another Brodbelt group member, is always ready to provide the neurotic, witty exchanges that I so desperately miss about the Northeast. I also thank my committee member Dr. Jennifer Brodbelt for allowing me to paint cartoons on the walls and floor of her lab. Former Stevenson lab undergraduates Monique Makos and Emily “$20,000” Barton have provided hours of stimulating conversation over margaritas and are extremely skilled at dressing fashionably in a laboratory setting, a truly underappreciated human quality.

I was lucky to enter graduate school with a great support network from my undergraduate research group at Penn State University, headed by Dr. Mary Elizabeth Williams, who continues to counsel me above and beyond the duties of a typical undergraduate research advisor. My Williams group co-workers Dr. Dave Fleming, Chris Morgan and Carly Jo Carter have continued to be great friends during my stay in Texas. I also thank Dr. Tom Mallouk for making my brief stint in his research lab rewarding. I thank Dr. (M.D., not Ph.D.) Adam Ehrlich for giving me most of the answers to

homework problems in Chemistry 451, 452, 410 and 431W, thus securing the GPA that probably helped me get into grad school, but more importantly for being my best friend in college.

Of course, I am most indebted to my family and closest loved ones. I thank my parents for their love and support. I thank my father for not making me become an engineer and I thank my mother for all the photos of her dogs. I thank my brother, Tim, for always entertaining me with pharmacy school stories while I'm home on break. I thank Annie, Toby and Taffy for gracefully decorating my cubicle walls, and because my parents probably won't read this dissertation unless their dogs are mentioned at least once. I am grateful to my cousin Janine Terry and my oldest friend, Leanne Himmler, for visiting me in Austin at times when I really needed some cheering up. Finally, I thank Dr. Sean McClure for the purchase of my iPod and iPhone, which I use to mentally escape this place on a daily basis, and for always siding with me. Oh yeah, and for all his love and support.

Having safely spaced two pages of text between the "Acknowledgements" heading and here, I may now thank Keith Stevenson for giving me so much creative freedom as a graduate student, with these long-winded acknowledgements serving as proof of concept. Through both lecture and example, Keith has taught me some valuable lessons concerning electrochemistry, viscosity at food–ceiling interfaces, breaking and entering, subtlety and nuance, snorkeling strategy for sea turtle sighting and the general not-putting-up-with of assorted crap. Clearly an advisor who provides so much deserves more than the standard "so glad to improve my research skills through him" spiel. Which is why I'm leaving that stinky, Salvation Army lab couch that you never reimbursed me for in the lab, Keith. You can thank me later, buddy.

Electrochemical Evaluation of Nanocarbons for Biogenic Analyte Detection

Publication No._____

Jennifer Lee Lyon, Ph.D.

The University of Texas at Austin, 2007

Supervisor: Keith J. Stevenson

This dissertation explores the use of nanocarbons both as conductive supports for redox enzyme electrochemistry and as electrocatalytic components for the nonmediated detection of biogenic analytes. More specifically, the influence of nitrogen doping of these nanocarbons (referred to herein as nitrogen-doped carbon nanotubes, or N-CNTs) on their bioelectrocatalytic performance is studied through direct enzyme adsorption and exploitation of the N-CNTs' inherent reactivity toward H_2O_2 to create H_2O_2-based sensing strategies. Both nondoped CNTs and N-CNTs may be effectively incorporated into biogenic sensing assemblies, as demonstrated herein using a variety of electrochemical techniques. Chapter 1 gives a general overview of the scope of this research and describes previous studies conducted within our laboratories that demonstrate our CNTs' promise as biogenic electrode materials. Chapter 2 describes the chemical vapor deposition (CVD) method used to prepare both CNTs and N-CNTs and establishes their suitability for use in the detection schemes outlined in later chapters through long-term stability studies. Additionally, the redox activity of Fe nanoparticles

entrapped in the CNTs as a result of this CVD growth process is examined using a host of electrochemical experiments. Importantly, the data presented in this chapter show that these Fe particles *do not* explain the observed electrocatalytic response of the CNTs. Chapter 3 explores the direct adsorption of horseradish peroxidase (HRP) at both nondoped and N-CNTs. Spectroscopic and electrochemical assays are used to compare the extent of HRP enzymatic activity upon immobilization at both types of CNTs. Both types of HRP/CNT composites are then utilized in a quantitative H_2O_2 sensing strategy. Chapter 4 discusses the intrinsic reactivity of N-CNTs toward H_2O_2. Koutecky–Levich plots are used to demonstrate differences in H_2O_2 consumption mechanisms between N-CNTs and traditional peroxidases. By replacing HRP with N-CNTs in an amperometric glucose detection scheme, the versatility of N-CNTs as a peroxidase substitute for biogenic analyte detection is demonstrated. Chapter 5 outlines future directions for this research, including possible strategies for improving electron transfer between HRP and both types of CNTs. This chapter also presents a newly developed, mediated oxidase–substrate electrochemical detection method that can easily be modified to incorporate CNTs.

Table of Contents

List of Tables

List of Figures

CHAPTER 1

Nanocarbons as an Electrode Material for Biogenic Analysis

1.1 INTRODUCTION

Beginning with Luigi Galvani's use of frog legs as supporting electrolytes,[1] biological systems have been evaluated by electrochemical means for more than two centuries. Modern bioanalytical electrochemistry focuses on the fast, sensitive quantification of biogenic analytes for both fundamental research and more applied medical biodiagnostic applications, such as determining glucose levels in blood and urine for diabetes detection[2] and monitoring cholesterol for the diagnosis of coronary heart disease, arteriosclerosis, and other clinical disorders.[3] To achieve these goals, electrochemical biosensors have been developed that utilize complementary enzymes in conjunction with an electrode, allowing redox reactions to be detected electrochemically by measurement of substrate consumption or product formation. Often, complementary enzymes are immobilized at electrode surfaces in order to create reagentless in vivo and in vitro sensors; the most widely recognized example of this type of biosensor is the FreeStyle™ amperometric glucose sensor used for diabetes management, in which glucose oxidase is "wired" to the electrode surface through an electron-conducting polymer hydrogel, which acts as a redox mediator to shuttle electrons between glucose oxidase and the electrode.[4] A simplified version of this electrode assembly is shown in Figure 1.1a.

Enzyme wiring components, such as the $Os^{2+/3+}$ redox polymer used in the FreeStyle™ sensor, are commonly employed in biosensor development[5] since many enzymes' redox active centers are buried within insulating protein layers and are thus

unable to directly exchange electrons with an electrode surface;[6] this process is commonly referred to as direct electron transfer. Direct electron transfer is also difficult to achieve because many biomolecules denature over time when directly adsorbed at an unmodified electrode surface.[7] Some proteins and enzymes, including the heme enzyme horseradish peroxidase (HRP)[8, 9] and hemoproteins cytochrome c (Cyt c),[7, 10] myoglobin (Mb),[11] and hemoglobin (Hb),[12] are capable of direct electron transfer when adsorbed at electrode surfaces, and their electron transfer is further stabilized when they are supported by surfactant films, lipid bilayer membranes, or linking molecules (such as polycationic-anionic polymers) at the electrode surface.[7, 13, 14]

Alternatively, redox reactions between products generated by enzyme–substrate interactions and the electrode surface can be monitored at the electrode. One of the most common examples of this biosensing strategy is the direct electrochemical oxidation of hydrogen peroxide (H_2O_2), which is produced stoichiometrically as a byproduct of oxidase–substrate interactions involving many physiologically important molecules, including glucose and cholesterol. (The balanced equations for H_2O_2 production through cholesterol consumption are provided in Chapter 5.) For example, Burgess et al. have developed a cholesterol sensor based on the general schematic depicted in Figure 1.1b, in which cholesterol oxidase is immobilized in a lipid bilayer membrane within a Pt cavity electrode. When the electrode is contacted to a plasma membrane, cholesterol in the membrane is oxidized to cholestenone by cholesterol oxidase, and the H_2O_2 byproduct oxidation at Pt is recorded amperometrically.[15-17] H_2O_2 produced in oxidase–substrate interactions also may be enzymatically reduced to water using a redox-active peroxidase, such as HRP, permitting detection of substrate consumption through the redox-mediated HRP response.[18] (HRP may undergo several different electron transfer mechanisms upon its reduction of H_2O_2, and these possible reaction pathways are discussed in detail in

Chapter 3.) An example of a HRP-mediated biosensor, in which both HRP and an oxidase are immobilized at an unspecified electrode surface, is shown in Figure 1.1c. Finally, the enzymatic reaction may be reported at the electrode surface via a freely diffusing, redox-active mediator, as depicted in Figure 1.1d. Examples of mediated electrochemical bioanalysis using a host of small redox molecules are abundant in the literature,[5, 6, 19] but we shall reserve discussion of these types of biosensors for Chapter 5.

Though many biosensors incorporating the assemblies depicted in Figure 1.1(a–d) have employed modified noble metal (i.e., Pt, Au) indicator electrodes,[2, 3, 15-17, 20, 21] carbon electrodes are becoming more popular in the biosensing arena for several reasons. In addition to the aforementioned possibility of biomolecule denaturation upon direct adsorption at electrodes, metal electrodes are more susceptible to fouling through protein adsorption than other types of electrodes, such as tin oxide electrodes.[7] By contrast, robust redox acitivty has been demonstrated when enzymes are directly adsorbed at graphite or glassy carbon (GC) electrodes,[22-30] thus eliminating the need for enzyme wiring components. In the case of H_2O_2-based sensing schemes, the electrochemical oxidation of generated H_2O_2 at Pt at physiological pH values (6.5–7.5) occurs at potentials (+0.6 to +0.9 vs. NHE) where other electroactive species (e.g., uric acid and ascorbic acid) interfere.[31] Furthermore, Pt-based electrodes exhibit decreased sensitivity and reproducibility due to the formation of PtO_2 at the electrode surface when large anodic overpotentials are used for H_2O_2 oxidation.[17, 32] In a more general sense, carbon has found ubiquitous application across many electroanalytical disciplines owing to its outstanding material properties, such as high electronic conductivity, stability, chemical inertness, and resistance to corrosion,[33, 34] making it an obvious choice for the fabrication of low-cost, durable biosensors.

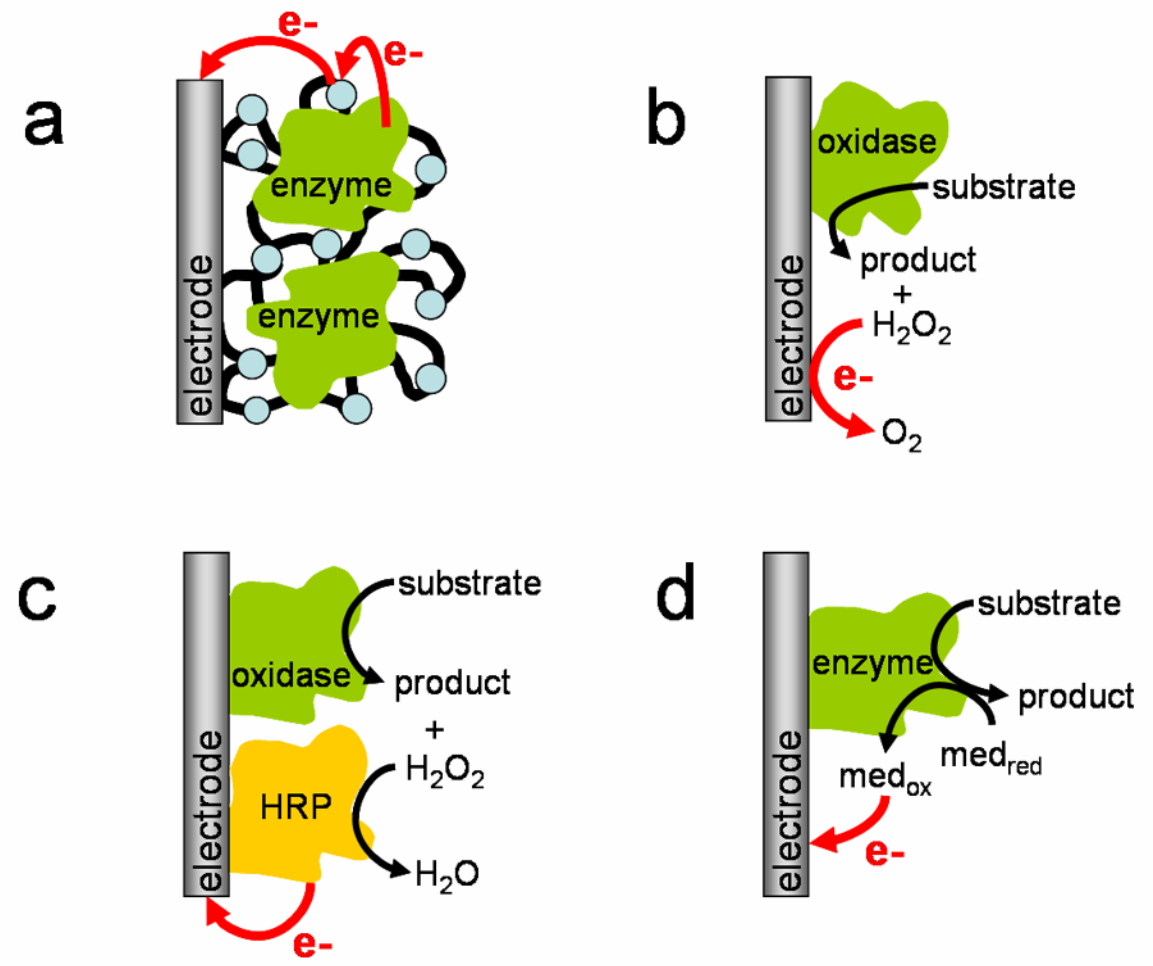

Figure 1.1. Schematic representations of assorted biosensing strategies, in which enzymes are immobilized at an unspecified electrode surface. Chemical reactions are not balanced, and electron transfer (denoted with red arrows) is grossly oversimplified. (a) "Wiring" of enzymes to an electrode through a redox polymer network. (b) H_2O_2-based electrochemical detection of oxidase–substrate interactions. (c) Peroxidase-mediated sensing of oxidase–substrate interactions using horseradish peroxidase (HRP). (d) Electrical wiring of an enzyme using a diffusional mediator, whose oxidized and reduced forms are denoted "med_{ox}" and "med_{red}," respectively.

Several examples of immobilized-enzyme carbon electrodes are available in the literature, including enzymes immobilized in polymeric films[18, 35] and supported by lipid bilayers[36] at highly oriented pyrolytic graphite (HOPG), mediated cholesterol sensors at GC,[19] and the aforementioned directly adsorbed enzymes at GC and graphite. This last type of electrode, in which no linking molecules or immobilizing films are used to tether the enzymes to the carbon surface, is often used to probe the correlation between carbon microstructure and extent of enzyme redox activity. It has long been known that the structure of a given sp^2 carbon material, namely its degree of basal or edge plane character, exerts a profound effect on electron transfer kinetics for both diffusional and adsorbed analytes.[34] A pictorial representation of a carbon sp^2 lattice, featuring basal and edge planes, is shown in Figure 1.2a. In early reports, Hill et al. demonstrated the correlation between increasing edge plane character and enhanced Cyt c electron transfer at graphite,[27, 28] and similar results have also been reported using HRP.[29, 30] The improved electrochemical signal of proteins and enzymes at edge plane graphite is largely attributed to increased biomolecule adsorption at edge plane sites, thus increasing the number of biomolecules available for signal transduction.[37-39] Edge plane character is induced in a graphitic lattice wherever a disruption in the sp^2 lattice occurs; these disruptions are most often caused by the presence of another atom, such as oxygen in the form of carboxylic, quinone, lactone, phenol, or carbonyl functional groups.[34]

In order to improve biogenic detection and to promote more facile electron transfer between biomolecules and carbon electrodes, many researchers have attempted to increase biomolecule loading at carbon electrodes by using physical and electrochemical roughening techniques to increase edge plane character. Figure 1.2b presents a pictorial adaptation of a study in which GC electrodes were mechanically roughened using sandpaper to improve HRP electrochemical signal.[22] Others have

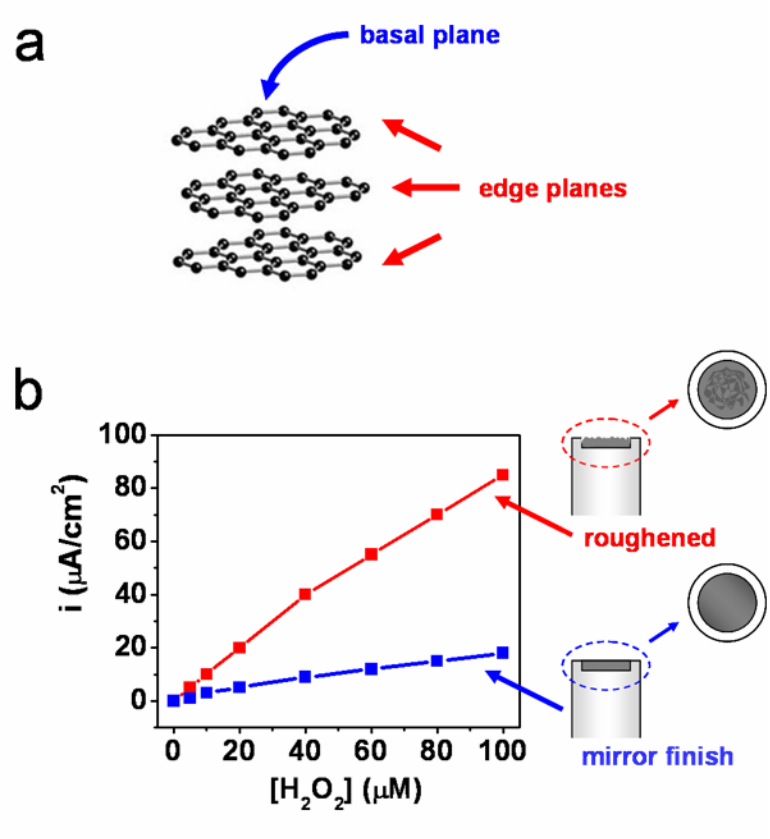

Figure 1.2. (a) Schematic representation of a graphitic sp^2 lattice, denoting basal and edge planes. (b) Adaptation from Reference 30, in which mechanically roughened graphite exhibits increased HRP adsorption, leading to an increased amperometric response to H_2O_2.

detailed electrochemical pretreatment procedures that cycle or hold carbon electrodes at anodic potentials, sometimes in the presence of acid, as a means of inducing oxygen-containing surface functionalities in order to increase the number of edge plane sites.[34, 40-43] However, these types of harsh surface roughening processes are not often reproducible and do not permit control over the extent or composition of functionalities introduced at the carbon electrode surface, nor do they necessarily increase edge plane character.[41, 43] Additionally, quinones and lactones introduced at the electrode surface may exhibit their own redox signatures, which complicate interpretation of the redox reaction mechanism and interfere with analyte detection by increasing the electrochemical background relative to the analyte signal.[34] We also note that carbon surfaces may be chemically modified so that biomolecules may be tethered to them, such as the carbodiimide coupling of HRP reported by Rusling et al.[44, 45] These types of modifications are mentioned briefly in Chapter 3, but they are largely beyond the scope of this discussion because they promote biomolecule loading through covalent attachment at modified electrode sites, rather than creation of an increased electrode surface area for adsorption.

Many of the problems associated with increasing the electroactive surface area and number of edge plane sites stem from the fact that these traditional carbons, e.g., GC and HOPG, are produced using bulk techniques, i.e., bulk thermal decomposition of solid and liquid precursors such as coconut shells and polyacrylonitrile.[33] Purification and activation of these materials requires aggressive processing procedures; therefore, the tailoring of these carbons for electrochemical applications is limited to post-synthetic processing. As such, optimization of various carbon properties is difficult. By contrast, nanocarbons or carbon nanotubes (CNTs), which consist of nanostructured, concentrically aligned graphene layers, may be synthesized using techniques that permit a

higher degree of control and tuning of resultant properties. More specifically, carbon nanotubes prepared using chemical vapor deposition (CVD) growth processes can be modified to tune CNT edge plane character by adjusting length, diameter, texture, composition, and surface functionalities.[46-48] CVD methods involve the dissociation of an organometallic (Fe, Ni, Co, Mo) precursor under high temperature (>600 °C) in a reducing (H_2) environment, resulting in the formation of metallic nanoparticles that act as nanotube nucleation sites. Carbon from the dissociated precursor diffuses to the surface of the nanoparticles, growing in concentric graphene sheets.[34, 47, 48] The degree of edge plane character in these CNTs may be increased through heteroatom doping with nitrogen, producing nitrogen functionalities (e.g., pyrrole, pyridine) that disrupt the sp^2 lattice.[49-55]

Previously, our research group has established methods for selectively and reproducibly tuning the extent of edge plane character at CNTs through N-doping using a floating catalyst CVD approach.[56] Through a series of carefully controlled, systematic studies utilizing microscopy, spectroscopic, surface analytical, and electrochemical methods, we have correlated structure–property relationships of these CNTs as a function of N-doping.[56-59] We have shown using X-ray photoelectron spectroscopy that nitrogen is integrated into the CNTs as pyridinic, pyrrolic, and quaternary functionalities, with the pyridinic content scaling with increasing NH_3 content.[56] As expected, CNT structural disorder escalates as the number of edge plane sites increases with increasing amounts of NH_3 used CNT growth process. Raman microprobe spectroscopy and high-resolution transmission electron microscopy studies support these correlations.[56, 59] Most notably, we have established correlations between structural disorder and number of edge plane sites at N-doped CNTs (referred to herein as N-CNTs) and electrochemical behavior. For example, the electron transfer rate constants for inner-sphere redox couples have been

shown to change susbstantially at N-CNTs relative to nondoped CNTs,[57] in agreement with previous findings using GC electrodes.[60, 61] We have also correlated increasing electrocatalytic activity toward both O_2 reduction and H_2O_2 decomposition with increasing N content in our CNTs.[58, 59] Most recently, we have exploited the adsorptive properties of our highly edge plane N-CNTs by creating synergistic catalytic assemblies, using N-CNTs as an electrode support for noble metal nanoparticle catalysts.[62]

The work presented in this dissertation examines the influence of N-doping of nanocarbons on enzyme activity and biosensing strategies, both by using nanocarbons as a conductive support for direct enzyme adsorption and by exploiting the inherent catalytic properties of N-doped nanocarbons toward H_2O_2 decomposition to create a new peroxidase mimetic sensing strategy. Studies of CNT-based biosensors are already abundant in the literature,[45, 63-73] partially owing to the purported electrical conductivity, chemical inertness, and stability of CNTs relative to the aforementioned traditional carbon electrode materials.[74-76] However, none of the above cited studies features a series of tailored CNTs, nor can these studies directly correlate biomolecule or sensor redox response with structural differences in CNTs. Our finely controlled synthetic approach, along with our exhaustive characterization studies, enable us to evaluate and correlate CNTs as potential biosensors in a more thorough manner than has been possible to date.

This dissertation is organized into five chapters, with Chapter 1 providing a broad overview of the motivation and scope of the work, as well as describing previous studies done in our group to establish structure–property relationships of these tunable CNTs. The remaining four chapters describe the use of both types of CNTs (nondoped and N-CNTs) in peroxidase-based electrochemical sensing schemes. Chapter 2 describes the electrochemical evaluation of CNTs, both nondoped and N-doped, in the absence of any substrates to confirm their suitability for use in biological electroanalysis schemes

detailed in later chapters. Their long-term stability is compared to that of Vulcan XC-72, an industry standard carbon support used in electroanalysis and fuel cell design. Additionally, the inherent redox activity of Fe nanoparticles entrapped in the CNTs as a result of the CVD growth process is examined, and a method for irreversibly suppressing this Fe redox activity through electrochemical passivation is established. Data in Chapter 2 demonstrate that neither the presence of Fe redox activity nor its passivation alters the inherent electrocatalytic properties of the CNTs.

Chapter 3 describes the direct adsorption of horseradish peroxidase (HRP) at both nondoped and N-CNTs, as well as spectroscopic and electrochemical assays used to quantify the extent of HRP activity upon immobilization. Spectroscopic assays indicate that HRP preferentially adsorbs to N-CNTs, in agreement with the prevalent literature assumption that increasing edge plane character in a carbon substrate promotes increasing enzyme adsorption. However, electrochemical detection of the HRP Fe heme redox couple suggests that HRP better maintains direct electron transfer with the CNT substrate at nondoped CNTs. Possible reasons for differences in electron transfer between the two types of CNTs are discussed, and electrochemical studies using both types of HRP/CNT composites in the direct, nonmediated detection of H_2O_2 are described.

Chapter 4 details the inherent peroxidase mimetic activity of N-CNTs and describes oxidase-coupled sensing schemes that utilize N-CNTs in lieu of a peroxidase for H_2O_2-based electrochemical detection of glucose. Differences between N-CNTs' and nondoped CNTs' reactivity toward H_2O_2 are explained, and N-CNT-modified electrodes are compared to previously reported HRP-modified electrodes via Koutecky–Levich analysis to investigate the catalytic mechanism of H_2O_2 consumption at N-CNTs. By replacing HRP with N-CNTs in a glucose oxidase-coupled glucose detection scheme, the

versatility of N-CNTs as a peroxidase substitute in biogenic electrochemical detection strategies is demonstrated.

Future directions for this research are discussed in Chapter 5, which outlines possible strategies for improving electron transfer between HRP and both types of CNTs. A mediated sensing scheme for H_2O_2-based electrochemical detection of cholesterol at carbon fiber ultramicroelectrodes is also presented, which can be applied to any oxidase-coupled sensing scheme. This method features lower H_2O_2 detection limits than those obtained using the sensing assemblies described in Chapters 3 and 4, and can easily be modified to incorporate CNTs.

1.2 REFERENCES

(1) Pera, M. *The Ambiguous Frog: The Galvani-Volta Controversy on Animal Electricity*; Princeton University Press: Princeton, NJ, 1992.

(2) Heller, A. *Annu. Rev. Biomed. Eng.* **1999**, *1*, 153-175.

(3) Wilson, G. S.; Hu, Y. *Chem. Rev.* **2000**, *100*, 2693-2704.

(4) Feldman, B.; McGarraugh, G.; Heller, A.; Bohannon, N.; Skyler, J.; DeLeeuw, E.; Clarke, D. *Diabetes Tech. Ther.* **2000**, *2*, 221-229.

(5) Willner, I.; Katz, E. Angew. Chem. **2000**, *39*, 1181-1218.

(6) Katz, E.; Shipway, A. N.; Willner, I. In *Electron Transfer in Chemistry*; Balzani, V., Ed.; Wiley-VCH: New York, 2001; Vol. 4, pp 127-201.

(7) Burgess, J. D.; Hawkridge, F. M. In *Electroanalytical Methods for Biological Materials*; Brajter-Toth, A., Chambers, J. Q., Eds.; Marcel Dekker, Inc.: New York, 2002, pp 109-142.

(8) Ferapontova, E.; Dominguez, E. *Bioelectrochem.* **2002**, *55*, 127-130.

(9) Ferapontova, E.; Gorton, L. *Bioelectrochem.* **2002**, *55*, 83-87.

(10) Reed, D. E.; Hawkridge, F. M. *Anal. Chem.* **1987**, *59*, 2334-2339.

(11) King, B. C.; Hawkridge, F. M.; Hoffman, B. M. *J. Am. Chem. Soc.* **1992**, *114*, 10603-10608.

(12) Jia, N.; Wang, L.; Liu, L.; Zhou, Q.; Jiang, Z. *Electrochem. Comm.* **2005**, *7*, 349-354.

(13) Yu, X.; Sotzing, G. A.; Papadimitrakopoulos, F.; Rusling, J. F. *Anal. Chem.* **2003**, *75*, 4565-4571.

(14) Rusling, J. F.; Zhang, Z. In *Electroanalytical Methods for Biological Materials*; Brajter-Toth, A., Chambers, J. Q., Eds.; Marcel Dekker, Inc.: New York, 2002, pp 195-231.

(15) Devadoss, A.; Burgess, J. D. *J. Am. Chem. Soc.* **2004**, *126*, 10214-10215.

(16) Jiang, D.; Devadoss, A.; Palencsar, M. S.; Fang, D.; White, N. M.; Kelley, T. J.; Smith, J. D.; Burgess, J. D. *J. Am. Chem. Soc.* **2007**, *129*, 11352-11353.

(17) Bokoch, M. P.; Devadoss, A.; Palencsar, M. S.; Burgess, J. D. *Anal. Chim. Acta* **2004**, *519*, 47-55.

(18) Bongiovanni, C.; Ferri, T.; Poscia, A.; Varalli, M.; Santucci, R.; Desideri, A. *Bioelectrochem.* **2001**, *54*, 17-22.

(19) Salinas, E.; Rivero, V.; Torriero, A. A. J.; Benuzzi, D.; Sanz, M. I.; Raba, J. *Talanta* **2006**, *70*, 244-250.

(20) Wagner, J. G.; Schmidtke, D. W.; Quinn, C. P.; Fleming, T. F.; Bernacky, B.; Heller, A. *Proc. Nat. Acad. Sci.* **1998**, *95*, 6379-6382.

(21) McMahon, C. P.; Rocchitta, G.; Serra, P. A.; Kirwan, S. M.; Lowry, J. P.; O'Neill, R. D. *Anal. Chem.* **2006**, *78*, 2352-2359.

(22) Ferapontova, E.; Puganova, E. J. *Electroanal. Chem.* **2002**, *518*, 20-26.

(23) Brusova, Z.; Ferapontova, E. E.; Sakharov, I. Y.; Magner, E.; Gorton, L. *Electroanalysis* **2005**, *17*, 460-468.

(24) Niculescu, M.; Ruzgas, T.; Nistor, C.; Frebort, I.; Sebela, M.; Pec, P.; Csoeregi, E. *Anal. Chem.* **2000**, *72*, 5988-5993.

(25) Wang, G.; Thai, N. M.; Yau, S.-T. *Electrochem. Comm.* **2006**, *8*, 987-992.

(26) Szucs, A.; Novak, M. J. *Electroanal. Chem.* **1995**, *384*, 47-55.

(27) Armstrong, F. A.; Bond, A. M.; Hill, H. A. O.; Oliver, B. N.; Psalti, I. S. M. *J. Am. Chem. Soc.* **1989**, *111*, 9185-9189.

(28) Frew, J. E.; Hill, H. A. O. *Eur. J. Biochem.* **1988**, *172*, 261-269.

(29) Csoeregi, E.; Joensson-Pettersson, G.; Gorton, L. J. *Biotech.* **1993**, *30*, 315-337.

(30) Ferapontova, E. E. *Electroanalysis* **2004**, *16*, 1101-1112.

(31) Moatti-Sirat, D.; Velho, G.; Reach, G. *Biosens. Bioelectr.* **1992**, *7*, 345-352.

(32) Garcia-Ruiz, E.; Vidal, J. C.; Aramendia, M. T.; Castillo, J. R. *Electroanalysis* **2004**, *16*, 497-504.

(33) Kinoshita, K. *Carbon: Electrochemical and Physicochemical Properties*; John Wiley and Sons, Inc.: New York, 1988.

(34) McCreery, R. L. In *Electroanalytical Chemistry*; Bard, A. J., Ed.; Marcel Dekker, Inc.: New York; Vol. 17, pp 221-292.

(35) Zhang, Z.; Chouchane, S.; Magliozzo, R. S.; Rusling, J. F. *Anal. Chem.* **2002**, *74*, 163-170.

(36) Nassar, A.-E. F.; Rusling, J. F.; Tominaga, M.; Yanagimoto, J.; Nakashima, N. *J. Electroanal. Chem.* **1996**, *416*, 183-185.

(37) Blanford, C. F.; Armstrong, F. A. J. *Solid State Electrochem.* **2006**, *10*, 826-832.

(38) Heng, L. Y.; Chou, A.; Yu, J.; Chen, Y.; Gooding, J. J. *Electrochem. Comm.* **2005**, *7*, 1457-1462.

(39) Kurusu, F.; Tsunoda, H.; Saito, A.; Tomita, A.; Kadota, A.; Kayahara, N.; Karube, I.; Gotoh, M. *Analyst* **2006**, *131*, 1292-1298.

(40) McCreery, R.; Cline, K. K. In *Laboratory Techniques in Electroanalytical Chemistry*, 2nd ed.; Kissinger, P. T., Heineman, W. R., Eds.; Marcel Dekker: New York, 1996, pp 293-332.

(41) Musameh, M.; Lawrence, N. S.; Wang, J. *Electrochem. Comm.* **2005**, *7*, 14-18.

(42) Downard, A. J.; Roddick, A. D. *Electroanalysis* **1994**, *6*, 409-414.

(43) Surmann, P.; Peter, B. *Electroanalysis* **1996**, *8*, 692-697.

(44) Yu, X.; Chattopadhyay, D.; Galeska, I.; Papadimitrakopoulos, F.; Rusling, J. F. *Electrochem. Comm.* **2003**, *5*, 408-411.

(45) Yu, X.; Kim, S. N.; Papadimitrakopoulos, F.; Rusling, J. F. *Mol. BioSys.* **2005**, *1*, 70-78.

(46) Kim, N. S.; Lee, Y. T.; Park, J.; Han, J. B.; Choi, Y. S.; Choi, S. Y.; Choo, J.; Lee, G. H. *J. Phys. Chem. B* **2003**, *107*, 9249-9255.

(47) Rao, C. N. R.; Govindaraj, A. *Acc. Chem. Res.* **2002**, *35*, 998-1007.

(48) Wang, X.; Hu, W.; Liu, Y. Q.; Long, C.; Xu, Y.; Zhou, S.; Zhu, D.; Dai, L. *Carbon* **2001**, *39*, 1533-1536.

(49) Blase, X.; Charlier, J. C.; De Vita, A.; Car, R.; Redlich, P.; Terrones, M.; Hsu, W. K.; Terrones, H.; Carroll, D. L.; Ajayan, P. M. *Phys. Rev. Lett.* **1999**, *83*, 5078-5081.

(50) Droppa, R.; Hammer, P.; Carvalho, A. C. M.; dos Santos, M. C.; Alvarez, F. *J. Non-Cryst. Sol.* **2002**, *299-302*, 874-879.

(51) Redlich, P.; Loeffler, J.; Ajayan, P. M.; Bill, J.; Aldinger, F.; Ruehle, M. *Chem. Phys. Lett.* **1996**, *260*, 465-470.

(52) Sen, R.; Satishkumar, B. C.; Govindaraj, A.; Harikumar, K. R.; Renganathan, M. K.; Rao, C. N. R. *J. Mater. Chem.* **1997**, *7*, 2335-2337.

(53) Terrones, M.; Jorio, A.; Endo, M.; Rao, A. M.; Kim, Y. A.; Hayashi, T.; Terrones, H.; Charlier, J. C.; Dresselhaus, G.; Dresselhaus, M. S. *Mater. Today* **2004**, *7*, 30-45.

(54) Terrones, M.; Terrones, H.; Grobert, N.; Hsu, W. K.; Zhu, Y. Q.; Hare, J. P.; Kroto, H. W.; Walton, D. R. M.; Kohler-Redlich, P.; Ruhle, M.; Zhang, J. P.; Cheetham, A. K. *Appl. Phys. Lett.* **1999**, *75*, 3932-3934.

(55) Yudasaka, M.; Kikuchi, R.; Ohki, Y.; Yoshimura, S. *Carbon* **1997**, *35*, 195-201.

(56) Maldonado, S.; Morin, S.; Stevenson, K. J. *Carbon* **2006**, *44*, 1429-1437.

(57) Maldonado, S.; Morin, S.; Stevenson Keith, J. *Analyst* **2006**, *131*, 262-267.

(58) Maldonado, S.; Stevenson, K. J. *J. Phys. Chem. B* **2004**, *108*, 11375-11383.

(59) Maldonado, S.; Stevenson, K. J. *J. Phys. Chem. B* **2005**, *109*, 4707-4716.

(60) Allred, C. D.; McCreery, R. L. *Anal. Chem.* **1992**, *64*, 444-448.

(61) DuVall, S. H.; McCreery, R. L. *Anal. Chem.* **1999**, *71*, 4594-4602.

(62) Vijayaraghavan, G.; Stevenson, K. J. *Langmuir* **2007**, *23*, 5279-5282.

(63) Zhao, G.-C.; Zhang, L.; Wei, X.-W. *Anal. Biochem.* **2004**, *329*, 160-161.

(64) Guiseppi-Elie, A.; Lei, C.; Baughman, R. H. *Nanotech.* **2002**, *13*, 559-564.

(65) Zeng, Y.-L.; Huang, Y.-F.; Jiang, J.-H.; Zhang, X.-B.; Tang, C.-R.; Shen, G.-L.; Yu, R.-Q. *Electrochem. Comm.* **2006**, *9*, 185-190.

(66) Yu, X.; Munge, B.; Patel, V.; Jensen, G.; Bhirde, A.; Gong, J. D.; Kim, S. N.; Gillespie, J.; Gutkind, J. S.; Papadimitrakopoulos, F.; Rusling, J. F. *J. Am. Chem. Soc.* **2006**, *128*, 11199-11205.

(67) Azamian, B. R.; Davis, J. J.; Coleman, K. S.; Bagshaw, C. B.; Green, M. L. H. *J. Am. Chem. Soc.* **2002**, *124*, 12664-12665.

(68) Vamvakaki, V.; Tsagaraki, K.; Chaniotakis, N. *Anal. Chem.* **2006**, *78*, 5538-5542.

(69) Rochette, J. F.; Sacher, E.; Meunier, M.; Luong, J. H. T. *Anal. Biochem.* **2005**, *336*, 305-311.

(70) Wang, Y.; Joshi, P. P.; Hobbs, K. L.; Johnson, M. B.; Schmidtke, D. W. *Langmuir* **2006**, *22*, 9776-9783.

(71) Luong, J. H. T.; Hrapovic, S.; Wang, D. *Electroanalysis* **2005**, *17*, 47-53.

(72) Luo, X.; Killard, A. J.; Smyth, M. R. *Electroanalysis* **2006**, *18*, 1131-1134.

(73) Joshi, P. P.; Merchant, S. A.; Wang, Y.; Schmidtke, D. W. *Anal. Chem.* **2005**, *77*, 3183-3188.

(74) Gooding, J. J. *Electrochim. Acta* **2005**, *50*, 3049-3060.

(75) Merkoci, A.; Pumera, M.; Llopis, X.; Perez, B.; del Valle, M.; Alegret, S. *Trend. Anal. Chem.* **2005**, *24*, 826-838.

(76) Musameh, M.; Wang, J.; Merkoci, A.; Lin, Y. *Electrochem. Comm.* **2002**, *4*, 743-746.

CHAPTER 2

Electrochemical Characterization of Carbon Nanotubes for Biogenic Analysis*

2.1 INTRODUCTION

Carbon nanotubes (CNTs), which are readily available through commercial sources, demonstrate much promise as electrochemical materials, largely due to their purported electrical conductivity, chemical inertness, and stability relative to traditional carbons such as carbon black.[1-3] Several reports have detailed the advantages of the apparent catalytic properties of CNTs when used as electrodes in electrochemical experiments. For example, CNTs have been used as conductive supports for electrocatalysis[4, 5] and bioelectrochemical applications.[6-9] The utility of CNTs for electrochemical applications depends strongly on the orientation and stacking of graphene layers, as the degree of ordered structure determines the inherent physicochemical properties and reactivity. Numerous electrochemical studies utilizing CNTs have described exceptional electrochemical characteristics of enhanced electron transfer reactivity occurring at low overpotentials for a variety of redox-active species including oxygen and hydrogen peroxide.[10]

Several recent studies have suggested that this enhanced electroactivity of CNT-based electrodes is a result of increased edge-plane character in CNTs, providing surface sites for chemical reactions to occur.[11-14] Edge plane character may be increased at CNTs, as well as on the surface of traditional carbons, through a variety of mechanical, chemical, and electrochemical "activation" procedures,[15] but synthetic methods including

* Portions of this chapter were published in Lyon, J. L.; Stevenson, K. J. *Langmuir* **2007**, *23*, 11311-11318.

laser ablation, arc discharge, and chemical vapor deposition (CVD) can be modified to directly tune CNT structural and chemical properties such as texture, diameter, length, composition, and surface functionalities.[16-18] In CVD, a carbonaceous metal precursor (usually a metallocene or metallophthalocyanine) containing Fe, Ni, Co, or Mo is decomposed at high temperatures (>600 °C) under a reducing (H_2) environment, forming metallic nanoparticles that act to catalyze CNT growth. Carbon from the dissociated precursor then diffuses to these nanoscopic metal catalysts, resulting in the growth of concentric graphene sheets in the form of single-walled and multiwalled CNTs.[11, 17, 18] The electronic, chemical, and structural properties of CNTs, including texture and crystallinity, can be changed by doping of heteroatoms such as N or B. We have previously reported on the influence of N-doping in CNTs on structural order, composition, chemical reactivity, and electrochemical properties.[10, 19-22] These studies have allowed us to make connections between structural and compositional CNT properties introduced by controlled N-doping with the observed electrocatalytic behavior of CNT-based electrode materials. However, our previous studies have been conducted largely in unbuffered supporting electrolytes (e.g., 1 M KNO_3, pH 6.4–12), which are not ideal for biogenic analysis. Therefore, prior to their use in biosensing assemblies, the electrochemical behavior of these CNTs should be studied in the buffered solutions (e.g., sodium phosphate) of physiological pH (6–7) that are necessary to use in our sensing strategies. Additionally, we have not performed any studies evaluating the long-term stability our CNTs upon subjection to extended use in electrochemical analysis. Such studies would be helpful in comparing the stability of our CNTs, and hence the practicality of their implementation in sensing strategies, to that of other commonly used carbon substrates.

One unfortunate result of catalytically prepared CNTs, including those fabricated

in our laboratory, is the incorporation of residual metal impurities (typically 3–30 wt%) into CNT materials. High-resolution transmission electron microscopy (HR-TEM) studies of CNTs indicate that metal contaminants exist as nanoscopic metal particles ranging from a few nm to several hundred nm in diameter, that are predominately entrapped within graphene layers,[16, 17, 23, 24] or present on the surface of the CNTs, yet covered with thin layers of amorphous carbon.[25] Even so, the influence of these metallic impurities on the apparent CNT properties cannot be easily ruled out. For example, previous studies by Compton et al. have suggested that occluded metal nanoparticles were responsible for observed CNT "electrocatalytic activity" toward H_2O_2 reduction,[26] halothane detection,[27] and hydrazine oxidation.[28] Of particular concern when considering the use of these CNTs for biogenic sensing is the possibility of encapsulated Fe oxide particles exhibiting peroxidase mimetic activity, as has been recently described by Gao et al.[29] Being aware of the potential problems incurred when using CNTs containing active metal nanoparticles, both commercial manufacturers and independent research laboratories have taken to "prewashing" CNTs in concentrated mineral acids in order to remove metal impurities. Nevertheless, it has been demonstrated that even "super washing" with concentrated acid fails to completely eliminate metal nanoparticles from CNTs.[23, 30] Commercially purified CNTs still contain lower but significant amounts of metallic impurities, as much as 15 wt%.[31] These findings indicate that a thorough knowledge of both the extent of metal incorporation into the CNT lattice and any residual metal redox activity when subjected to selected experimental conditions is essential for accurate understanding of structure–property–activity relationships for experimental studies using CNT materials.

In this chapter, we present data to demonstrate the electrochemical stability of our CVD-prepared nanocarbons, thus justifying their use as an enzyme support for biogenic

analysis. We show that our CNTs, both nondoped and N-doped, are more stable throughout long-term electrochemical oxidation in acid than Vulcan XC-72, a standard carbon substrate used in catalysis studies. We also present evidence of the electrochemically induced dissolution and passivation of Fe particles encapsulated within both non-doped and N-doped CNTs, prepared via a ferrocene floating catalyst CVD method,[21] when used as electrodes in the aqueous supporting electrolytes chosen for our biosensing schemes. While the Fe contained within these CNTs does not demonstrate direct Fe^{II} dissolution or $Fe^{II/III}$ redox activity in neutral pH (pH = 6.40 ± 0.03) solutions of potassium nitrate, a pronounced $Fe^{II/III}$ redox response is consistently observed when CNT electrodes are immersed in phosphate-, acetate-, or citrate-containing supporting electrolyte solutions. By controlling the applied potential vs. Hg/Hg_2SO_4, both Fe^{II} dissolution behavior and $Fe^{II/III}$ redox transitions may be observed. Repeated cycling within the $Fe^{II/III}$ potential window completely suppresses the observed $Fe^{II/III}$ redox activity due to passivation processes. Similar behavior is observed upon addition of a known passivation agent, sodium benzoate, which inhibits Fe^{II} dissolution. Lastly, we present data for the electroreduction of oxygen at N-CNT electrodes that displays a unique electrocatalytic response in which neither the presence of active $Fe^{II/III}$ redox activity nor the subsequent passivation of $Fe^{II/III}$ surface oxides affects the onset of oxygen reduction, suggesting that surface bound $Fe^{II/III}$ active sites are not required for observing enhanced oxygen reduction behavior.

2.2 EXPERIMENTAL

2.2.1 CNT Synthesis

CNTs (both nondoped and 5 at% N-doped, referred to herein as N-CNTs) were prepared via a floating catalyst CVD process using a ferrocene growth catalyst and

xylene (or pyridine) carbon (and nitrogen) source as previously described.[10] Briefly, 1.0 mL of a 20 mg/mL ferrocene-xylene (for non-doped CNTs) or ferrocene-pyridine (for N-CNTs) mixture was injected at 0.1 mL/min into a dual-zone quartz tube furnace. The mixture was volatilized at 150 °C in the first zone and then carried downstream to the second zone by carrier gases (Ar–H_2 or Ar–NH_3 for nondoped and N-CNTs, respectively) at a total flow rate of 575 sccm.[21] Upon reaching the second zone, the mixture was pyrolyzed at 700 °C or 800 °C, respectively, resulting in the base-catalyzed growth of multiwalled CNTs from Fe nanoparticle nucleation sites.[10] The CNTs were deposited along the walls of the quartz tube and were collected after cooling the tube to room temperature under Ar. The nominal lengths and diameters of the as-prepared CNTs are 10 μm and 20–40 nm, respectively.[10] CNTs were stored in airtight vials prior to electrochemical analysis. The Vulcan XC-72 used in control studies was a gift from Dr. Arumugam Manthiram (UT-Austin) and was also stored in an airtight vial.

2.2.2 X-ray Photoelectron Spectroscopy

X-ray photoelectron spectroscopy (XPS) was performed using a PHI 5700 ESCA system with a scan step size of 0.1 eV and an Al Kα monochromatic line (1486.6 eV), calibrated with the signals for Au $4f_{7/2}$, Ag $3d_{5/2}$, and Cu $2p_{3/2}$. Spectra were scan-averaged ten times and analyzed using the FITT 1.2 software package (Photoelectron Spectroscopy Lab, Seoul National University) with Shirley background corrections. Atomic percentages were determined from elemental survey scans and are reported relative to the total signal for carbon, nitrogen, and iron.

2.2.3 Electrochemical Analysis

For electrochemical analysis, nondoped CNTs and N-CNTs were drop-cast onto a 0.5 cm diameter glassy carbon (GC) electrode (PINE Instruments AFE2M050GC).

Before each experiment, the GC was polished successively with 0.3 and 0.05 μm almunia slurries on microcloth (Buehler) to a mirror finish and sonicated in ultrapure H_2O for 15 min. The electrode was then mounted securely in an inverted position, and 5 μL of 5 mg/mL CNTs or N-CNTs in absolute ethanol were carefully pipetted onto the GC surface. The GC-CNT assembly was covered to prevent contamination and allowed to dry (~10 min). Upon drying, the CNTs were immediately immersed into solution for use in electrochemical experiments. CNTs appeared to be strongly adherent to the GC surface, as no CNTs dislodged upon immersion. For control studies using Vulcan XC-72, a 5 mg/mL suspension in absolute ethanol was prepared and drop cast at the GC electrode using the method described above.

In addition to the CNT working electrode, a gold wire counter electrode and Hg/Hg_2SO_4 (sat'd. K_2SO_4) reference electrode (CH Instruments, E° = +0.640 V vs. NHE) were used in all electrochemical measurements. All electrode potentials are reported versus Hg/Hg_2SO_4. Electrochemical measurements were performed at room temperature (23 ± 2 °C) using an Autolab PGSTAT30 potentiostat interfaced with Autolab GPES version 4.9 software. Electrodes were contained within a 125 mL volume, 5-neck glass cell containing ~100 mL of supporting electrolyte solution. Prior to each experiment, solutions were purged with Ar for at least 15 min. All experiments were conducted under flowing Ar unless otherwise noted.

As prepared, the CNTs are somewhat hydrophobic; therefore, the CNTs were wetted prior to electrochemical measurements by cycling between +0.4 and -1.2 V at 0.1 V/s in Ar-purged 1 M KNO_3 (Fisher Scientific) until the CNTs were visibly wet. Effective CNT wetting was also confirmed by the increase in current density in the corresponding cyclic voltammograms (CVs) as the CNTs became fully saturated with electrolyte. At neutral pH, these potentials are not extreme enough to induce anion

intercalation or electrochemical oxidation of the CNTs, thus ensuring that the CNTs were not structurally altered during the wetting process.[11] Following wetting, excess KNO_3 was carefully wicked off the GC-CNT electrode using a Kimwipe before the electrode was immersed into the solution to be used in electrochemical analysis.

To study CNT long-term stability, a 0.1 M H_2SO_4 supporting electrolyte was prepared by diluting a 0.5 M H_2SO_4 stock solution with ultrapure (>18.2 MΩ/cm) water. To study CNT Fe redox activity in physiological pH solutions, several supporting electrolyte solutions commonly used in biogenic electroanalysis were prepared. Trisodium citrate was obtained from Alfa Aesar. All other supporting electrolyte materials were obtained from Fisher. All solutions were prepared with ultrapure water. Solutions of 1 M trisodium citrate, dibasic sodium phosphate and sodium acetate were adjusted to pH = 6.40 ± 0.03 using 1 M solutions of their respective acids, and the pH was measured using a portable pH meter (Orion). Solutions of 1 M KNO_3 in ultrapure H_2O typically exhibited pH values of 6.40 ± 0.03 without further adjustment.

2.3 RESULTS AND DISCUSSION

2.3.1 CNT Long-Term Stability

The durability of potential catalytic substrates, including those used for both inorganic (e.g., fuel cell) and biochemical catalysis, when subjected to normal operating conditions is a critical factor in determining the suitability of a given support in experimental design. To study the stability of traditional carbon blacks, CNTs, and Pt/CNT composites for use in fuel cells, others have used ex situ isothermal heating[32] or in situ electrochemical oxidative cycling[32-34] applied over several hours or days to simulate typical corrosion processes under realistic operating conditions. The latter of these methods can quantify catalyst support corrosion by monitoring the degree of carbon

surface oxidation as reflected by changes in the integrated current observed during electrochemical conditioning. As such, the formation of surface oxides serves as a direct indicator of catalyst support corrosion, as these disruptions to the graphene lattice hinder performance efficiency.[33] Though the experimental conditions used in such studies are harsh compared to conditions typically used in biogenic electrochemical sensing schemes, the information these studies provide about the long-term stability of carbon substrates can be used to evaluate their suitability for use in a variety of sensing schemes. Therefore, we subjected our CNTs, both nondoped and N-doped, to 12 h electrochemical oxidation at +0.66 V v. Hg/Hg_2SO_4 in 0.1 M H_2SO_4, and subjected Vulcan XC-72 carbon to the same electrochemical treatment as a control study. Periodically during the extended oxidations, CVs were collected to monitor the appearance and growth of any surface oxides. Figure 2.1 (top) shows collected for both types of CNTs, as well as Vulcan XC-72, after the 12 h oxidation period was complete. The formation of surface oxides is much more prevalent at the Vulcan carbon than at either CNT variety as indicated by the large peaks between -0.4 and +0.1 V, which are attributed to the redox chemistry of quinone, carboxylic, and phenol functionalities induced in the graphene lattice upon electrochemical oxidation.[35] We note that the increased background current or double layer charging current for N-CNTs relative to nondoped CNTs is a result of increased edge plane character due to turbostratic disorder induced by the incorporation of nitrogen into the graphene lattice, as described extensively in previous reports by us.[10, 22]

The oxidative stabilities of both types of CNTs, as well as Vulcan XC-72, were assessed quantitatively by integrating the amount of charge associated with the redox activity of these surface oxides. The integrated charge as a function of oxidation time is plotted in Figure 2.1 (bottom). Remarkably, our CNT supports appear to quickly stabilize after introduction to oxidative conditions: while both CNT varieties initially develop

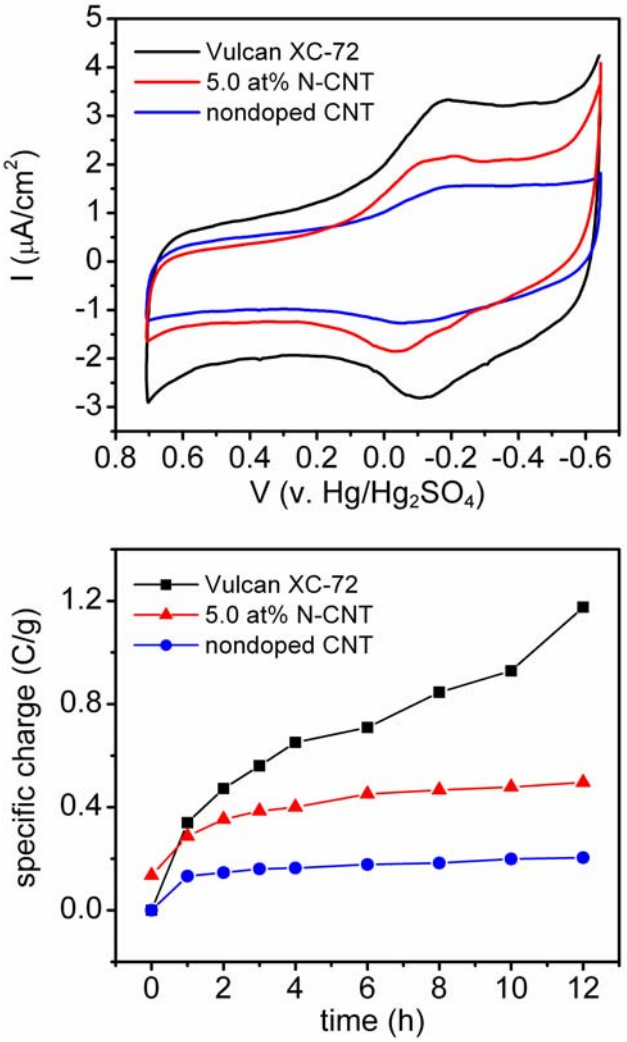

Figure 2.1. (top) Cyclic voltammograms of carbon supports after oxidative polarization for 12 h at +0.66 V v. Hg/Hg_2SO_4 in 0.1 M H_2SO_4 under Ar. (bottom) Integrated charge as a function of oxidative polarization time associated with the formation of surface oxides at the various carbon supports.

surface oxides (t = 0–1 h), they exhibit a self-limiting plateau for the duration of the study, indicating an inherent stabilization despite being subjected to oxidative conditions. The N-CNTs display a higher surface oxide coverage than nondoped CNTs, both before (t = 0) and after the oxidative potential has been applied. Again, this observed response most likely reflects the increased structure disorder within N-CNTs relative to nondoped CNTs, which may promote the formation of more surface oxide functionalities. Nevertheless, the surface oxides present in both types of CNTs are much less prevalent than those in Vulcan XC-72, which continues to develop surface oxides at a markedly increased rate throughout the 12 h period. Thus, our CVD-prepared CNTs demonstrate reduced corrosion vulnerability relative to currently employed fuel cell carbons, and are expected to remain electrochemically stable within the milder potential limits and shorter time durations of our planned experiments (vida infra).

2.3.2 Fe Redox Activity in CNTs

As mentioned in the Introduction, the growth mechanism of our floating catalyst CVD method involves a base-catalyzed, diffusion-controlled mechanism in which CNTs grow as the carbonaceous precursor adsorbs and dissociates at Fe nanoparticles nucleated under high temperature in the reducing environment contained within the quartz tube furnace. As a result of this growth process, the CVD-prepared nondoped CNTs and N-CNTs contain 7 ± 1 (1σ) and 12 ± 1 (1σ) wt% Fe, respectively, as determined previously using thermogravimetric (TGA) analysis.[10, 21] Because the CNT growth mechanism relies upon outgrowth from Fe catalyst seed particles, much of this Fe is encased within graphene layers (see TEM images in Reference 21). Analysis of the XPS Fe 2p spectra shown in Figure 2.2 reveals that the Fe within the CNTs exists both as metallic Fe^0/Fe carbide (707 and 720 eV bands) and as $Fe^{II/III}$ oxides (711 and 725 eV bands),[36-38] with the relative Fe oxide content being inversely proportional to the extent of

N-doping. From these spectra, it is evident that roughly 1.2 and 1.1 at% (~4.5 wt%), or approximately half of the total amount of Fe contained within the nondoped CNTs and N-CNTs, respectively, is located near the CNT surface (defined by the ~10 nm penetration depth of the XPS[39]). These results agree with those we have previously reported for our CNTs.[10]

Previously, we had not observed electrochemical Fe^{II} dissolution or $Fe^{II/III}$ redox behavior related to any of these Fe species when using CNTs in our chosen supporting electrolytes (typically 1 M KNO_3 at neutral to basic pH).[10, 22] Recently, we have discovered that the composition of supporting electrolyte can induce Fe^{II} dissolution and $Fe^{II/III}$ redox activity when CNT electrodes are immersed and cycled between various potential extremes. Figure 2.3 shows representative CVs obtained from GC-CNT assemblies containing ~25 μg CNTs immersed in pH = 6.4, 1 M solutions of (a) KNO_3, (b) Na_2HPO_4 (phosphate), (c) $Na_3C_6H_5O_7$ (citrate), and (d) $NaC_2H_3O_2$ (acetate). These CVs were collected by initially sweeping the potential negative from open circuit (~0 V) to -1.1 V, and then returning to 0 V. Note that the voltammetric response of CNT electrodes in KNO_3 (Figure 2.3a) is essentially featureless for both nondoped CNTs (solid line) and N-CNTs (dashed line), whereas the voltammetric response of these electrodes in other electrolytes (Figure 2.3(b-d)) display very prominent features characteristic of surface confined, $Fe^{II/III}$-based redox chemistry.[23, 24, 40, 41] We are indeed able to confirm that the redox activity observed in Figure 2.3(b-d) corresponds to surface-confined $Fe^{II/III}$ electron transfer by adding 1 mM $Fe^{II}SO_4$ to each of the supporting electrolytes, which results in an increase of both cathodic and anodic peak intensities at the same potential in all cases without the appearance of additional peaks, as shown in Figure 2.4. The $Fe^{II/III}$ redox activity seen Figure 2.4, as well as the disappearance of redox activity upon extensive cycling, are more closely examined in Figures 2.6 and 2.7 (vida infra).

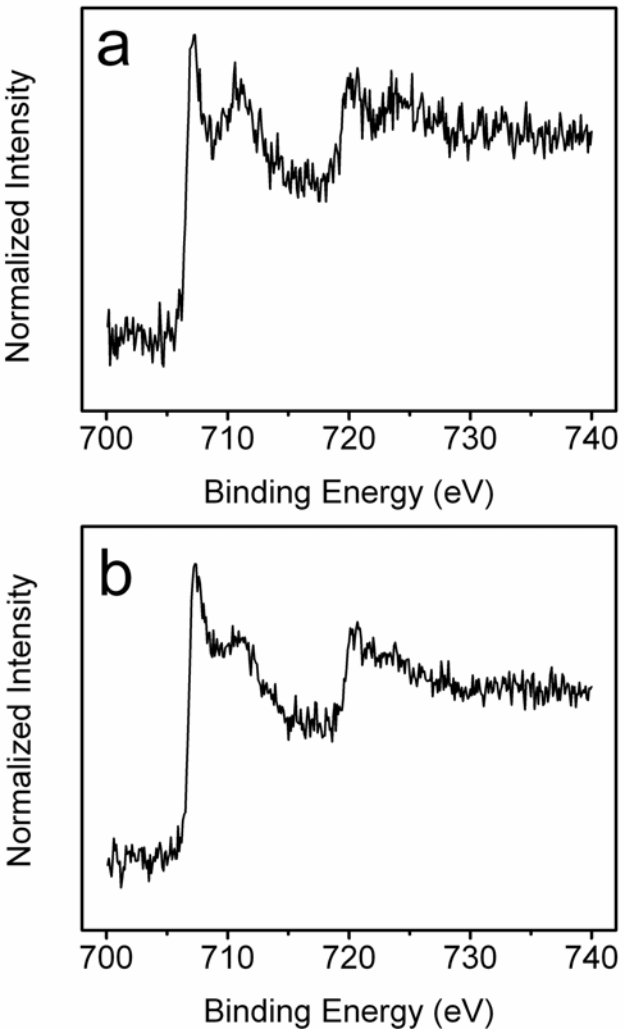

Figure 2.2. Normalized XPS Fe 2p spectra (10-scan average) of (a) nondoped and (b) N-CNTs.

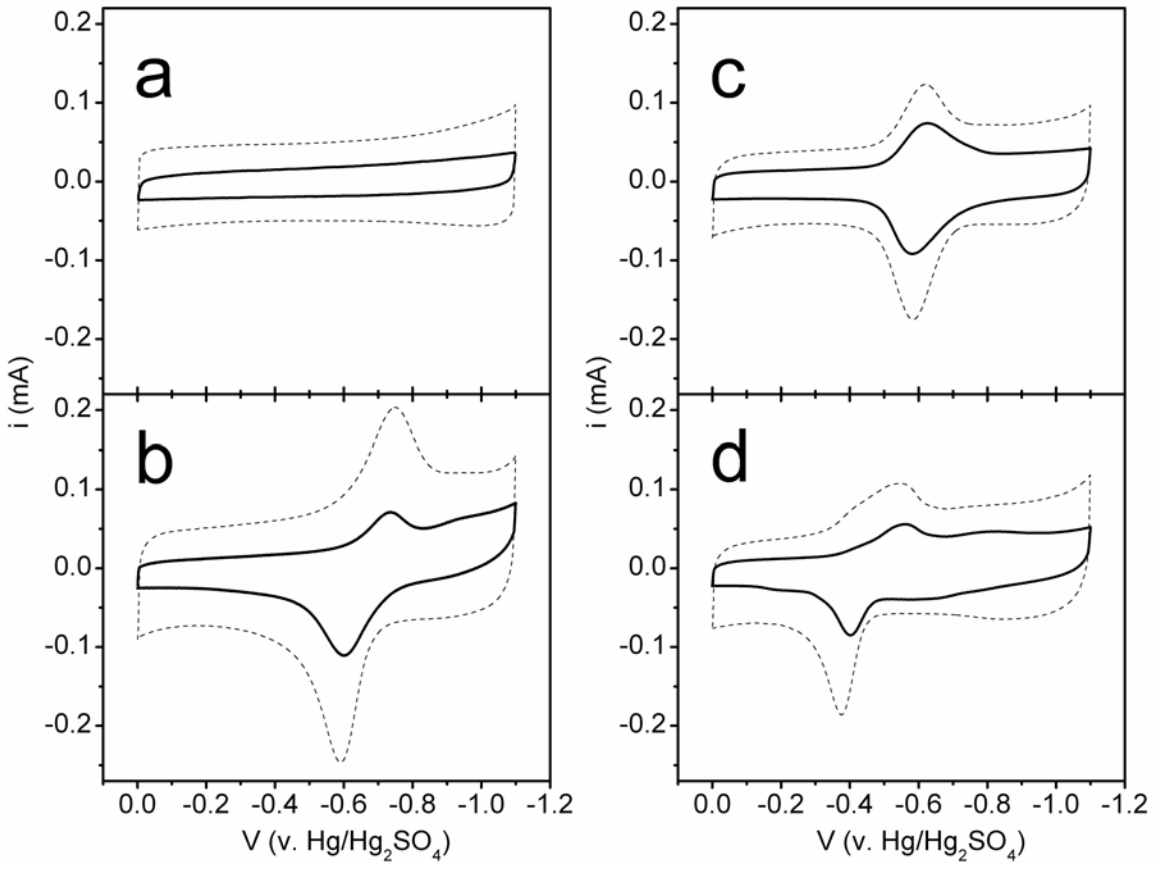

Figure 2.3. Representative CVs of nondoped CNTs (solid lines) and N-CNTs (dashed lines) in Ar-purged, 1 M, pH = 6.40 ± 0.03 solutions of (a) potassium nitrate, (b) sodium phosphate, (c) sodium citrate, and (d) sodium acetate. Scan rate: 100 mV/s.

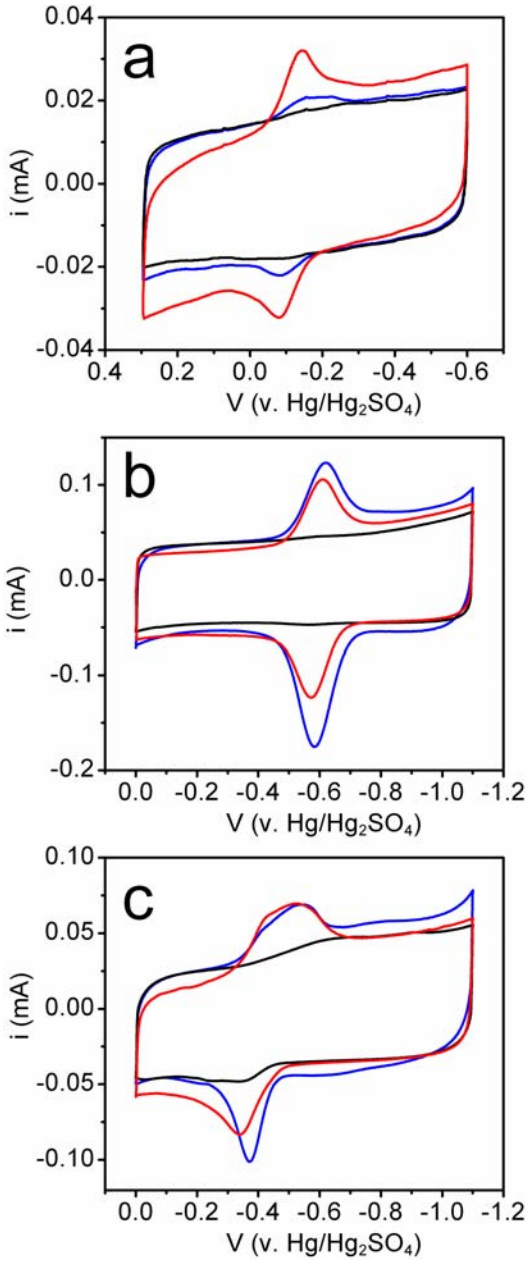

Figure 2.4. Electrochemical response of N-CNTs in 1 M solutions of (a) phosphate, (b) citrate, and (c) acetate both before (red line) and after (black line) exhaustive potential cycling, followed by the addition of 1 mM $FeSO_4$ (blue line). Note that for (a), the pH had to be adjusted to ~2 so that $FePO_4/Fe_2(PO_4)_3$ formed from addition of $FeSO_4$ would be soluble. All other experimental conditions are the same as in Figure 2.3.

We note that in all supporting electrolytes, both the background (double layer charging) current and peak current densities appear larger for N-CNTs than for nondoped CNTs. As mentioned in discussion of Figure 2.1, the increased background current at N-CNTs is a result of increased edge plane character due to turbostratic disorder induced by the nitrogen incorporation into the graphene lattice.[10, 22] Because there are more structural defects or breaks within the graphitic N-CNT lattice in comparison to nondoped CNTs, the increased current response for $Fe^{II/III}$ redox activity conceivably reflects increased Fe dissolution from N-CNTs with more easily accessible sites, while Fe contained within the nondoped CNTs is more protected from electrochemically induced oxidation.

Another interesting aspect is that the shapes of the peaks in Figure 2.3(b-d) vary considerably in different supporting electrolytes. This observation can be explained by considering the influence of the coordinating anion and its tendency to complex with Fe species, since the pH and ionic strength of these solutions are maintained at equivalent values in all supporting electrolytes. For example, the anodic peaks observed in all three supporting electrolytes containing phosphate, citrate, and acetate (Figure 2.3(b-d)) are noticeably larger than their corresponding cathodic peaks. This effect is most pronounced in phosphate solution (Figure 2.3b), and consistent with the fact that Fe^{III} phosphates are known to precipitate at Fe electrode surfaces at neutral pH.[40, 42, 43] The increase in anodic peak current in Figure 2.3b may thus be concurrent with the formation of a surface immobilized complex of $Fe^{III}PO_4$ ($K_{sp} = 9.91 \times 10^{-16}$)[44] on the CNT surface. In a separate instance, close inspection of Figure 2.3d reveals broad "pre-peaks" following the cathodic peaks and preceding the anodic ones, which provide evidence for overlapping redox activity for both soluble and surface immobilized Fe^{III} species in acetate. Additionally, the cathodic peaks for both nondoped CNTs and N-CNTs in acetate are

rather broad and misshapen compared with the anodic ones, reflective of variation in the kinetics of formation different redox-active, surface immobilized $Fe^{II/III}$ oxides in the presence of different complexing anions. It is well known that solvated anions in aqueous solutions may insert and deinsert into graphitic lattices as a result of electrochemical potential variation,[45-47] and that such intercalation is enhanced in the presence of disordered graphitic lattices, such as those in our CNTs.[48] Therefore, we believe that the differences in observed $Fe^{II/III}$ redox activity in varying supporting electrolytes are a result of the differing anions' interactions with encased Fe particles, which are accessed via anion intercalation into the graphitic lattice.

Values of $E_{1/2}$ and ΔE_p with their associated standard deviations (1σ) for 3 trials taken in each supporting electrolyte are shown in Table 2.1. The $E_{1/2}$ values presented in Table 2.1 are in close agreement with previously reported literature values for $Fe^{II/III}$ redox activity in phosphate,[23, 40, 42] citrate,[49] and acetate[50] electrolytes at neutral pH observed for a variety of electrochemical systems including dissolved Fe^{III},[49, 50] $Fe^0/Fe^{II/III}$ oxide thin films,[40, 42] and CVD-prepared, Fe catalyst CNTs.[23] Interestingly, Rusling et. al. have observed a redox couple at -300 mV when using CNTs aligned vertically on a $Fe(OH)_x$-coated substrate in phosphate buffer, though these peaks were attributed to carboxylate groups on the CNTs.[6, 7]

The peak-to-peak separation, ΔE_p, for the $Fe^{II/III}$ redox couple varies widely between different supporting electrolytes. The extreme sensitivity of soluble $Fe^{II/III}$ to surface conditions and microstructure at carbon electrodes has been demonstrated previously,[11, 51-54] and we believe that the unique surface chemistries arising from differences in coordinating anion interactions with both soluble and surface immobilized $Fe^{II/III}$ species contribute to the observed variance in ΔE_p. Such surface chemistries include adsorption of anions from the varying supporting electrolytes at the CNT/Fe sites,

Table 2.1. Peak potentials, peak-to-peak separations and apparent electron transfer rate constants for $Fe^{II/III}$ at nondoped CNT and N-CNT electrodes.

	nondoped CNT			N-CNT (5 at% N)		
Electrolyte[a]	**$E_{1/2}$[b,c]**	**ΔE_p**	**k° (s^{-1})[d]**	**$E_{1/2}$**	**ΔE_p**	**k° (s^{-1})**
(a) nitrate	--	--	--	--	--	--
(b) phosphate	-0.671 ± 0.008	0.132 ± 0.006	0.63 ± 0.03	-0.670 ± 0.003	0.160 ± 0.004	0.45 ± 0.01
(c) citrate	-0.599 ± 0.005	0.027 ± 0.009	5.2 ± 1.7	-0.606 ± 0.004	0.037 ± 0.006	3.6 ± 0.6
(d) acetate	-0.474 ± 0.007	0.156 ± 0.005	0.47 ± 0.02	-0.464 ± 0.006	0.176 ± 0.004	0.38 ± 0.01

[a]All electrolyte solutions are 1 M, pH 6.40 ± 0.03.

[b]Potentials are reported in V vs. Hg/Hg_2SO_4; N=3.

[c]Scan rate: 100 mV/s.

[d]Apparent electron transfer rate constant determined from ΔEp at 100 mV/s using the method of Laviron.[55]

as well as formation of surface immobilized Fe-anion complexes at CNTs. Overall, ΔE_p observed for $Fe^{II/III}$ redox activity at our CNTs is more narrow than that reported in previous studies of soluble $Fe^{II/III}$ at glassy carbon[54] and diamond thin film electrodes.[51, 52] This is an expected result, since $Fe^{II/III}$ is an inner-sphere redox couple in which surface adsorption of $Fe^{II/III}$ promotes more facile and reversible electron transfer, as previously described by McCreery et al.[54] Additionally, CNTs have a greater sp^2 character than HOPG, micro- or nano-crystalline diamond or boron-doped diamond thin film electrodes, so they should display more facile redox activity relative to basal plane sp^2 or B-doped sp^3 carbon electrode materials. Apparent electron transfer rate constants (k^0_{obs}), determined using Laviron's method for surface-confined redox species,[55] can be estimated from the ΔE_p values and are also listed in Table 2.1. For both nondoped CNTs and N-CNTs, k^0_{obs} decreased as a function of anion composition in the order of citrate > phosphate > acetate. The k^0_{obs} in citrate is an order of magnitude larger than either phosphate or acetate. Also evident from analysis of the data in Table 2.1 is that on average, the overall electron transfer process appears less facile at N-CNTs than at nondoped CNTs, as k^0_{obs} is smaller at N-CNTs in all supporting electrolytes. We have previously observed a similar, though more pronounced (k^0_{obs} decreased by an order of magnitude) effect at our N-CNTs relative to nondoped CNTs when studying the oxidation of catecholamines.[20] Like the $Fe^{II/III}$ redox couple, catecholamines are also inner-sphere systems that are very sensitive to carbon electrode surface conditions and microstructure.[56, 57]

To estimate the amount of electroactive $Fe^{II/III}$ present in the CNTs, the anodic peak of each of the CVs shown in Figure 2.3(b-d) was integrated and the charge obtained was used to calculate the number of moles of oxidized Fe^{II}.[58] An electroactive weight percent of $Fe^{II/III}$ was then determined using the mass of the CNTs drop-cast at the GC-

CNT electrode. These weight percents are reported in Table 2.2. The amount of electroactive $Fe^{II/III}$ varies appreciably with supporting electrolyte composition, although it represents only a small fraction (<5%) of the total amount of Fe encapsulated within the CNTs. We attribute the voltammetric differences seen in the respective electrolytes to the variation in the solubility of the Fe–anion complexes. For instance, the solubilities of the Fe^{III}–anion species ($Fe^{III}PO_4$, $Fe^{III}C_6H_5O_7$, and $Fe^{III}(C_2H_3O_2)_3$) are inversely proportional to the integrated anodic peak currents;[44] therefore, as the Fe^{III}–anion complex decreases in solubility, the apparent electroactive percentage of $Fe^{II/III}$ increases, reflective of the formation of insoluble Fe^{III}–anion complexes and their subsequent adsorption/precipitation on the CNT surface.

In addition to the $Fe^{II/III}$ redox process, we are able to observe Fe^{II} dissolution by holding the potential at values more negative than -1.3 V. Figure 2.5 shows CVs of nondoped CNTs (initial scan direction: positive) preceded by a 30 s potential hold at -1.5 V. This potential is near the onset of the hydrogen evolution reaction (HER), which is observed most notably in supporting electrolyte containing nitrate anions (Figure 2.5). We note that the onset of the HER in phosphate supporting electrolyte occurs at a much lower potential, as $H_2(g)$ formation was observed at the CNTs along with liftoff of CNTs from the GC support. Therefore, the phosphate preconditioning potential was limited to -1.3 V (Figure 2.5). Nonetheless, the CVs acquired in all supporting electrolytes display an anodic peak (or pair of peaks, in the case of acetate) at potentials <-0.9 V, which corresponds to the oxidation of Fe, dissolution of Fe^{II} from the Fe nanoparticle surface, and formation of insoluble $Fe(OH)_2$ at the surface, along with competitive adsorption of Fe^{II}–anion complexes. This voltammetric response is similar to that seen for iron electrodes in supporting electrolytes containing acetate anions, where $Fe(OH)_2$ precipitation has been shown to precede the competitive anion adsorption step, giving

Table 2.2. Mass percentage of electroactive $Fe^{II/III}$ from nondoped CNT and N-CNT electrodes, determined by integration of anodic peak currents in Figure 2.3.

	Mass % $Fe^{II/III}$[a]	
Electrolyte	**nondoped CNT**	**N-CNT (5 at% N)**
(a) nitrate	--	--
(b) phosphate	0.50 ± 0.02	0.62 ± 0.03
(c) citrate	0.30 ± 0.01	0.41 ± 0.04
(d) acetate	0.26 ± 0.01	0.34 ± 0.04

[a]Mass percentages are determined using the total mass of CNTs loaded onto GC for electrochemical analysis; N=3.

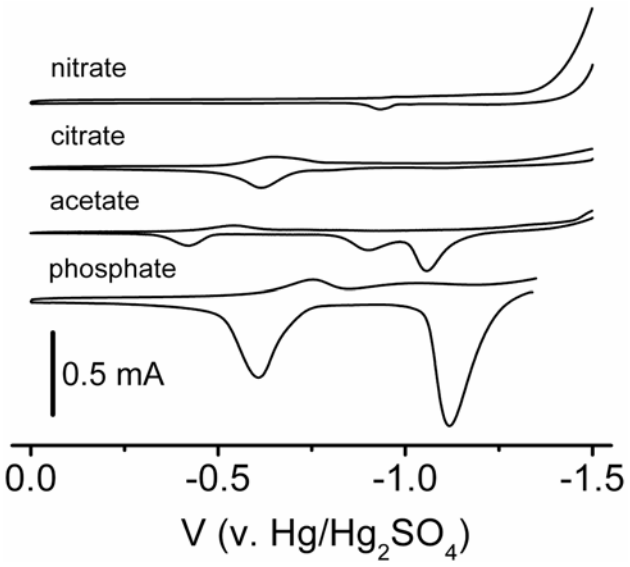

Figure 2.5 CVs of nondoped CNTs collected after a 30 s potential hold at -1.5 V (-1.3 V for phosphate, bottom scan) vs. Hg/Hg_2SO_4 in various 1 M solutions of supporting electrolytes (labeled). Scan rate: 30 mV/s. Other experimental conditions are the same as Figure 2.3.

rise to a pair of observed peaks rather than a single peak.[59-62]

Along with the large anodic peaks observed upon $Fe(OH)_2$ precipitation and Fe^{II} dissolution, changes in $Fe^{II/III}$ peaks were also evident, as shown in Figure 2.5 in citrate, phosphate, and acetate electrolytes. The peak potentials for $Fe^{II/III}$ in Figure 2.5 agree with those presented in Table 2.1. However, both anodic and cathodic peak areas at potentials >-0.8 V deviate from those shown in Figure 2.3. While $Fe^{II/III}$ redox peaks are still not observed in nitrate (despite a small amount of Fe^{II} dissolution seen at -0.934 V), both the anodic and cathodic $Fe^{II/III}$ peaks in citrate, acetate, and phosphate increase in size relative to those observed in Figure 2.3. In comparing Figure 2.5 to Figure 2.3, the relative change in current densities observed for the $Fe^{II/III}$ redox response most likely results from the formation of an $Fe(OH)_2$ layer at Fe particle surfaces after inducing a more negative preconditioning potential. This layer is then oxidized to $Fe^{II/III}$ oxides as the potential is swept anodically, causing the observed increase in $Fe^{II/III}$ redox response.

Analogous electrochemical behavior has been seen for iron electrodes studied in the context of corrosion and passivation processes.[42, 43, 59-78] Based on this earlier research precedence, we can qualitatively depict which Fe species may be responsible for the observed potential-dependent electrochemical responses shown in Figures 2.3, 2.4, and 2.5 using Figure 2.6. For visual clarity of correlating the redox responses with passivation and dissolution processes occurring at the Fe surface, the acetate CV from Figure 2.5 is shown in Figure 2.6 along with pictorial representations of graphene-encased Fe in four potential regions (labeled a–d). We note that this scheme can be used to describe the general behavior of Fe in citrate and phosphate supporting electrolytes, as well. We begin our discussion with the $Fe^{II/III}$ redox couple present >-0.7 V (Figure 2.6, regions a and b). The primary Fe-based species that are redox active within regions a–b are typically $Fe^{II/III}$ oxides/oxyhydroxides, consistent with thermodynamic predictions of Fe^{II} oxides being

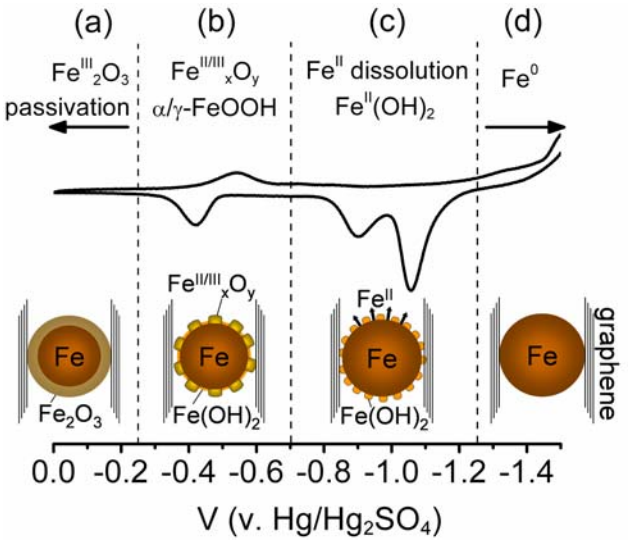

Figure 2.6. Scheme depicting the dissolution and passivation of graphene-encased Fe in neutral pH, aqueous supporting electrolyte as a function of potential.

electroactive at -1.1 V.[64] However, the distinct assignment of these peaks to one particular Fe oxide species is difficult, as many types of Fe species are known to form in this potential window. According to potential–pH diagrams for solid Fe^0 immersed in aqueous systems, Fe oxides of hematite (α-$Fe^{III}_2O_3$) and magnetite ($Fe^{II}Fe^{III}_2O_4$), as well as hydrated $Fe^{II}(OH)_2$, can exist between potentials of 0 and -1.1 V at pH 6.4.[64] Previous electrochemical studies coupled with XANES analysis of Fe^0 thin films have confirmed that the mixed $Fe^{II/III}$ oxide magnetite, as well as substoichiometric Fe oxides with oxidation states between those of magnetite and pure Fe^{III} oxide, are present in solutions of acetate at pH 6.4.[69] Furthermore, though maghemite (γ-$Fe^{III}_2O_3$) is not explicitly included in the Pourbaix discussion of Fe potential–pH diagrams, it has been shown experimentally to form from electrochemical oxidation of Fe thin films in acetate; however, we note that a more positive applied potential than that used here (>+0.35 V) is required to observe a surface layer consisting entirely of Fe^{III} oxide.[69] Additionally, both Fe corrosion and its passivation by layers of hematite and magnetite occur within the potential window of Figure 2.6, regions a–b, according to the Pourbaix diagrams. The thermodynamic active-to-passive transition occurs at ~-0.7 V, though it is noted in discussion of these diagrams that the presence of Fe complexing anions can shift the experimental activation potential to more negative potential values than -1 V at neutral pH.[64] The Pourbaix diagrams also do not consider Fe^{III} oxyhydroxides as possible species, but recent experiments have shown that goethite (α-$Fe^{III}OOH$) and lepidocrocite (γ-$Fe^{III}OOH$) oxyhydroxides, along with magnetite, may coexist within the potential window of -0.9 to -0.4 V in acetate at pH 6.[67] Considering all of these observations, the data displayed in Figures 2.3 and 2.4 is most characteristic of Fe surface oxides comprising mixed $Fe^{II/III}$ oxide/Fe^{III} oxyhydroxides, with the nature of the coordinating anion within the supporting electrolyte composition influencing formation and relative

amounts of these species.

The determination of Fe species in Figure 2.6, regions c–d is more straightforward, as many literature references have attributed the peaks occurring during an anodic sweep from -1.5 V to -0.75 V to Fe^{II} dissolution and $Fe(OH)_2$ formation.[49, 60, 61] Returning to the Pourbaix diagrams for Fe, cathodic potentials <-1.3 V at pH 6.4 lie within the "activation" region of the potential–pH diagram where $Fe(OH)_2$ is sparingly soluble, supporting the concept of $Fe(OH)_2$ surface coverage and competitive adsorption.[64] As the potential is swept anodically from region d toward region a, the $Fe(OH)_2$ layer may be oxidized to mixed $Fe^{II/III}$ oxides, as demonstrated in studies of Fe in borate solutions.[72] Finally, as the potential is swept anodically to potentials more positive than the 0 V limit in region a, a mixed $Fe^{II/III}$ oxide can be further oxidized to an almost entirely insulating Fe^{III} oxide film,[69] thereby passivating the surface of the Fe particle as depicted in the pictorial representation of Figure 2.6, region a.

A notable exception to this discussion of electroactive $Fe^{II/III}$ species at CNTs is the case of CNTs immersed in supporting electrolyte containing nitrate anions, in which no surface bound $Fe^{II/III}$ redox activity (Figure 2.3a) and very little Fe^{II} dissolution (Figure 2.5) is observed. The chemistry of Fe^0 in nitrate electrolytes at neutral pH has been studied extensively in the context of corrosion[73, 78] and denitrification processes.[74-77] Fe^0 electrodes immersed in nitrate electrolytes are known to form passivating oxide layers such as amorphous magnetite and Fe^{III} oxyhydroxides. These insulating oxides form outer coatings on Fe^0 surfaces that inhibit nitrate reduction[74-78] in addition to reduction of chlorinated solvents such as tricholorethylene.[79, 80] As evident from the voltammetric response shown in Figure 2.5, the Fe^0 particles within the CNTs exhibit a passivating response preventing not only nitrate reduction but also the dissolution of Fe^{II}, as well as subsequent surface-bound $Fe^{II/III}$ redox activity associated with the formation of mixed

$Fe^{II/III}$ oxides. Only a small transient peak at -0.934 V is seen, most likely due to dissolution of Fe^{II} from residual surface Fe. As documented extensively by Huang and coworkers, the addition of soluble Fe^{II} to nitrate solutions containing Fe^0 has been shown to promote the transition of an amorphous, non-redox-active magnetite layer to a crystalline, redox-active magnetite layer.[73, 76-78] Soluble Fe^{II} is believed to adsorb strongly at $Fe^{II/III}$ oxide layers, facilitating the transformation between non-redox-active, amorphous $Fe^{II/III}$ oxides/oxyhydroxides to redox-active, $Fe^{II/III}$ magnetite phases that catalyze nitrate reduction.[73, 76-78] While the exact role of surface-bound Fe^{II} in nitrate reduction is not entirely clear, it is evident from our studies shown in Figures 2.3 and 2.5 that Fe^{II} dissolution directly increases surface $Fe^{II/III}$ oxide/oxyhyroxide redox activity at CNTs immersed in acetate, phosphate, and citrate electrolytes.

Repeated cycling of CNTs in these supporting electrolytes results in the complete diminishment or suppression of the $Fe^{II/III}$ redox activity, as shown in Figure 2.7 for nondoped CNTs in (a) phosphate and (b) acetate. In contrast, other researchers have shown that repeated oxidative cycling of CNT electrodes prepared by CVD using Fe catalysts results in an increase in $Fe^{II/III}$ redox behavior as amorphous C coating the Fe particles is oxidized, exposing Fe^0 to the solution where it can then be more easily oxidized to Fe^{II}.[25] While the potentials used here are not positive enough to induce the oxidation of amorphous C, we do observe an initial increase in $Fe^{II/III}$ redox activity for CNTs in acetate electrolyte (Figure 2.7b). However, after the first few (<5) scans, peak currents for the $Fe^{II/III}$ redox process decrease with each subsequent scan. Furthermore, following the diminishment of $Fe^{II/III}$ redox activity (as seen for scan 200 in Figure 2.7), the $Fe^{II/III}$ redox response does not reappear, even after holding the electrode potential for 20 min at open circuit, or at cathodic (-1.1 V) or anodic (0 V) potential extremes. We believe the observed voltammetric behavior in acetate, citrate, and phosphate electrolytes

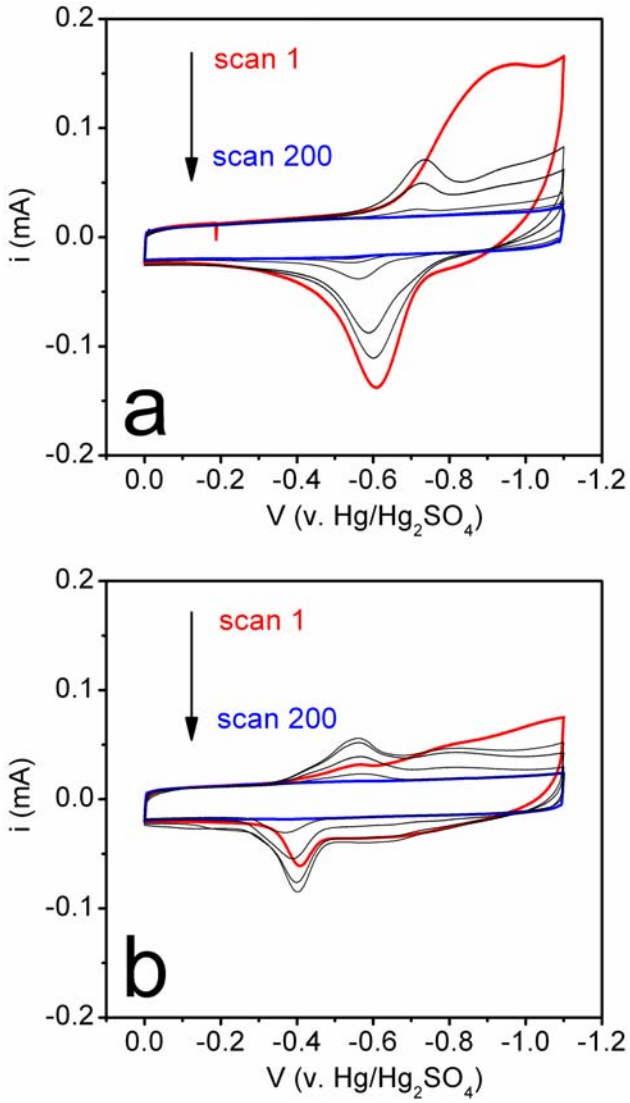

Figure 2.7. Repetitive cycling of nondoped CNTs in (a) 1 M phosphate and (b) 1 M acetate. Experimental conditions are the same as in Figure 2.3.

is a result of the combination of Fe oxidation/dissolution from graphene-encased Fe particles into solution to form surface-bound $Fe^{II/III}$–anion complexes, along with passivation of exposed Fe^0 and $Fe^{II/III}$ oxides/oxyhydrxides confined to the CNTs as the potential is repeatedly swept between activating and passivating regions (see discussion of Figure 2.6).

An alternative to electrochemical passivation of Fe is its chemical passivation, which may be achieved through addition of a chemical species that inhibits Fe^{II} dissolution and $Fe^{II/III}$–anion complex formation in solution. For example, it has been well documented that the addition of sodium benzoate to neutral pH acetate solutions inhibits Fe dissolution and the formation of $Fe^{II/III}$–anion complexes and $Fe^{II/III}$ oxides/oxyhydroxides, as benzoate anions strongly adsorb and passivate the Fe surface.[65, 70] Figure 2.8 shows CVs collected using the same electrochemical parameters as that shown in Figure 2.5 for nondoped CNTs in solutions with varying ratios of 1 M acetate:1 M benzoate. As evident in Figure 2.8, Fe^{II} dissolution is severely inhibited as the benzoate concentration is increased, consistent with the voltammetric response seen at Fe^0 electrodes reported previously. Takahashi et. al.[70] have shown through galvanostatic reduction of solid Fe^0 electrodes immersed in 1 M benzoate that $Fe(OH)_2$ and $Fe(OH)_3$, as well as $Fe^{II}(OH)$–benzoate complexes, are present at potentials more negative than +0.5 V vs. Hg/Hg_2SO_4, contributing to the marked decrease in Fe^{II} dissolution observed in Figure 4. One key difference with our system is that the current density for the $Fe^{II/III}$ redox response *increases* in the presence of benzoate relative to the peaks observed in acetate alone (Figure 2.8). Thus it appears that while benzoate adsorption at the Fe particle surface inhibits Fe^{II} dissolution at potentials <-0.8 V, benzoate adsorption does not inhibit the redox activity of pre-existing $Fe^{II/III}$ oxides, nor does it inhibit the oxidation of $Fe(OH)_x$/Fe(OH)–benzoate complexes to $Fe^{II/III}$ oxides.

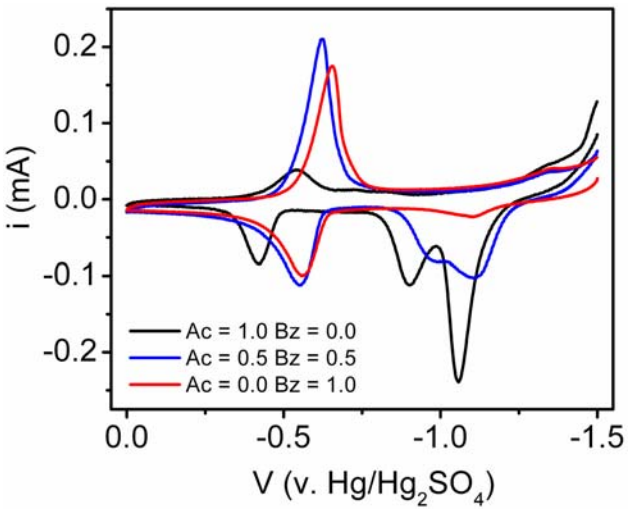

Figure 2.8. CVs of nondoped CNTs collected after a 30 s potential hold at -1.5 V vs. Hg/Hg_2SO_4 in 1 M solutions of varying acetate:benzoate concentration, as denoted in the figure legend. Scan rate: 30 mV/s. Other experimental conditions are the same as Figure 2.3.

We have previously reported the enhanced O_2 reduction at nondoped and N-CNTs relative to GC electrodes,[10, 22] and found distinct mechanistic differences toward O_2 reduction as a function of nitrogen doping and solution pH. Both ourselves[10, 19, 22] and other recent reports by Ozkan et al.[24, 81-84] have documented that N-CNTs, even after rigorous washing in concentrated HCl or HF, display pronounced oxygen reduction activity that does not appear to be directly related to the residual iron content. Several previous studies have speculated that iron species may participate in the observed O_2 reduction activity in as many as three ways: as exposed solid iron on the carbon surface, as dissolved Fe^{II} species leaching out of the CNTs into solution, or as nitrogen-chelated $Fe^{II/III}$ sites. A common feature of O_2 reduction with Fe and Fe oxides is the formation of Fe^{II} surface sites simultaneously with the electroreduction of oxygen, which is associated with the specific interaction of Fe^{II} with O_2.[85-87] Previously, we have observed no voltammetric peaks commensurate with the oxidation of metallic iron or reduction of iron oxide at N-CNTs in neutral pH solutions containing nitrate that would provide evidence for the formation of surface Fe^{II} sites. However, we do see this behavior for CNTs immersed in other supporting electrolytes at neutral pH. Figure 2.9 shows CVs of ~10 μg N-CNTs supported on a GC electrode immersed 1 M phosphate both in deaerated (dashed line) and O_2 saturated solutions before (solid black line) and after (red line) excessive potential cycling (50 cycles), where a pair of peaks corresponding to $Fe^{II/III}$ redox response occurs initially at -0.670 V for N-CNTs along with a cathodic peak at -0.343 V, consistent with the irreversible reduction of O_2. Note that the O_2 reduction peak at N-CNT electrodes is shifted significantly positive (~0.227 V) to that where $Fe^{II/III}$ redox activity is seen and to that where O_2 reduction occurs at nondoped CNT electrodes (-0.760 V)[10] or at GC (Figure 2.9, dotted line) in neutral pH solutions.[22] By cycling the N-CNTs repeatedly for 50 cycles in O_2 saturated phosphate electrolyte, the $Fe^{II/III}$ redox

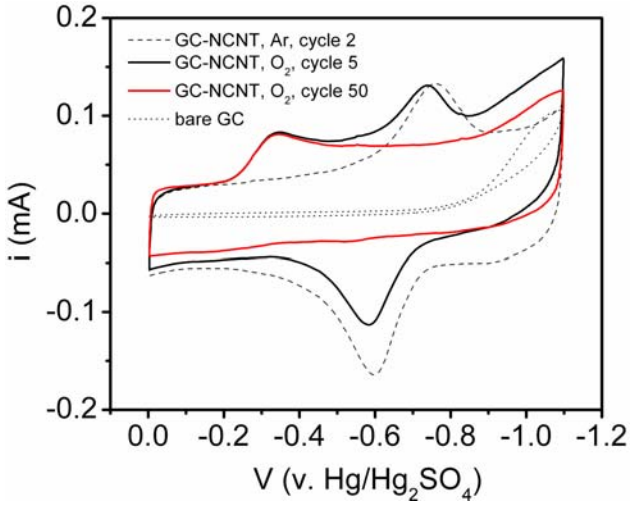

Figure 2.9. CVs of ~10 μg N-CNTs supported on a GC electrode immersed in O_2 saturated, 1 M phosphate both before (solid black line) and after (red line) suppression of $Fe^{II/III}$ redox activity. For comparison, CVs of N-CNTs in Ar-purged phosphate (dashed line) and of bare GC in O_2 saturated phosphate (dotted line) are also shown. Scan rate: 100 mV/s.

peaks are suppressed, as demonstrated previously in Figure 2.7, and the CV shown in Figure 2.9 (red line) is obtained. Remarkably, the O_2 reduction peak *does not shift* from its original potential of -0.343 V upon suppression of $Fe^{II/III}$ redox activity. Figure 2.9 suggests that neither the presence of Fe nor its subsequent passivation directly influences N-CNTs' catalytic behavior toward O_2 reduction. Similar electrochemical behavior for O_2 reduction at nondoped CNTs (data not shown) were obtained when using acetate buffer. These findings, combined with earlier studies by ourselves[10, 19, 22] and others[24, 81-84] suggest that nitrogen-chelated $Fe^{II/III}$ sites or surface-bound $Fe^{II/III}$ oxide species are *not* the primary catalytically active sites for O_2 reduction within these N-CNTs. These observations are supported by extensive studies[88-91] of O_2 reduction on Fe and Fe oxides, in which the formation of Fenton-like, redox-active surface Fe^{II} sites is essential for reducing O_2.[85-87] If Fe^{II} sites were involved in O_2 reduction, then the passivating behavior for $Fe^{II/III}$ seen after significant potential cycling should inhibit O_2 reduction, evidenced by diminishment and shifting of O_2 reduction peak to more negative potentials. Finally, we note with curiosity that the peak potential for O_2 reduction in Figure 2.9 is ~0.35 V positive of potentials we have previously reported for N-CNTs in 1 M KNO_3.[10] We have observed similar positive shifts using N-CNTs in buffered acetate solutions, and we are currently investigating the cause of this apparent increased catalytic activity for oxygen reduction.

2.4 CONCLUSIONS

In this chapter, we have examined CNTs prepared via a floating catalyst CVD method to determine their suitability for use in biogenic electrochemical sensing schemes. We have determined that both nondoped CNTs and CNTs doped with 5 at% nitrogen exhibit increased long-term stability relative to Vulcan XC-72, an industry standard carbon support material. We have also demonstrated that Fe particles

encapsulated in nondoped and N-doped CNTs as a result of catalytic synthesis methods may exhibit both $Fe^{II/III}$ and $Fe^{0/II}$ redox activity, depending upon the nature of the supporting electrolyte and experimental conditions chosen for electrochemical analysis. While no $Fe^{II/III}$ redox activity is observed in 1 M KNO_3 solutions, a pronounced $Fe^{II/III}$ response associated with surface-confined $Fe^{II/III}$ is observed between 0 and -1.1 V vs. Hg/Hg_2SO_4 in solutions of acetate, citrate, and phosphate. Iron (II) dissolution may also be induced by applying more negative potentials. The dissolution of Fe^{II} contained within CNTs is inhibited by benzoate anions, in accordance with previous findings at solid Fe^0 electrodes. Importantly, $Fe^{II/III}$ redox activity within the CNTs may be completely suppressed by repeated electrochemical cycling, and doing so does not alter their apparent electrocatalytic response to O_2, suggesting that O_2 reduction at neutral pH is not catalyzed by surface bound $Fe^{II/III}$ species. These findings confirm that CNTs prepared in our laboratory using a floating catalyst CVD method are suitable for use in biogenic electrochemical sensing schemes. Furthermore, these findings underscore the importance of thoroughly investigating the inherent electrochemical activity of catalytically prepared CNTs in a chosen set of experimental parameters (supporting electrolyte, potential window) prior to their use as conductive supports in electrochemical studies.

2.5 REFERENCES

(1) Musameh, M.; Wang, J.; Merkoci, A.; Lin, Y. *Electrochem. Comm.* **2002**, *4*, 743-746.

(2) Gooding, J. J. *Electrochim. Acta* **2005**, *50*, 3049-3060.

(3) Merkoci, A.; Pumera, M.; Llopis, X.; Perez, B.; del Valle, M.; Alegret, S. *Tr. Anal. Chem.* **2005**, *24*, 826-838.

(4) Li, W.; Liang, C.; Qiu, J.; Zhou, W.; Han, H.; Wei, Z.; Sun, G.; Xin, Q. *Carbon* **2002**, *40*, 791-794.

(5) Wang, X.; Li, W.; Chen, Z.; Waje, M.; Yan, Y. *J. Pow. Sour.* **2006**, *158*, 154-159.

(6) Yu, X.; Chattopadhyay, D.; Galeska, I.; Papadimitrakopoulos, F.; Rusling, J. F. *Electrochem. Comm.* **2003**, *5*, 408-411.

(7) Yu, X.; Kim, S. N.; Papadimitrakopoulos, F.; Rusling, J. F. *Mol. BioSys.* **2005**, *1*, 70-78.

(8) Yu, X.; Munge, B.; Patel, V.; Jensen, G.; Bhirde, A.; Gong, J. D.; Kim, S. N.; Gillespie, J.; Gutkind, J. S.; Papadimitrakopoulos, F.; Rusling, J. F. *J. Am. Chem. Soc.* **2006**, *128*, 11199-11205.

(9) O'Connor, M.; Kim Sang, N.; Killard Anthony, J.; Forster Robert, J.; Smyth Malcolm, R.; Papadimitrakopoulos, F.; Rusling James, F. *Analyst* **2004**, *129*, 1176-1180.

(10) Maldonado, S.; Stevenson, K. J. *J. Phys. Chem. B* **2005**, *109*, 4707-4716.

(11) McCreery, R. L. In *Electroanalytical Chemistry*; Bard, A. J., Ed.; Marcel Dekker, Inc.: New York; Vol. 17, pp 221-292.

(12) Bowling, R. J.; Packard, R. T.; McCreery, R. L. *J. Am. Chem. Soc.* **1989**, *111*, 1217-1223.

(13) Moore, R. R.; Banks, C. E.; Compton, R. G. *Anal. Chem.* **2004**, *76*, 2677-2682.

(14) Morcos, I.; Yeager, E. *Electrochim. Acta* **1970**, *15*, 953-975.

(15) Ranganathan, S.; Kuo, T.-C.; McCreery, R. L. *Anal. Chem.* **1999**, *71*, 3574-3580.

(16) Kim, N. S.; Lee, Y. T.; Park, J.; Han, J. B.; Choi, Y. S.; Choi, S. Y.; Choo, J.; Lee, G. H. *J. Phys.Chem. B* **2003**, *107*, 9249-9255.

(17) Wang, X.; Hu, W.; Liu, Y. Q.; Long, C.; Xu, Y.; Zhou, S.; Zhu, D.; Dai, L. *Carbon* **2001**, *39*, 1533-1536.

(18) Rao, C. N. R.; Govindaraj, A. *Acc. Chem. Res.* **2002**, *35*, 998-1007.

(19) Vijayaraghavan, G.; Stevenson, K. J. *Langmuir* **2007**, *23*, 5279-5282.

(20) Maldonado, S.; Morin, S.; Stevenson, K. J. *Analyst* **2006**, *131*, 262-267.

(21) Maldonado, S.; Morin, S.; Stevenson, K. J. *Carbon* **2006**, *44*, 1429-1437.

(22) Maldonado, S.; Stevenson, K. J. *J. Phys. Chem. B* **2004**, *108*, 11375-11383.

(23) Pumera, M. *Langmuir* **2007**, *23*, 6453-6458.

(24) Matter, P. H.; Wang, E.; Millet, J.-M. M.; Ozkan, U. S. *J. Phys. Chem. C* **2007**, *111*, 1444-1450.

(25) Fang, H.-T.; Liu, C.-G.; Liu, C.; Li, F.; Liu, M.; Cheng, H.-M. *Chem. Mater.* **2004**, *16*, 5744-5750.

(26) Sljukic, B.; Banks, C. E.; Compton, R. G. *Nano Lett.* **2006**, *6*, 1556-1558.

(27) Dai, X.; Wildgoose, G. G.; Compton, R. G. *Analyst* **2006**, *131*, 901-906.

(28) Banks, C. E.; Crossley, A.; Salter, C.; Wilkins, S. J.; Compton, R. G. *Angew. Chem.* **2006**, *45*, 2533-2537.

(29) Gao, L.; Zhuang, J.; Nie, L.; Zhang, J.; Zhang, Y.; Gu, N.; Wang, T.; Feng, J.; Yang, D.; Perrett, S.; Yan, X. *Nature Nanotech.* **2007**, *2*, 577-583.

(30) Jurkschat, K.; Ji, X.; Crossley, A.; Compton, R. G.; Banks, C. E. *Analyst* **2007**, *132*, 21-23.

(31) "Purified" and "Super Purified" HiPCO(c) CNTs containing <5-15 wt% ash content are available from Carbon Nanotechnologies, http://www.cnanotech.com.

(32) Stevens, D. A.; Hicks, M. T.; Haugen, G. M.; Dahn, J. R. *J. Electrochem. Soc.* **2005**, *152*, A2309-A2315.

(33) Li, L.; Xing, Y. *J. Electrochem. Soc.* **2006**, *153*, A1823-A1828.

(34) Shao, Y.; Yin, G.; Gao, Y.; Shi, P. *J. Electrochem. Soc.* **2006**, *153*, A1093-A1097.

(35) Kinoshita, K. In *Carbon: Electrochemical and Physicochemical Properties*; John Wiley & Sons, Inc.: New York, 1988, pp 1-19.

(36) In *Handbook of X-Ray Photoelectron Spectroscopy*; Chastain, J., King, R. C., Eds.; Physical Electronics, Inc.: Eden Prairie, 1995, pp 80.

(37) Choudhury, T.; Saied, S. O.; Sullivan, J. L.; Abbot, A. M. *J. Phys. D* **1989**, *22*, 1185-1195.

(38) Sethuraman, A. R.; Stencel, J. M.; Rubel, A. M.; Cavin, B.; Hubbard, C. R. *J. Vac. Sci. Tech. A* **1994**, *12*, 443-451.

(39) Christie, A. B. In *Methods of Surface Analysis*; Walls, J. M., Ed.; Cambridge University Press: Cambridge, 1989, pp 136.

(40) Borras, C. A.; Romagnoli, R.; Lezna, R. O. *Electrochim. Acta* **2000**, *45*, 1717-1725.

(41) Gojkovic, S. L.; Gupta, S.; Savinell, R. F. *J. Electrochem. Soc.* **1998**, *145*, 3493-3499.

(42) Benzakour, J.; Derja, A. *Electrochim. Acta* **1993**, *38*, 2547-2550.

(43) Masek, J.; Mesickova, E. *J. Electroanal. Chem.* **1971**, *33*, 219-223.

(44) In *CRC Handbook of Chemistry and Physics,* 86th ed.; Lide, D. R., Ed.; Taylor & Francis: Boca Raton, 2005, pp 8-118.

(45) Alliata, D.; Haring, P.; Haas, O.; Kotz, R.; Siegenthaler, H. *Electrochem. Comm.* **1999**, *1*, 5-9.

(46) Conway, B. E. In *Electrochemical Supercapacitors: Scientific Fundamentals and Technological Applications*; Kluwer Academic/Plenum: New York, 1999, pp 218.

(47) Goss, C. A.; Brumfield, J. C.; Irene, E. A.; Murray, R. W. *Anal. Chem.* **1993**, *65*, 1378-1389.

(48) Gnanaraj, J. S.; Levi, M. D.; Levi, E.; Salitra, G.; Aurbach, D.; Fischer, J. E.; Claye, A. *J. Electrochem. Soc.* **2001**, *148*, A525-A536.

(49) Danilov, F. I.; Protsenko, V. S.; Ubiikon, A. V. *Russ. J. Electrochem.* **2005**, *41*, 1282-1289.

(50) Domenech-Carbo, A.; Sanchez-Ramosa, S.; Domenech-Carbo, M. T.; Gimeno-Adelantado, J. V.; Bosch-Reig, F.; Yusa-Marco, D. J.; Sauri-Peris, M. C. *Electroanal.* **2002**, *14*, 685-696.

(51) Bennett, J. A.; Wang, J.; Show, Y.; Swain, G. M. *J. Electrochem. Soc.* **2004**, *151*, E306-E313.

(52) Fischer, A. E.; Show, Y.; Swain Greg, M. *Anal. Chem.* **2004**, *76*, 2553-2560.

(53) Pupkevich, V.; Glibin, V.; Karamanev, D. *Electrochem. Comm.* **2007**, *9*, 1924-1930.

(54) Chen, P.; Fryling, M. A.; McCreery, R. L. *Anal. Chem.* **1995**, *67*, 3115-3122.

(55) Laviron, E. *J. Electroanal. Chem.* **1979**, *101*, 19-28.

(56) Allred, C. D.; McCreery, R. L. *Anal. Chem.* **1992**, *64*, 444-448.

(57) DuVall, S. H.; McCreery, R. L. *Anal. Chem.* **1999**, *71*, 4594-4602.

(58) Bard, A. J.; Faulkner, L. R. *Electrochemical Methods: Fundamentals and Applications*, 2nd ed.; John Wiley & Sons: Hoboken, NJ, 2001.

(59) Azambuja, D. S.; Muller, I. L.; Feris, L. A.; Ladeira, F.; Ries, L. S. *Corr. Sci.* **1996**, *38*, 1235-1244.

(60) Takahashi, K.; Bardwell, J. A.; MacDougall, B.; Graham, M. J. *Electrochim. Acta* **1992**, *37*, 477-487.

(61) Kladekova, D.; Galova, M.; Pikna, L. u. *Part. Sci. Tech.* **2005**, *23*, 189-199.

(62) Azambuja, D. S.; Mueller, I. L. *Corr. Sci.* **1994**, *36*, 1835-1845.

(63) Jovanovic, V. M.; Hackerman, N. *J. Phys. Chem. B* **1998**, *102*, 9855-9860.

(64) Pourbaix, M. *Atlas of Electrochemical Equilibria in Aqueous Solutions*; Pergamon Press: Oxford, 1966.

(65) Azambuja, D. S.; Holzle, L. R.; Muller, I. L.; Piatnicki, C. M. S. *Corr. Sci.* **1999**, *41*, 2083-2097.

(66) Hang, B. T.; Watanabe, T.; Eashira, M.; Watanabe, I.; Okada, S.; Yamaki, J.-i. *Electrochem. Sol.-St. Lett.* **2005**, *8*, A476-A480.

(67) Martinez, L.; Leinen, D.; Martin, F.; Gabas, M.; Ramos-Barrado, J. R.; Quagliata, E.; Dalchiele, E. A. *J. Electrochem. Soc.* **2007**, *154*, D126-D133.

(68) Merkofer, M.; Kissner, R.; Hider, R. C.; Brunk, U. T.; Koppenol, W. H. *Chem. Res. Toxic.* **2006**, *19*, 1263-1269.

(69) Oblonsky, L. J.; Ryan, M. P.; Isaacs, H. S. *Corr. Sci.* **2000**, *42*, 229-241.

(70) Takahashi, K.; Bardwell, J. A.; MacDougall, B.; Graham, M. J. *Electrochim. Acta* **1992**, *37*, 489-494.

(71) Thomas, J. G. N.; Nurse, T. J. *Brit. Corr. J.* **1967**, *2*, 13-20.

(72) Diez-Perez, I.; Gorostiza, P.; Sanz, F.; Muller, C. *J. Electrochem. Soc.* **2001**, *148*, B307-B313.

(73) Huang, Y. H.; Zhang, T. C. *Chemosphere* **2006**, *64*, 937-943.

(74) Mishra, D.; Farrell, J. *Environ. Sci. and Tech.* **2005**, *39*, 645-650.

(75) Zhang, T. C.; Huang, Y. H. *J. Environ. Eng.* **2005**, *131*, 461-470.

(76) Zhang, T. C.; Huang, Y. H. *J. Environ. Eng.* **2006**, *132*, 527-536.

(77) Zhang, T. C.; Huang, Y. H. *Water Res.* **2006**, *40*, 2311-2320.

(78) Huang, Y. H.; Zhang, T. C. *Water Res.* **2005**, *39*, 1751-1760.

(79) Farrell, J.; Kason, M.; Melitas, N.; Li, T. *Environ. Sci. Tech.* **2000**, *34*, 514-521.

(80) Ritter, K.; Odziemkowski, M. S.; Simpgraga, R.; Gillham, R. W.; Irish, D. E. *J. Contam. Hydr.* **2003**, *65*, 121-136.

(81) Matter, P. H.; Wang, E.; Arias, M.; Biddinger, E. J.; Ozkan, U. S. *J. Mol. Catal. A* **2007**, *264*, 73-81.

(82) Matter, P. H.; Wang, E.; Ozkan, U. S. *J. Catal.* **2006**, *243*, 395-403.

(83) Matter, P. H.; Wang, E.; Arias, M.; Biddinger, E. J.; Ozkan, U. S. *J. Phys. Chem. B* **2006**, *110*, 18374-18384.

(84) Matter, P. H.; Ozkan, U. S. *Catal. Lett.* **2006**, *109*, 115-123.

(85) Moura, F. C. C.; Araujo, M. H.; Costa, R. C. C.; Fabris, J. D.; Ardisson, J. D.; Macedo, W. A. A.; Lago, R. M. *Chemosphere* **2005**, *60*, 1118-1123.

(86) Moura, F. C. C.; Oliveira, G. C.; Araujo, M. H.; Ardisson, J. D.; Macedo, W. A. A.; Lago, R. M. *App. Catal. A* **2006**, *307*, 195-204.

(87) Nurmi, J. T.; Tratnyek, P. G.; Sarathy, V.; Baer, D. R.; Amonette, J. E.; Pecher, K.; Wang, C.; Linehan, J. C.; Matson, D. W.; Penn, R. L.; Driessen, M. D. *Environ. Sci. Tech.* **2005**, *39*, 1221-1230.

(88) Castro, P. A.; Vago, E. R.; Calvo, E. J. *J. Chem. Soc. Farad. Trans.* **1996**, *92*, 3371-3379.

(89) Vago, E.; Calvo, E. J. *J. Chem. Soc. Farad. Trans.* **1995**, *91*, 2323-2329.

(90) Vago, E. R.; Calvo, E. J. *J. Electroanal. Chem.* **1992**, *339*, 41-67.

(91) Vago, E. R.; Calvo, E. J.; Stratmann, M. *Electrochim. Acta* **1994**, *39*, 1655-1659.

CHAPTER 3

Electron Transfer of Peroxidase Assemblies at Tailored Nanocarbon Electrodes*

3.1 INTRODUCTION

Electrochemical biosensors frequently employ carbon-based indicator electrode materials because carbon electrodes promote facile electron transfer without inducing biomolecule denaturation at the electrode surface over time, in contrast to traditional metal electrodes (i.e., Pt, Au).[1] Several studies have demonstrated that the electrochemical response and electron transfer rates observed for proteins and enzymes can vary widely based on the carbon source (e.g., GC, HOPG), pretreatment or activation conditions and surface properties (chemical functionalities, defect sites, edge plane sites). In particular, it has been demonstrated that increasing the edge plane character within the graphitic lattice results in enhanced electron transfer of several heme proteins and enzymes, including cytochrome c and horseradish peroxidase (HRP).[2-4] It is believed that the improved electron transfer reactivity results from increased biomolecule adsorption at edge plane sites, and that the presence of functional groups (e.g., carboxylic groups) assists in promoting favorable carbon–enzyme interactions.[5-7] As such, many researchers have attempted to optimize biomolecule adsorption and electron transfer characteristics at carbon electrodes by using physical, chemical, and electrochemical means for surface modification specifically to increase the number of edge plane sites and surface functional groups. For example, glassy carbon electrodes may be roughened with abrasives (e.g., sandpaper) to enhance surface area and number of defect sites[8] or

* Portions of this chapter were accepted for publication by *Electrochimica Acta*.

electrochemically pretreated by cycling to oxidative potentials in order to create both oxygen-containing surface functionalities and improve the edge plane character.[9] Alternatively, enzyme linkage to carbon materials may be promoted through chemical coupling at the electrode surface using small linker molecules, such as carbodiimides.[10-13] A major drawback to such mechanical, chemical, and electrochemical "surface activation" processes is that only limited control may be exerted over the degree of edge plane character or specific composition of functionalities introduced at the carbon electrode surface. These methods also dramatically change other properties such as surface cleanliness, electrical conductivity, and mechanical stability. Therefore, reproducibility between experiments is poor, and many oxygen-containing functionalities that exhibit their own unique redox chemistries, such as quinones and lactones, may be present on the electrode surface, interfering with analyte detection and possibly leading to misinterpretation of mechanistic steps.[9]

Recent studies have touted carbon nanotubes (CNTs) as a promising alternative to the traditional carbon electrodes used in biosensing schemes because they feature enhanced electrical conductivity, chemical inertness, and stability.[14-16] Notably, CNTs' inherent properties, including edge plane character, may be increased by direct adjustment of growth conditions using laser ablation, chemical vapor deposition (CVD), etc. rather than induced by post-synthetic activation steps.[17-19] We have previously described a floating catalyst CVD method that has enabled the selective and reproducible preparation of multiwalled carbon nanotubes (CNTs). In particular, controlled heteroatom doping of CNTs with nitrogen provides a means for tuning the degree of edge plane character in CNTs in addition to other properties.[20] Previous studies from our group have thoroughly explored the influence of nitrogen doping on the electrocatalytic activity at N-doped CNTs (referred to herein as N-CNTs) when used as both an electrode material and

as a catalyst support for noble metal nanoparticles.[20-24] Several other reports in this area have investigated enzyme- and protein-functionalized CNT electrodes.[10-13, 25-30] In an effort to gain deeper insight into the mechanisms that define the electron transfer reactivity and catalytic function of redox enzymes at CNT electrodes, this chapter extends our studies to understand the influence of nitrogen doping of CNTs on the adsorption of HRP and subsequent HRP electrochemical activity. In particular, this chapter attempts to correlate trends of nitrogen content and edge plane character with HRP redox activity at tailored (nondoped and N-doped) CNTs.

HRP, an Fe heme enzyme, is one of the most widely employed enzymes in electrochemical sensing schemes because of its role in oxidase-coupled substrate detection: HRP reduces H_2O_2 that is stoichiometrically produced as a byproduct of oxidase–substrate interactions, permitting quantitative substrate detection through HRP-mediated redox processes. Many examples of HRP-modified carbon electrodes are available in the literature;[2, 31-35] more specifically, HRP has been immobilized at CNTs in previous electrochemical studies, allowing us to compare the efficiency of our immobilization strategy to others reported in the literature.[10-13, 29] In our study, HRP has been adsorbed at both nondoped and N-CNTs containing 5 at% N to evaluate HRP enzymatic activity upon immobilization. Both optical and electrochemical assays are used to assess HRP catalytic activity, and these studies along with other complementary surface characterization data allow for correlation of structure–property relationships. Spectrophotometric enzymatic assays suggest that HRP adsorption is indeed increased at N-CNTs relative to nondoped CNTs. However, cyclic voltammetry studies indicate that a greater percentage of adsorbed HRP is electroactive at nondoped CNTs than at N-CNTs, revealing that the carbon–enzyme interactions and coordination environments differ between the two types of CNTs. When these composites are utilized as peroxide

biosensors, the response of HRP as measured by rotating disk amperometry in the presence of 10–100 μM H_2O_2 is more sensitive at CNTs than at bare GC, though the reaction pathway governing the reduction of the activated enzyme to native HRP appears to involve chemical reduction by a second H_2O_2 molecule, rather than direct electrochemical reduction.

3.2 EXPERIMENTAL

3.2.1 CNT Synthesis

CNTs (both nondoped and 5 at% N-doped) were prepared via a floating catalyst CVD process using a ferrocene growth catalyst and xylene (or pyridine) carbon (and nitrogen) source as previously described in Chapter 2.2.[20] Again, 1.0 mL of a 20 mg/mL ferrocene–xylene (for nondoped CNTs) or ferrocene–pyridine (for N-CNTs) mixture was injected at 0.1 mL/min into a dual-zone quartz tube furnace. The mixture was volatilized at 150 °C in the first zone and then carried downstream to the second zone by carrier gases (Ar–H_2 or Ar–NH_3 for nondoped and N-CNTs, respectively) at a total flow rate of 575 sccm.[20] Upon reaching the second zone, the mixture was pyrolyzed at 700 °C or 800 °C, respectively, resulting in the base-catalyzed growth of multi-walled CNTs from Fe nanoparticle nucleation sites. The CNTs were deposited along the walls of the quartz tube and were collected after cooling the tube to room temperature under Ar. The nominal lengths and diameters of the as-prepared CNTs are 10 μm and 20–40 nm, respectively.[23] CNTs were stored in airtight vials prior to enzyme immobilization.

3.2.2 HRP Immobilization

Horseradish peroxidase (HRP; EC 1.11.1.7, MW ~44 kDa, 1280 ABTS U/mg solid, where 1 U = 1 μmol 2,2'-azino-bis(3-ethylbenzothiazoline-6-sulfonic acid) (ABTS) oxidized per min at pH 6.0 at 25 °C) was purchased from Sigma (Product #P-6782). To

prepare stock solutions of HRP, a solution of 0.1 M Na_2HPO_4 (phosphate, Fisher Scientific) was adjusted to pH 6.00 ± 0.03 using 0.1 M o-phosphoric acid. Stock solutions of 1000 U/mL HRP were prepared and diluted with the phosphate solution as necessary. These solutions were stored at 4 °C when not in use and maintained consistent enzymatic activity for 3 weeks, as determined via UV-Vis spectrophotometric assay of enzyme activity (Sigma Quality Control Test Procedure for Product #P-6782; this procedure is available via the Sigma website at www.sigma.com). For direct immobilization of HRP at CNTs, 1.0 mg of either nondoped or N-CNTs was suspended in 1.00 mL of phosphate solution containing 150, 250, 375, 650 or 1000 U/mL HRP. The solutions were briefly sonicated to disperse the CNTs and then stirred with magnetic stirbars at 4 °C for 24 h. Following this period, the HRP-loaded CNTs (HRP/CNT or HRP/N-CNT for nondoped and N-CNTs, respectively) were collected via vacuum filtration and washed three times with 2.00 mL aliquots of phosphate solution. The HRP/CNT or HRP/N-CNT composites were redispersed in 0.1 M phosphate solution at a final concentration of ~2 mg/mL and stored in airtight vials at 4 °C for further use. The filtrate was also collected and used to determine unbound HRP activity for HRP adsorption isotherms (vida infra).

3.2.3 Spectrophotometric Activity Assays

The enzymatic activity of HRP immobilized at both types of CNTs was determined using a UV-Vis spectrophotometric assay based on the oxidation of ABTS (see Sigma Quality Control Test listed above in the HRP Immobilization section) with minor modifications. A cuvette containing 2.90 mL of 9.1 mM ABTS (Sigma) in 0.1 M phosphate solution, pH 6.00 ± 0.03, and 1-5 μL of ~2 mg/mL HRP/CNT or HRP/N-CNT was placed in the beam path of an Agilent Instruments 8453 UV-Visible spectrometer with a photodiode array detector. The solution in the cuvette was stirred constantly throughout the assay using magnetic stirring, and the temperature was maintained at 25

°C using an isothermal bath (Fisher Scientific Isotemp 9100). The absorption maximum at 420 nm, A_{420}, was monitored until stable (~10 s), and then 100 μL of freshly prepared 0.3 wt% H_2O_2 (diluted from 30 wt% H_2O_2 in ultrapure water, Fisher Scientific) was added to the cuvette. The increase in A_{420} due to HRP-induced oxidation of ABTS was recorded for 2 min following the addition of H_2O_2 and used to determine HRP enzymatic activity in ABTS units (U/mg, using the mass of HRP/CNTs introduced into the assay). An ABTS extinction coefficient of 31.1 mM^{-1} cm^{-1} was used in the calculations.[34] The enzymatic activity of HRP filtrates collected from HRP immobilization at CNTs was conducted using the same protocol except that 50 μL of HRP filtrate, diluted with phosphate solution to ~0.5 U/mL HRP based on the original concentration of HRP used in the immobilization solution, was used rather than HRP/CNTs or HRP/N-CNTs.

For determination of HRP activity at CNTs supported on GC electrodes, HRP/CNTs or HRP/N-CNTs were drop-cast onto a 0.3 cm diameter GC electrode prepared in-house from a GC rod (GC-20, Tokai Carbon) insulated with Shell® EPON 825 resin cured with *m*-phenylenediamine (Aldrich).[36] Before each experiment, the GC electrode was polished successively with 0.3 and 0.05 μm alumina slurries on microcloth (Buehler) to a mirror finish and sonicated in ultrapure H_2O (>18.2 MΩ/cm) for 15 min. For adherence of HRP/CNT and HRP/N-CNT solutions to the GC surface, a 5 wt% Nafion® persulfonated ion exchange polymer solution (Sigma-Aldrich, Inc.) was modified with tetrabutylammonium bromide (referred to herein as TBABr-Nafion®) using Minteer's method.[37, 38] The TBABr-Nafion® solution was diluted to 0.075 wt% using absolute ethanol and vortexed in a 1:2 (v/v) ratio with nondoped HRP/CNTs or HRP/N-CNTs immediately prior to drop casting. The GC electrode was then mounted securely in an inverted position, and 3 μL of this mixture was carefully pipetted onto the GC surface. The assembly was covered to prevent contamination and allowed to dry (~1

h). Upon drying, the HRP/CNT- or HRP/N-CNT-modified GC electrodes were immediately immersed into a cuvette containing 2.90 mL ABTS solution for use in assays, being careful to keep the electrode out of the beam path. H_2O_2 was added as described above, and again A_{420} was monitored for 2 min following H_2O_2 addition. The HRP/CNT assemblies appeared to be strongly adherent to the GC surface, as no CNTs dislodged upon immersion. Data analysis was performed using Origin 7.0 software. All enzymatic electroactivity is reported in ABTS units (U) as described above.

3.2.4 Electrochemical Analysis

For electrochemical analysis, HRP/CNTs or HRP/N-CNTs were drop-cast in 5 μL aliquots onto a 0.5 cm diameter GC electrode (PINE Instruments AFE2M050GC) using the same TBABr-Nafion® solution and polishing and drying procedures described above. For control studies, a 1000 U/mL HRP stock solution was diluted 2:1 (v/v) with 0.075 wt% TBABr-Nafion® and drop-cast in 5 μL aliquots onto the GC surface. In addition to the GC working electrode, a Au wire counter electrode and Hg/Hg_2SO_4 (sat'd. K_2SO_4) reference electrode (CH Instruments, E° = +0.64 V vs. NHE) were used in all electrochemical measurements. All electrode potentials are reported vs. Hg/Hg_2SO_4. Electrochemical measurements were performed at room temperature (23 ± 2 °C) using an Autolab™ PGSTAT30 potentiostat interfaced with Autolab™ GPES version 4.9 software. Electrodes were contained within a 125-mL volume, 5-neck glass cell containing 100 mL of 0.1 M Na_2HPO_4 at pH 6.00 ± 0.03. Experiments were conducted under flowing Ar at all times.

To determine electroactive surface coverages of HRP, a U/mol conversion factor was created by dividing the enzymatic activity of a HRP stock solution by its molar concentration as determined from the HRP Soret band absorbance (ε_{402} = 100 mM^{-1} cm^{-1} [39]). The number of moles of HRP determined from CV analysis was then converted to

ABTS units using the conversion factor and normalized to the electroactive surface area. Electroactive surface areas were determined from chronocoulometric analysis of nondoped and N-CNTs (without HRP) adsorbed at GC in 1.02 mM ruthenium hexaaminechloride in 90 mM Na_2HPO_4, pH 7.4 (D_o = 5.3x10^{-6} cm^2 s^{-1} [40]), using a potential step from open circuit (~0 V vs. Hg/Hg_2SO_4) to -1 V.

For rotating disk (RDE) amperometry experiments, a PINE Instruments AFMSRX analytical rotator was used at a rotation rate (ω) of 1000 rpm. For H_2O_2 calibration curves, solutions of H_2O_2 prepared with ultrapure H_2O (18.2 mΩ cm) were injected into the cell in 30 s intervals using an automated syringe pump (New Era, Inc.).

3.3 RESULTS AND DISCUSSION

The HRP catalytic cycle can be expressed using the following three reactions:[35, 41, 42]

$$HRP(Fe^{3+}) + H_2O_2 \rightarrow E1(Fe^{4+}=O, P^{\bullet+}) + H_2O \quad (1)$$

$$E1(Fe^{4+}=O, P^{\bullet+}) + AH_2 \rightarrow E2(Fe^{4+}=O) + HA\cdot \quad (2)$$

$$E2(Fe^{4+}=O) + AH_2 \rightarrow HRP(Fe^{3+}) + HA\cdot + H_2O \quad (3)$$

In the above reactions, "HRP(Fe^{3+})" refers to the native or resting enzyme and "E1" refers to an oxidized form of HRP (Compound I) consisting of an oxyferryl Fe (Fe^{4+}=O) and porphyrin π cation radical ($P^{\bullet+}$).[43] E1, which is produced through reduction of H_2O_2 to H_2O (Reaction 1), is reduced to native HRP by an electron donor substrate, denoted AH_2 in the above reactions. In the first electron transfer step (Reaction 2), AH_2 reduces $P^{\bullet+}$, producing E2 (Compound II), which still contains Fe^{4+}=O. E2 is then reduced to native HRP through a second reduction step (Reaction 3), in which AH_2 converts Fe^{4+}=O to Fe^{3+}, thus regenerating the native enzyme (H_2O is formed from the

ferryl oxygen atom). Though the above reactions have been written in the most simplified manner possible, it should be noted that Reactions 2 and 3 also involve proton transfer from AH_2 to E1 and E2.[35, 41, 42] Additionally, the reduction of E1 to native HRP may be achieved in a single, two-electron transfer step if a two-electron donor (e.g., iodide) is present.[43]

While the catalytic cycle depicted in Reactions 1-3 cannot be transduced directly at an electrode surface, HRP activity may be observed electrochemically through direct electrochemical reduction of E1 to native HRP following Reaction 1:

$$E1(Fe^{4+}=O, P^{\bullet+}) + 2H^+ + 2e^- \rightarrow HRP(Fe^{3+}) + H_2O \quad (4)$$

The onset of this reduction should occur near +0.220 V vs. Hg/Hg_2SO_4,[2, 35] but many electrochemical schemes that involve the detection of HRP immobilized at electrode surfaces report an electrocatalytic potential significantly more negative, between -0.140 and -0.500 V vs. Hg/Hg_2SO_4.[31, 34] Such potentials are nearer to that of the HRP $Fe^{2+/3+}$ redox couple in the absence of H_2O_2:

$$HRP(Fe^{3+}) + e^- + H^+ \rightarrow HRP(Fe^{2+}) \quad (5)$$

This reversible one-electron, one-proton process has been reported to occur between -0.580 and -0.795 V vs. Hg/Hg_2SO_4 at pH 6-7 using HRP immobilized in organic films at GC electrodes[44] and in lipid films[33] and polyion films[32] immobilized at pyrolytic graphite (PG) electrodes, as well as HRP at CNTs.[10-12, 29] Furthermore, it has been noted that in the presence of excess H_2O_2, E1 may be reduced to native HRP by another H_2O_2 molecule, rather than by direct electrochemical reduction:[32, 33]

$$E1(Fe^{4+}=O, P^{\bullet+}) + H_2O_2 \rightarrow HRP(Fe^{3+}) + O_2 + H_2O \quad (6)$$

The chemical and electrochemical processes described by Reactions 1-6 are presented in Figure 3.1, which depicts HRP molecules adsorbed at a CNT-modified GC electrode. We employ such an electrode assembly in the present studies to determine HRP enzymatic activity upon immobilization at both nondoped CNTs and N-CNTs.

3.3.1 Spectrophotometric Activity Assays

Following adsorption of HRP at CNTs and filtration of the HRP/CNT composites (see Experimental section), the enzymatic activity of both types of composites was determined spectrophotometrically using an ABTS optical assay. In this assay, ABTS acts as the electron donor substrate (denoted as AH_2 in Reactions 2 and 3), becoming oxidized in the presence of both HRP and H_2O_2. The oxidized form of ABTS exhibits an absorption maximum at 420 nm in our system, which may be monitored as a function of time after H_2O_2 addition to determine the activity of adsorbed HRP in U/mg. The activity of unbound HRP (i.e., the HRP in the filtrate) was also assessed in U/mL using the ABTS assay. By plotting the determined activities of the HRP/CNT composites against the HRP activity in each filtrate, we are able to construct HRP adsorption isotherms for our CNTs, as shown in Figure 3.2. For both nondoped CNTs and N-CNTs, the sum of the adsorbed and unbound HRP (in U) at each concentration approximately equals the amount of HRP originally introduced in the CNT suspensions, indicating that HRP was not denatured in solution after stirring for 24 h with CNTs, nor was HRP substantially denatured upon adsorption to the CNTs. The data plotted in Figure 3.2 were fitted to a Langmuir-type adsorption isotherm, and the resulting adsorption maxima (Γ_m, in U/mg) and equilibrium dissociation constants (K_d, in mL/U) are also reported in Figure 3.2.[45, 46] The maximum HRP adsorption at N-CNTs (75 ± 4 U/mg) is nearly twice that at nondoped CNTs (33 ± 5

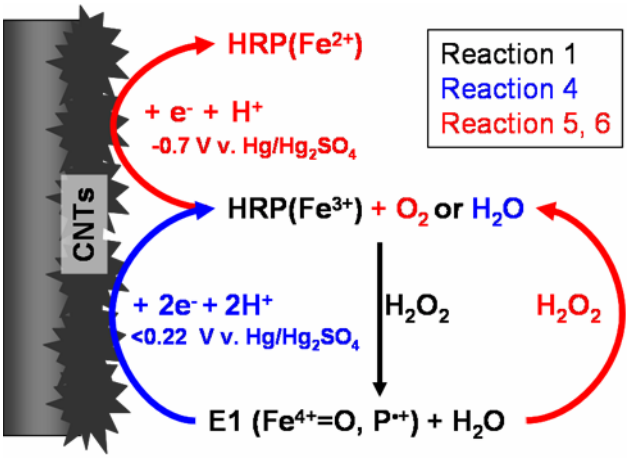

Figure 3.1. Possible HRP electron transfer pathways in the presence of H_2O_2 at a CNT-modified GC electrode. The colored arrows correspond to the numbered reactions detailed in the text.

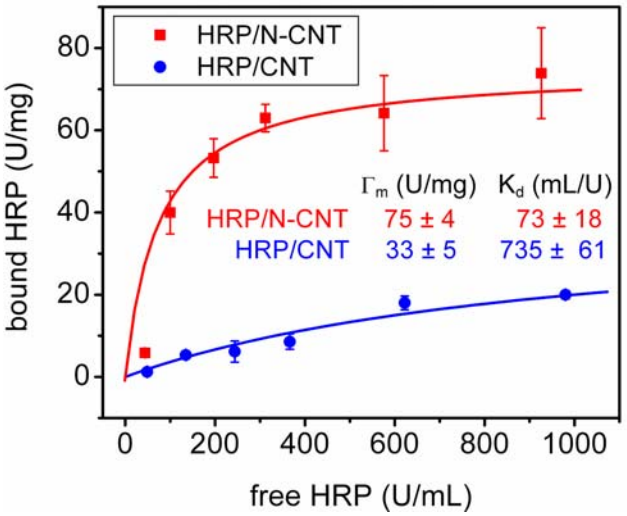

Figure 3.2. HRP adsorption isotherms at non-doped (blue) and N-CNTs (red), as determined using spectrophotometric enzymatic activity assays.

U/mg), while the dissociation constant at nondoped CNTs is an order of magnitude greater than that at N-CNTs. We have observed similar adsorption trends when investigating noble metal nanocatalyst adsorption at our CNTs.[24] Our previous studies have determined that the N-CNTs prepared for this study contain approximately three times the amount of edge plane sites per unit crystallite size as nondoped CNTs. [20] These observations suggest that the amount of HRP adsorbed at our CNTs is proportional to the degree of edge plane character or number of edge plane sites present in the CNTs, in agreement with previous findings in the literature.[2, 5-8]

We note that, as a result of the CVD growth process, our nondoped and N-CNTs contain 7 ± 1 (1σ) and 12 ± 1 (1σ) wt. % Fe, respectively, as discussed in Chapter 2.3.2 and determined previously using thermogravimetric (TGA) analysis.[20,23] This residual Fe is present as <100 nm sized particles, consisting of both Fe^0 and mixed Fe oxides, occluded by several graphene layers.[20, 47] Though we have previously shown both in the literature and in Chapter 2.3.2 that this residual Fe is not responsible for the electrocatalytic activity observed at our CNTs,[47] a recent report has demonstrated peroxidase mimetic activity at Fe_3O_4 nanoparticles.[48] Therefore, control assays were conducted in which nondoped and N-CNTs without adsorbed HRP were mixed with H_2O_2 and ABTS. ABTS was not oxidized as evidenced by the lack of an increased absorbance at 420 nm for these assays (data not shown), indicating that the CNTs themselves do not contribute to the observed optical activity of HRP/CNT composites.

To assess the long-term stability of both types of HRP/CNT composites, ABTS assays were performed periodically for 21–30 d, with the composites being refrigerated in airtight vials when not in use. The calculated HRP activity from these periodic assays is shown in Figure 3.3, with t = 0 being defined as the day during which the HRP/CNT composites were filtered. As seen in the figure, both HRP/CNTs and HRP/N-CNTs retain

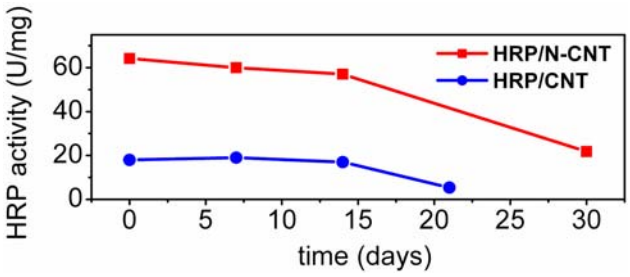

Figure 3.3. Enzymatic activity of HRP adsorbed to non-doped and N-CNTs as a function of time following the initial 24 h adsorption period.

>90% of their original activity for a period of 14 d, followed by a substantial dropoff in activity. Therefore, HRP/CNT composites were used for optical assays and electrochemical analyses within 14 d of their assembly and filtration.

The HRP/CNT composites used to generate the data shown in Figures 3.2 and 3.3 were freely suspended in solution (herein referred to as "soluble") during the ABTS assays. However, in order to determine HRP electroactivity in these composites, they must be immobilized at an electrode surface. While our CNTs are hydrophobic enough to remain adsorbed at a GC surface in aqueous supporting electrolyte,[47] the enzyme-loaded CNTs are sufficiently hydrophilic to desorb from the GC surface upon immersion in aqueous solution. Therefore, an immobilizing membrane is necessary to entrap the HRP/CNT composites at the GC surface. Previous reports by Minteer et al. have detailed a hydrophobic modification of Nafion® in which the membrane is mixture-cast with quaternary ammonium bromides to increase the size of its micellar pores. Enzymes immobilized in this TBABr-Nafion® exhibit increased activity relative to those immobilized in unmodified Nafion®, and improved electrochemical flux of redox couples through the modified membrane has been demonstrated.[37,38] For our experiments, TBABr-Nafion® was vortexed briefly with HRP/CNT composites and immediately drop cast at a GC electrode surface (see Experimental section). ABTS assays were performed on these GC electrodes to determine the extent of enzymatic activity for the immobilized composites, and these activities were compared to those obtained using soluble HRP/CNT composites. The activities (in total U per assay) were calculated using varying amounts of HRP/CNT composites and plotted as a function of HRP/CNT mass (in mg). The slope obtained from such a plot is equivalent to the enzymatic activity in U/mg. Figure 3.4 compares the activity of soluble, nondoped HRP/CNT to HRP/CNT immobilized at GC in TBABr-Nafion®. Upon immobilization, HRP/CNT retains 75% of

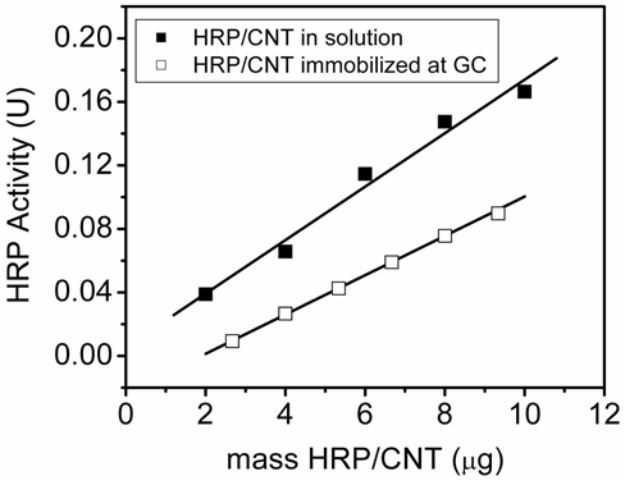

Figure 3.4. Enzymatic activity of HRP/CNT when dispersed in ABTS-phosphate solution (solid squares) and immobilized at GC with TBABr-Nafion® (open squares).

the enzymatic activity measured from soluble composites, with activities of 16 ± 1 and 12 ± 1 U/mg measured for soluble and immobilized HRP/CNT, respectively. The results obtained using HRP/N-CNT are similar (data not shown), with activities of 63 ± 7 and 46 ± 5 U/mg for soluble and immobilized HRP/N-CNT, respectively. The enzymatic activities determined for immobilized HRP/CNT composites are used in comparing electroactive and optically active HRP surface coverages (vida infra).

3.3.2 Electrochemical Analysis

To determine the electroactivity of HRP/CNT composites, the composites were immobilized in TBABr-Nafion® at GC electrodes as described in Section 3.2. Additionally, control experiments were conducted in which HRP (without CNTs) was drop cast with TBABr-Nafion® at the GC surface. Figure 3.5 shows CVs collected at 0.1 V/s for a) immobilized HRP without CNTs, b) HRP/CNT and c) HRP/N-CNT. The amount of HRP in optically active ABTS units immobilized at each GC electrode is 3.00, 0.07 and 0.20 U for the HRP control, HRP/CNT and HRP/N-CNT, respectively. We note that the 3.00 U of HRP immobilized at GC in the control is substantially higher than the amount of HRP immobilized with either nondoped or N-CNTs; this control study corresponds to the minimum amount of HRP (in the absence of CNTs) necessary to observe a detectable amperometric response to H_2O_2 injections. The dashed lines in Figure 4a-c correspond to CVs obtained in the absence of H_2O_2, and the solid lines correspond to CVs obtained upon addition of 100 μM H_2O_2 to the electrochemical cell. The background charging (capacitive) currents of both HRP/CNT composites are significantly higher than that of the control, and the HRP/N-CNT capacitance exceeds the HRP/CNT capacitance by a factor of ~3. The increased background current at HRP/N-CNTs reflects the increased edge plane character in N-CNTs, which is due to

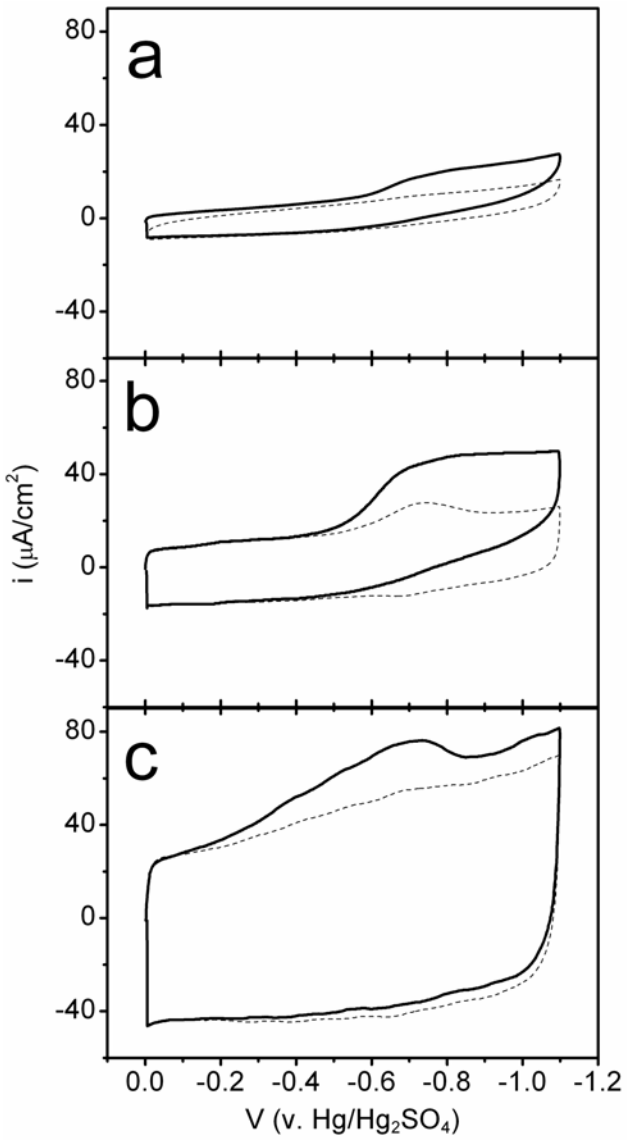

Figure 3.5. Performance of TBABr-Nafion® suspensions drop-cast at GC in the absence (dashed lines) and presence (solid lines) of 100 μM H_2O_2: (a) HRP only; (b) HRP/CNT; (c) HRP/N-CNT. Experimental conditions: 0.1 V/s scan rate, 0.1 M Na_2HPO_4, pH 6.00 ± 0.03 supporting electrolyte.

turbostratic disorder induced by the incorporation of nitrogen into the graphene lattice,[20, 22] i.e., it is not reflective of increased HRP adsorption.

The native HRP $Fe^{2+/3+}$ redox couple (Reaction 5) is observed most notably in the dashed CV of Figure 3.5b, and to a lesser extent in Figure 3.5c. The $Fe^{2+/3+}$ couple is not readily observed in Figure 3.5a, most likely because the directly adsorbed HRP is randomly oriented at GC and does not promote facile electron transfer, though some reports have demonstrated more distinct HRP redox activity upon direct adsorption at GC or graphite using similar quantities of HRP.[34, 44] By contrast, the $Fe^{2+/3+}$ couple is more apparent at the CNT-modified GC electrodes, even though these electrodes contain less than 10% of the amount of HRP used in the control study. The midpoint potential for $Fe^{2+/3+}$ is -0.712 V at HRP/CNT and -0.683 V at HRP/N-CNT. These values are similar to those previously reported for HRP immobilized at carbon and CNT electrodes.[10-12, 32, 33, 44] In order to determine the electroactive surface coverage of HRP in Figures 3.5b and c, the dashed CVs were background subtracted using CVs collected at CNTs without adsorbed HRP, and the areas beneath the cathodic peaks were integrated and converted to ABTS units as described in Section 3.2. The electroactive surface coverage of HRP is 2.5 ± 0.7 pmol/cm^2 for HRP/CNT and and 3.1 ± 0.9 pmol/cm^2 for HRP/N-CNT. For comparison, the surface coverage of HRP determined by optical ABTS assays is 2.3 ± 0.2 and 8.8 ± 0.9 pmol/cm^2 for HRP/CNT and HRP/N-CNT, respectively. Although HRP-N-CNT exhibits a nearly 300% higher HRP surface coverage obtained by spectroscopic means than HRP/CNT, only ~40% of the adsorbed HRP is electroactive, as opposed to HRP/CNT, at which nearly 100% of adsorbed HRP is electroactive. These results suggest that HRP orientation and carbon–enzyme interactions at the CNT surface differ between nondoped and N-CNTs, making electron transfer at HRP/N-CNT less facile than at HRP/CNT composites. A possible explanation for the difference in enzyme interactions

and orientation is that the nitrogen functionalities located at the edge planes in N-CNTs promote electrostatic binding of HRP through its exterior carbohydrate residues. HRP is a heavily glycosylated enzyme, with ~18% carbohydrate groups, and theoretical docking calculations have shown that electron transfer between HRP and a planar graphite surface can decrease by more than 10^{19} s^{-1} if the enzyme is adsorbed at the electrode surface through its carbohydrate moieties.[35] Furthermore, Gorton et al. have demonstrated that recombinant HRP, which does not contain carbohydrate groups, exhibits more facile direct electrochemistry at graphite than native HRP, presumably because the lack of glycosylation permits a greater number of enzymes to be properly oriented at the electrode surface for direct electron transfer.[35, 49] This sensitivity of HRP electron transfer to enzyme orientation at carbon surfaces could explain why a smaller relative percentage of HRP is electroactive at HRP/N-CNT than at HRP/CNT. Importantly, these results demonstrate that HRP redox activity is not controlled solely by the availability of edge plane sites, but that the chemical nature of these surface sites and carbon–enzyme interactions also influence the enzyme's electrochemical response.

The CVs denoted with solid lines in Figure 3.5a-c were obtained after the addition of 100 μM H_2O_2 to the electrochemical cell, as stated above. Again, the HRP control exhibits the smallest increase in current density upon exposure to H_2O_2. The HRP/CNT and HRP/N-CNT composites display a more pronounced Fe^{3+} reduction peak, while the Fe^{2+} oxidation peak disappears. Note that for both HRP/CNT and HRP/N-CNT, these catalytic peaks are not centered near the potential associated with Reaction 4, but are instead observed as a current increase near -0.7 V. Similar responses to H_2O_2 addition have been observed for HRP immobilized in lipids[33] and supported by polyion films[32] at PG, as well as HRP that has been chemically coupled to vertically aligned CNTs.[11, 12] However, catalytic currents positive of our observed response—beginning near +0.300 V

and reaching a maximum at -0.500 V—have been reported for HRP physisorbed at graphite electrodes.[8, 34] The fact that our HRP catalytic peak potentials are not shifted positive relative to the $Fe^{2+/3+}$ potentials indicates that the direct electrochemical reduction of E1 (Reaction 4, blue pathway in Figure 3.1) is not observed in our system. Instead, it is more likely that H_2O_2 reduces E1 to native HRP (Reaction 6), which then exhibits an increase in cathodic current density as Fe^{3+} is reduced to Fe^{2+} (Reaction 5). This two-step E1 reduction pathway is denoted in red in Figure 3.1.

To measure the amperometric response of our HRP/CNT composites to incremental H_2O_2 additions, we employed rotating disk (RDE) amperometry, since this method has been shown to provide better sensitivity and lower H_2O_2 detection limits than CV when used to measure HRP enzymatic activity.[11-13, 32, 33] RDE was performed at various applied potentials, and it was determined that a potential of -0.6 V, which is ~100 mV positive of the $Fe^{2+/3+}$ redox couple, demonstrated the best sensitivity toward H_2O_2 for both HRP/CNT and HRP/N-CNT composites. Rusling et al. have also demonstrated that RDE potentials near the onset of HRP Fe^{3+} reduction provide the most sensitive amperometric response to H_2O_2.[32] The amperometric response of HRP/CNT and HRP/N-CNT composites, as well as the HRP control, to 10 μM additions of H_2O_2 up to 100 μM are shown in Figure 3.6. Again, HRP shows a much more pronounced response to H_2O_2 when immobilized at CNTs rather than being directly adsorbed to GC. The amperometric response at 100 μM H_2O_2 is nearly eight times greater at HRP/CNT than at the HRP control. The response at 100 μM H_2O_2 using HRP/N-CNT is two orders of magnitude greater than that observed for HRP/CNT, even though the electroactive surface coverage of HRP appears to be equivalent for both types of HRP/CNT composites. Amperometric sensitivities normalized to electroactive surface areas were determined for the linear ranges of each of the plots in Figure 3.6, and they are 0.008 ± 0.001 A/M·cm^2 for the

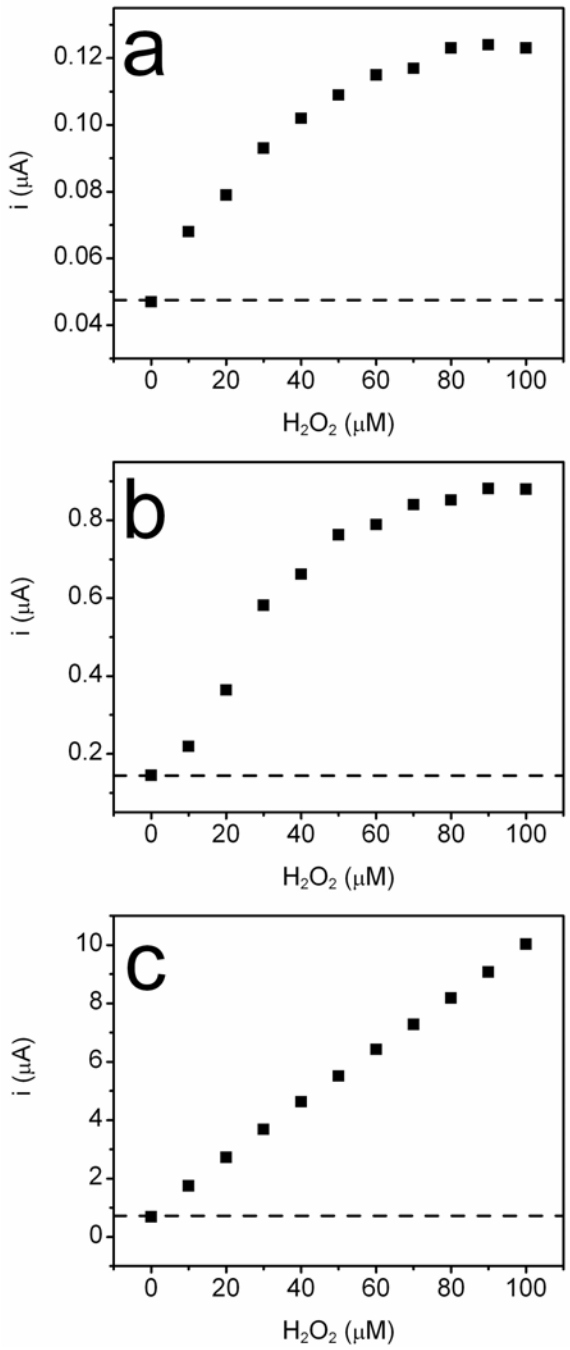

Figure 3.6. Rotating disk amperometric response at -0.6 V and 1000 rpm under saturated Ar to H_2O_2 injections at (a) HRP-GC (b) HRP/CNT-GC and (c) HRP/N-CNT-GC electrodes. Experimental conditions are the same as in Figure 3.5. Note that the current scales differ in a-c.

HRP control, 0.065 ± 0.005 A/M·cm^2 for HRP/CNT and 0.163 ± 0.002 A/M·cm^2 for HRP/N-CNT. Compared to the reported sensitivities of some other HRP-modified carbon electrodes, the sensitivity of the HRP control is poor, but those of both types of HRP/CNT composites are typical,[12, 31] and in some cases better than reported sensitivities of HRP-modified CNT electrodes.[11] Note that the blank signals, marked with dashed lines in Figures 3.5a-c, vary substantially between electrode assemblies. By dividing $3\sigma_b$ by the amperometric sensitivity, where σ_b is the standard deviation of the blank signal (i.e., $[H_2O_2] = 0$), the limits of detection are 8, 5 and 1 μM for the HRP control, HRP/CNT and HRP/N-CNT, respectively. Differences in the amperometric sensitivities and electroactive surface areas of each electrode assembly contribute to the observed differences in these (non-normalized) detection limits. The detection limits for both types of HRP/CNT composites are similar to those reported for other HRP-modified CNTs.[11, 12] Finally, we note that the amperometric response of HRP/N-CNTs to H_2O_2 displays a much larger linear range than that of HRP/CNT. We believe this enhanced response is reflective of the N-CNTs' ability to decompose H_2O_2 to O_2, which is then catalytically reduced at the N-CNTs.[23] We are currently investigating the use of these N-CNTs in other oxidase-coupled biosensing schemes.

3.4 CONCLUSIONS

In this chapter, we have demonstrated that nitrogen doping of carbon nanotubes effects the loading density and subsequent redox activity of an adsorbed heme enzyme, HRP. While the loading density of HRP at N-doped CNTs is nearly twice that of nondoped CNTs, a greater percentage of adsorbed HRP exhibits $Fe^{2+/3+}$ redox activity at nondoped CNTs. These results emphasize the importance of HRP coordination environment and orientation at the electrode surface for efficient electron transfer, and suggest that not only surface site availability, but also the nature of given surface sites,

influences the resulting redox activity of the adsorbed enzyme. Nevertheless, HRP/N-CNT composites are more sensitive to the addition of H_2O_2 than HRP/CNT, though we believe this result is partially due to the previously demonstrated ability of our N-CNTs to catalytically decompose H_2O_2 as discussed in further detail in the next chapter.

3.5 REFERENCES

(1) Katz, E.; Shipway, A. N.; Willner, I. In *Electron Transfer in Chemistry*; Balzani, V., Ed.; Wiley-VCH: New York, 2001, pp 127-201.

(2) Ferapontova, E. E. *Electroanalysis* **2004**, *16*, 1101-1112.

(3) Frew, J. E.; Hill, H. A. O. *Eur. J. Biochem.* **1988**, *172*, 261-269.

(4) Csoeregi, E.; Joensson-Pettersson, G.; Gorton, L. *J. Biotech.* **1993**, *30*, 315-337.

(5) Blanford, C. F.; Armstrong, F. A. *J. Solid State Electrochem.* **2006**, *10*, 826-832.

(6) Heng, L. Y.; Chou, A.; Yu, J.; Chen, Y.; Gooding, J. J. *Electrochem. Comm.* **2005**, *7*, 1457-1462.

(7) Kurusu, F.; Tsunoda, H.; Saito, A.; Tomita, A.; Kadota, A.; Kayahara, N.; Karube, I.; Gotoh, M. *Analyst* **2006**, *131*, 1292-1298.

(8) Ferapontova, E.; Puganova, E. *J. Electroanal. Chem.* **2002**, *518*, 20-26.

(9) McCreery, R. L. In *Electroanalytical Chemistry*; Bard, A. J., Ed.; Marcel Dekker, Inc.: New York; Vol. 17, pp 221-292.

(10) Yin, Y.; Lu, Y.; Wu, P.; Cai, C. *Sensors* **2005**, *5*, 220-234.

(11) Yu, X.; Chattopadhyay, D.; Galeska, I.; Papadimitrakopoulos, F.; Rusling, J. F. *Electrochem. Comm.* **2003**, *5*, 408-411.

(12) Yu, X.; Kim, S. N.; Papadimitrakopoulos, F.; Rusling, J. F. *Mol. BioSys.* **2005**, *1*, 70-78.

(13) Yu, X.; Munge, B.; Patel, V.; Jensen, G.; Bhirde, A.; Gong, J. D.; Kim, S. N.; Gillespie, J.; Gutkind, J. S.; Papadimitrakopoulos, F.; Rusling, J. F. *J. Am. Chem. Soc.* **2006**, *128*, 11199-11205.

(14) Gooding, J. J. *Electrochim. Acta* **2005**, *50*, 3049-3060.

(15) Merkoci, A.; Pumera, M.; Llopis, X.; Perez, B.; del Valle, M.; Alegret, S. *Trends Anal. Chem.* **2005**, *24*, 826-838.

(16) Musameh, M.; Wang, J.; Merkoci, A.; Lin, Y. *Electrochem. Comm.* **2002**, *4*, 743-746.

(17) Kim, N. S.; Lee, Y. T.; Park, J.; Han, J. B.; Choi, Y. S.; Choi, S. Y.; Choo, J.; Lee, G. H. *J. Phys. Chem. B* **2003**, *107*, 9249-9255.

(18) Rao, C. N. R.; Govindaraj, A. *Acc. Chem. Res.* **2002**, *35*, 998-1007.

(19) Wang, X.; Hu, W.; Liu, Y. Q.; Long, C.; Xu, Y.; Zhou, S.; Zhu, D.; Dai, L. *Carbon* **2001**, *39*, 1533-1536.

(20) Maldonado, S.; Morin, S.; Stevenson, K. J. *Carbon* **2006**, *44*, 1429-1437.

(21) Maldonado, S.; Morin, S.; Stevenson, K. J. *Analyst* **2006**, *131*, 262-267.

(22) Maldonado, S.; Stevenson, K. J. *J. Phys. Chem. B* **2004**, *108*, 11375-11383.

(23) Maldonado, S.; Stevenson, K. J. *J. Phys. Chem. B* **2005**, *109*, 4707-4716.

(24) Vijayaraghavan, G.; Stevenson, K. J. *Langmuir* **2007**, *23*, 5279-5282.

(25) Baker, S. E.; Colavita, P. E.; Tse, K.-Y.; Hamers, R. J. *Chem. Mater.* **2006**, *18*, 4415-4422.

(26) Guiseppi-Elie, A.; Lei, C.; Baughman, R. H. *Nanotechnology* **2002**, *13*, 559-564.

(27) O'Connor, M.; Kim Sang, N.; Killard Anthony, J.; Forster Robert, J.; Smyth Malcolm, R.; Papadimitrakopoulos, F.; Rusling James, F. *Analyst* **2004**, *129*, 1176-1180.

(28) Jia, N.; Wang, L.; Liu, L.; Zhou, Q.; Jiang, Z. *Electrochem. Comm.* **2005**, *7*, 349-354.

(29) Zeng, Y.-L.; Huang, Y.-F.; Jiang, J.-H.; Zhang, X.-B.; Tang, C.-R.; Shen, G.-L.; Yu, R.-Q. *Electrochem. Comm.* **2006**, *9*, 185-190.

(30) Azamian, B. R.; Davis, J. J.; Coleman, K. S.; Bagshaw, C. B.; Green, M. L. H. *J. Am. Chem. Soc.* **2002**, *124*, 12664-12665.

(31) Ruzgas, T.; Csoeregi, E.; Emmneus, J.; Gorton, L.; Marko-Varga, G. *Anal. Chim. Acta* **1996**, *330*, 123-138.

(32) Yu, X.; Sotzing, G. A.; Papadimitrakopoulos, F.; Rusling, J. F. *Anal. Chem.* **2003**, *75*, 4565-4571.

(33) Zhang, Z.; Chouchane, S.; Magliozzo, R. S.; Rusling, J. F. *Anal. Chem.* **2002**, *74*, 163-170.

(34) Brusova, Z.; Ferapontova, E. E.; Sakharov, I. Y.; Magner, E.; Gorton, L. *Electroanalysis* **2005**, *17*, 460-468.

(35) Ruzgas, T.; Lindgren, A.; Gorton, L.; Hecht, H.-J.; Reichelt, J.; Bilitewski, U. In *Electroanalytical Methods for Biological Materials*; Brajter-Toth, A., Chambers, J. Q., Eds.; Marcel Dekker, Inc.: New York, 2002, pp 233-254.

(36) Groat, K. A.; Creager, S. E. *Langmuir* **1993**, *9*, 3668-3675.

(37) Klotzbach, T.; Watt, M.; Ansari, Y.; Minteer, S. D. *J. Membr. Sci.* **2006**, *282*, 276-283.

(38) Thomas, T. J.; Ponnusamy, K. E.; Chang, N. M.; Galmore, K.; Minteer, S. D. *J. Membr. Sci.* **2003**, *213*, 55-66.

(39) Delincee, H.; Radola, B. J. *Eur. J. Biochem.* **1975**, *52*, 321-330.

(40) Wightman, R. M.; Wipf, D. O. In *Electroanalytical Chemistry*; Bard, A. J., Ed.; Marcel Dekker: New York, 1989; Vol. 15, pp 343.

(41) Dunford, H. B. In *Peroxidases in Chemistry and Biology*; Everse, J., Everse, K. E., Grisham, M. B., Eds.; CRC Press: Boca Raton, FL, 1991; Vol. 2, pp 5-7.

(42) Dunford, H. B. *Heme Peroxidases*; Wiley-VCH: New York, 1999, pp 9-12.

(43) Dunford, H. B. *Heme Peroxidases*; Wiley-VCH: New York, 1999, pp 63-67.

(44) Guo, Y.; Guadalupe, A. R. *Chem. Comm.* **1997**, 1437-1438.

(45) Lozzi, I.; Calamai, L.; Fusi, P.; Bosetto, M.; Stotzky, G. *Soil Bio. Biochem.* **2001**, *33*, 1021-1028.

(46) Miranda, M. V.; Magri, M. L.; Cabrera, R. B.; Fernandez Lahore, H. M.; Cascone, O. *Lat. Am. App. Res.* **2003**, *33*, 67-71.

(47) Lyon, J. L.; Stevenson, K. J. *Langmuir* **2007**, *23*, 11311-11318.

(48) Gao, L.; Zhuang, J.; Nie, L.; Zhang, J.; Zhang, Y.; Gu, N.; Wang, T.; Feng, J.; Yang, D.; Perrett, S.; Yan, X. *Nature Nanotech.* **2007**, *2*, 577-583.

(49) Lindgren, A.; Tanaka, M.; Ruzgas, T.; Gorton, L.; Gazaryan, I.; Ishimori, K.; Morishima, I. *Electrochem. Comm.* **1999**, *1*, 171-175.

CHAPTER 4

Peroxidase Mimetic Activity at Tailored Nanocarbon Electrodes

4.1. INTRODUCTION

Carbon nanotubes are often modified with enzymes for use in electrochemical enzymatic sensing schemes.[1-15] For many oxidase–substrate interactions, these schemes must be bi-enzymatic, because the cofactors of many oxidases are not able to participate in direct electron transfer with an electrode surface.[16] Therefore, a second, redox-active enzyme must be employed to mediate detection of oxidase–substrate interactions. For example, glucose oxidase (GOx) and horseradish peroxidase (HRP) have been covalently linked to CNTs through poly(amidoamine) dendrimers,[13] permitting the detection of glucose through HRP-mediated H_2O_2 consumption, as detailed in Chapter 3. Additionally, small redox molecules such as ferrocenes have been used to mediate glucose and glutamate detection.[4, 17] Alternatively, the "peroxidase mimetic" activity of microperoxidases and Fe protoporphyrin IX in electrode assemblies has been reported.[18, 19] These "miniature versions" of HRP, which are capable of reducing H_2O_2 to H_2O through the 2-electron, Fe-mediated process outlined in Chapter 3, may exchange electrons more efficiently than HRP in electrochemical biosensing schemes due to the lack of protein residues surrounding their active sites. Most recently, peroxidase mimetic activity has been reported for Fe_3O_4 nanoparticles,[20] and non-heme Fe^{3+} macrocycles were shown by computational calculation to decompose H_2O_2 through formation of an E1 complex similar to that discussed in Chapter 3,[21] though neither of these moieties were implemented in any electrochemical detection schemes.

"Reagentless" CNT-based biosensors—that is, sensing assemblies that rely on intrinsic CNT reactivity rather than a separate redox mediator for analyte detection—may also provide an alternative to traditional bi-enzymatic sensing schemes. Some reports claim that GOx direct electron transfer may be attained at CNTs,[1, 6] but most rely on the CNTs' electrocatalytic activity toward either substrates or H_2O_2 generated from oxidase–substrate interactions for detection.[5, 22] However, the redox responses obtained at these CNTs are characteristically sluggish, require large overpotentials (-0.5 to -0.9 V vs. Hg/Hg_2SO_4),[5, 6] and in some cases use extreme pH conditions[22] in order to detect substrates. By contrast, previous studies in our own laboratories have demonstrated an inherent reactivity toward H_2O_2 at our nitrogen-doped carbon nanotubes (N-CNTs) in neutral pH, aqueous supporting electrolytes at open circuit (~0 V v. Hg/Hg_2SO_4).[23]

In this chapter, we evaluate the inherent peroxidase mimetic activity of our N-CNTs for the development of a nonmediated, amperometric glucose sensing scheme. We briefly discuss differences between N-CNTs' and nondoped CNTs' reactivity toward H_2O_2, and compare the behavior of N-CNT-modified GC electrodes to previously described HRP-modified graphite electrodes through Koutecky–Levich analysis of H_2O_2 consumption. We then utilize N-CNTs in lieu of HRP in a traditional bi-enzymatic sensing scheme for glucose detection to demonstrate the N-CNTs' ability to supplant peroxidase components for low-overpotential, oxidase-coupled electrochemical sensing. Importantly, we note that though we refer to our N-CNT assembly as a peroxidase mimetic both in the title and discussion of this chapter, the assembly does not truly "mimic" the HRP-catalyzed H_2O_2 reduction pathway, i.e. H_2O_2 is not reduced to H_2O through a 2-electron transfer from the N-CNTs as discussed in detail vida infra.

4.2 EXPERIMENTAL

4.2.1 CNT Synthesis

CNTs (both nondoped and 5 and 7.5 at% N-doped) were prepared via a floating catalyst CVD process using a ferrocene growth catalyst and xylene (or pyridine) carbon (and nitrogen) source as previously described in Chapter 2. Again, 1.0 mL of a 20 mg/mL ferrocene–xylene (for nondoped CNTs) or ferrocene–pyridine (for N-CNTs) mixture was injected at 0.1 mL/min into a dual-zone quartz tube furnace. The mixture was volatilized at 150 °C in the first zone and then carried downstream to the second zone by carrier gases (Ar–H_2 or Ar–NH_3 for nondoped and N-CNTs, respectively) at a total flow rate of 575 sccm.[24] Upon reaching the second zone, the mixture was pyrolyzed at 700 °C or 800 °C, respectively, resulting in the base-catalyzed growth of multi-walled CNTs from Fe nanoparticle nucleation sites. The CNTs were deposited along the walls of the quartz tube and were collected after cooling the tube to room temperature under Ar. The nominal lengths and diameters of the as-prepared CNTs are 10 μm and 20–40 nm, respectively.[23] CNTs were stored in airtight vials prior to enzyme immobilization.

4.2.2 Electrochemical Analysis

For oxygen reduction reaction (ORR) analysis, CNTs were drop-cast from absolute ethanol at a concentration of ~2 mg/mL onto a 0.5-cm diameter glassy carbon (GC) electrode (PINE Instruments AFE2M050GC) in the absence of any immobilizing films, as described in Chapter 2. Before each experiment, the GC was polished successively with 0.3 and 0.05 μm almunia slurries on microcloth (Buehler) to a mirror finish and sonicated in ultrapure H_2O (>18.2 MΩ cm) for 15 minutes. For H_2O_2 detection experiments, CNTs were immobilized at the GC surface using a 5 wt % Nafion® persulfonated ion exchange polymer solution in aliphatic alcohols (Sigma-Aldrich) that

was modified with tetrabutylammonium bromide to form a TBABr-Nafion® membrane as described previously by Minteer et al.[25, 26] The TBABr-Nafion® solution was diluted to 0.075 wt% in absolute ethanol, and CNTs were suspended in this solution at a concentration of ~2 mg/mL and drop-cast at the GC surface as described in Chapter 3.

For glucose determination using co-immobilized glucose oxidase (GOx; Sigma, 106,000 U/g), 10 mg GOx was added to 200 μL of 7.5 at% N-CNTs (2 mg/mL) in 0.075 wt% TBABr-Nafion® and vortexed for 10 s before drop-casting 5 μL of the mixture onto the GC surface. GC surfaces were covered to prevent contamination and allowed to dry for about 10 minutes. Upon drying, the N-CNT and N-CNT/GOx composite-modified GC electrodes were used immediately in electrochemical experiments.

In addition to the GC working electrode, a Au wire counter electrode and Hg/Hg_2SO_4 (sat'd. K_2SO_4) reference electrode (CH Instruments, $E° = +0.64$ V vs. NHE) were used in all electrochemical measurements. All electrode potentials are reported vs. Hg/Hg_2SO_4. Electrochemical measurements were performed at room temperature (23 ± 2 °C) using an Autolab™ PGSTAT30 potentiostat interfaced with Autolab™ GPES version 4.9 software. All reported amperometric sensitivities are normalized to the electroactive surface area of the CNT-modified working electrode, as determined using the chronocoulometry method described in Chapter 3. Electrodes were contained within a 125-mL volume, 5-neck glass cell containing 100 mL of 0.1 M Na_2HPO_4 at pH 6.00 ± 0.03. Prior to collecting analytical data, CNT-modified GC assemblies were cycled at least 50 times between 0 and -1.2 V in supporting electrolyte to passivate residual Fe growth catalysts in the CNTs (see Chapter 2). Experiments were conducted under saturated O_2 conditions by flowing O_2 through the cell at all times. For rotating disk (RDE) amperometry experiments, a PINE Instruments AFMSRX analytical rotator was used at rotation rates (ω) between 1000 and 3200 rpm as noted in Section 4.3.

Solutions of H_2O_2 (Fisher) and D-glucose (Sigma-Aldrich) were injected into the cell in 30 second intervals using an automated syringe pump (New Era, Inc.). Solutions of both analytes, KNO_3 and Na_2HPO_4 supporting electrolyte were prepared with ultrapure (>18.2 MΩ cm) water. Solutions of 0.1 M Na_2HPO_4 were adjusted to pH 6.00 ± 0.03 using 0.1 M *o*-phosphoric acid (Fisher), and 1 M phosphate solutions (pH 6.40 ± 0.03) were similarly adjusted using 1 M *o*-phosphoric acid. Solutions of 1 M KNO_3 exhibited a pH of 6.40 ± 0.03 without any adjustment.

4.3 RESULTS AND DISCUSSION

4.3.1 CNT ORR Potentials as a Function of Supporting Electrolyte

Previous reports from our group have studied mechanistic differences in oxygen reduction between nondoped and N-CNTs. These studies showed that the oxygen reduction reaction (ORR), an overall 4-electron process, proceeds through two 2-electron transfer steps at both types of CNTs, with hydrogen peroxide formed as an intermediate species in the first step:[23]

$$O_2 + 2H^+ + 2e^- \rightarrow H_2O_2 \quad (1)$$

At nondoped CNTs, this reaction is followed by a second 2-electron reduction of H_2O_2 to H_2O:

$$H_2O_2 + 2H^+ + 2e^- \rightarrow 2H_2O \quad (2)$$

However, at N-CNTs, H_2O_2 is rapidly decomposed to regenerate O_2 and produce H_2O:

$$2H_2O_2 \rightarrow O_2 + 2H_2O \quad (3)$$

The catalytic decomposition of H_2O_2 occurs more than 1000 times faster at N-CNTs than at nondoped CNTs, as previously determined using gasometric analysis.[23] This catalytic behavior toward H_2O_2 contributes to an observed positive potential shift for the ORR at N-CNTs relative to nondoped CNTs, as we have documented in previous reports.[23, 27] Figure 4.1 shows representative cyclic voltammograms (CVs) of nondoped, 5 at% and 7.5 at% N-CNTs drop-cast at a GC electrode (without any supporting binder, such as Nafion®) in 1 M solutions of KNO_3 (black lines) and 1 M Na_2HPO_4 (phosphate, blue lines), both at pH 6.40 ± 0.03. Table 4.1 reports the ORR peak potentials extracted from the CVs in Figure 4.1. Note that the ORR process at nondoped CNTs (Figure 4.1a) shows two clearly resolved cathodic peaks, which are reflective of Reactions 1 and 2 mentioned above, while both types of N-CNTs exhibit only one cathodic peak. The shapes of the CVs in Figure 4.1 agree with our previously reported results in pH ~6.4 KNO_3,[23, 27] and the ORR potentials reported in Table 4.1 for nondoped CNTs correspond to the more positive of the two peaks for each nondoped CNT CV (i.e., the peak corresponding to Reaction 1). Remarkably, the ORR peak potential observed at both types of N-CNTs in phosphate (Figure 4.1b and c) is shifted dramatically positive relative to the ORR peak potentials observed for the same N-CNTs in KNO_3. For example, the ORR peak potential at 5 at% N-CNTs in Figure 4.1 is -0.277 V, a 208 mV positive shift relative to the ORR peak potential at the same N-CNTs in KNO_3. Similarly, the ORR peak potential at 7.5 at% N-CNTs in phosphate exhibits a 213 mV positive shift relative that seen in KNO_3. By contrast, the ORR peak potential at nondoped CNTs occurs at -0.831 V in Figure 4.1, which is 88 mV *negative* of the nondoped CNT ORR potential in KNO_3. At this point in time, it is speculative to explain why the observed positive ORR

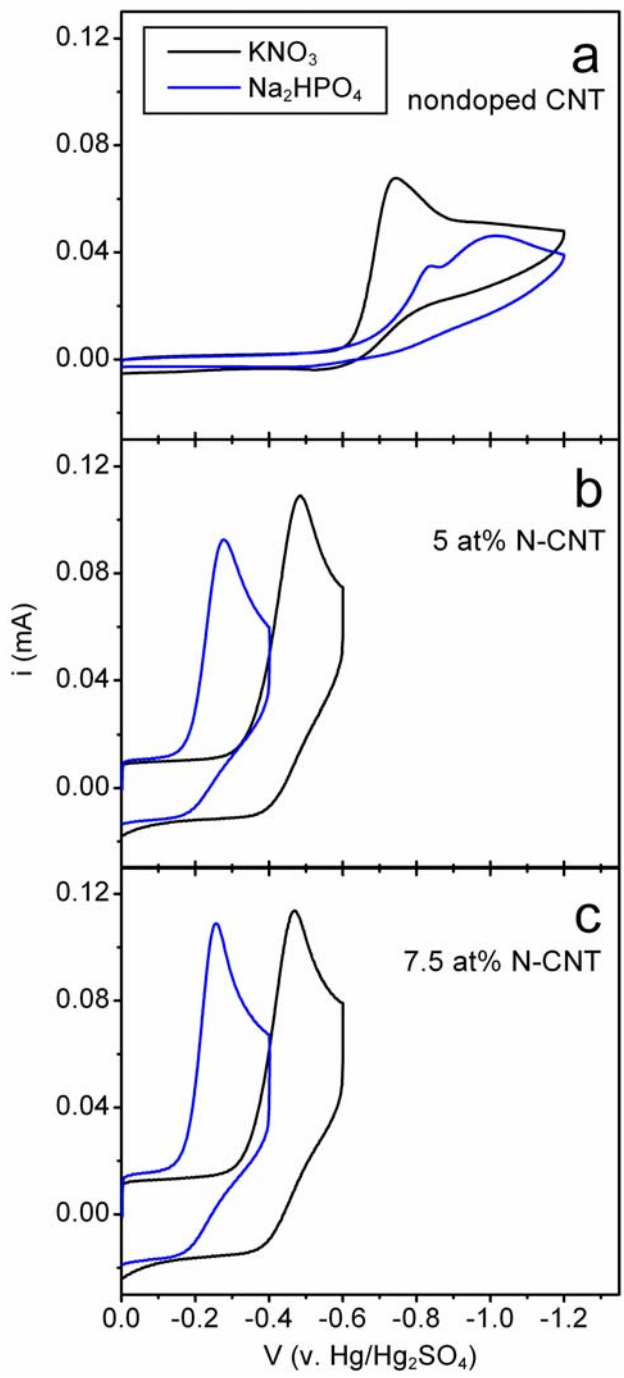

Figure 4.1. ORR response of (a) nondoped, (b) 5 and (c) 7.5 at% N-CNTs drop-cast at a GC electrode without any immobilizing binder, as measured by CV in KNO_3 (black lines) or Na_2HPO_4 (blue lines). Both supporting electrolytes were pH 6.40 ± 0.03, 1 M. Scan rate: 20 mV/s.

Table 4.1. ORR peak potentials for the CVs shown in Figure 4.1.

	ORR Peak Potential (V v. Hg/Hg_2SO_4)	
Sample	**1 M KNO_3**	**1 M Na_2HPO_4**
(a) nondoped CNT	-0.743	-0.831
(b) 5 at% N-CNT	-0.485	-0.277
(c) 7.5 at% N-CNT	-0.469	-0.256

potential shift between the two supporting electrolytes occurs selectively at N-CNTs, but we believe that the observed behavior is a result of double layer effects and interactions between oxygen species (e.g. adsorbed O_2, superoxide) and the N-CNTs' nitrogen functionalities, and we are currently conducting studies to investigate this hypothesis. Nevertheless, we have exploited the low-overpotential oxygen reduction/H_2O_2 decomposition at our N-CNTs to develop the biogenic, H_2O_2-based sensing strategy detailed below.

4.3.2 H_2O_2 Detection at N-CNTs Using RDE Amperometry

Figure 4.2 shows a schematic of the RDE amperometry experimental setup used to obtain amperometric response curves for successive additions of H_2O_2 to an O_2-saturated supporting electrolyte solution of 0.1 M phosphate, pH 6.00 ± 0.03. As H_2O_2 is injected into the supporting electrolyte solution via the syringe pump, the amperometric response generated at the N-CNT-modified GC (or CNT-modified GC, for control studies) working electrode is recorded. By rotating the working electrode, hydrodynamic transport occurs to facilitate faster mass transport of reactants in order to permit the fastest response time possible. In order to secure the CNTs at the GC surface while using such fast rotation rates (>1000 rpm), the CNTs in this configuration are immobilized within a 0.075 wt% TBABr-Nafion® membrane film, as described in Chapter 3. The experimental conditions detailed here were chosen with the foresight of introducing biological substrates and enzymes into this configuration after conducting the control experiments shown in Figure 4.3.

Figure 4.3a shows ORR CVs collected for nondoped, 5 and 7.5 at% N-CNTs in 0.1 M phosphate. Note that the ORR potentials observed here are within 10 mV of those reported in Table 4.1 using 1 M phosphate, indicating that the changing ionic strength of the supporting electrolyte and the incorporation of the TBABr-Nafion® film have not

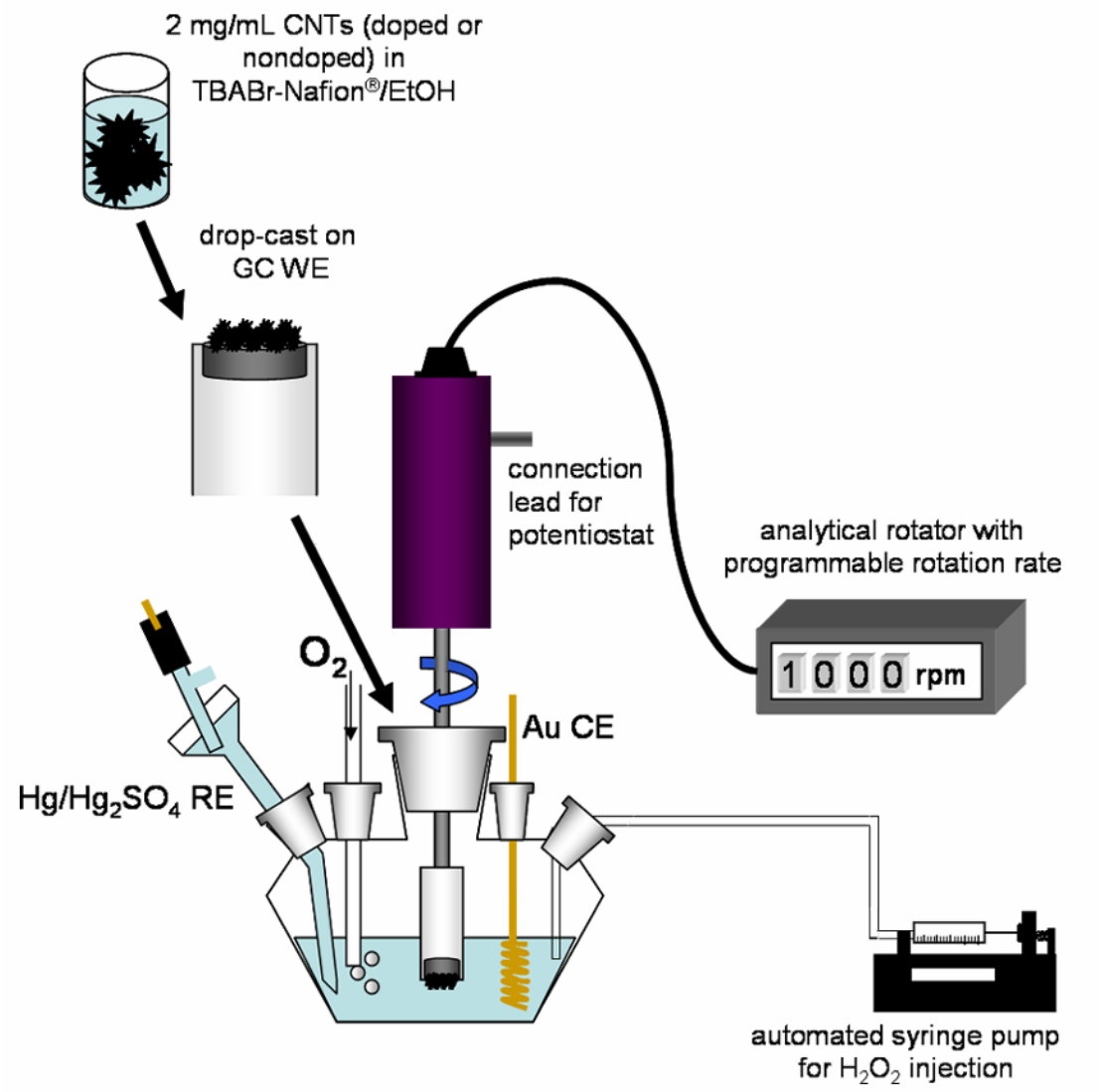

Figure 4.2. Schematic of RDE configuration used for amperometric H_2O_2 detection. WE, RE, and CE are abbreviations for working electrode, reference electrode, and counter electrode, respectively.

altered the CNTs' activity toward O_2 reduction. Since the observed ORR peak potential at N-CNTs reflects both O_2 reduction and H_2O_2 decomposition (Reactions 1 and 3, respectively), we detected the addition of H_2O_2 to the supporting electrolyte solution by monitoring the working electrode current at a fixed potential slightly positive of the ORR potential for each type of CNT.

The same CNTs used in Figure 4.3a were used to detect H_2O_2 via RDE amperometry, as shown in Figure 4.3b. The dashed lines along the y-axis in Figure 4.3a denote the potentials at which the CNT-modified GC electrode was poised during RDE amperometry experiments, as it was determined that these potentials (-0.18, -0.21, and -1.00 V for 7.5 at% N-CNTs, 5 at% N-CNTs, and nondoped CNTs, respectively) gave the most sensitive response to the addition of 25–500 μM H_2O_2 in 25 μM intervals. Though it may seem as though the most sensitive response should occur at the apex of the ORR peak, previous H_2O_2-based RDE amperometry studies using enzyme-modified electrodes have reported optimal H_2O_2 detection at potentials near the onset of the enzyme's redox peak, as well.[12, 28] As evident in Figure 4.3b, the sensitivity to H_2O_2 additions increases with increasing nitrogen content in the nanotubes. While nondoped CNTs exhibit no measurable response to H_2O_2 addition, the 5 and 7.5 at% N-CNTs exhibit amperometric sensitivities of 0.48 ± 0.02 and 0.26 ± 0.01 A/M*cm^2, respectively. The linear ranges of the N-CNT-modified GC assemblies' response to H_2O_2 ($R^2 > 0.999$) are denoted by the lines through the data points in Figure 4.3b. Both types of N-CNTs exhibit a linear range of 25–275 μM H_2O_2. The response of the N-CNT-modified GC electrodes to H_2O_2 was rapid, with an amperometric response occurring <1 s following H_2O_2 injection.

As mentioned in Section 4.1, several research groups have reported "peroxidase mimetic" activity of several Fe-based species.[18-20, 29] Fe in these species reduces H_2O_2 to

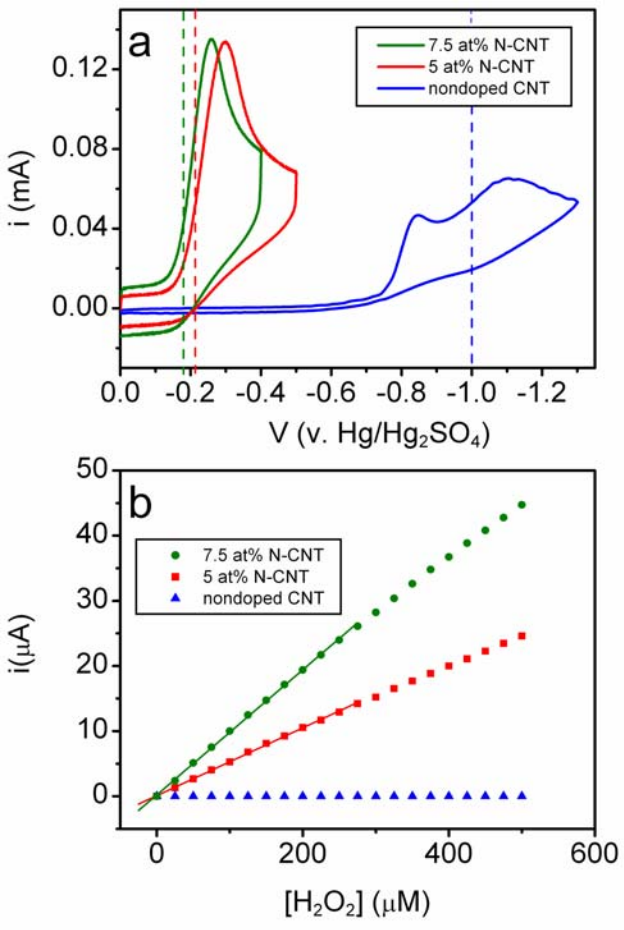

Figure 4.3. ORR response of nondoped, 5 and 7.5 at% N-CNTs immobilized at a GC electrode using TBABr-Nafion®, as measured by CV. Supporting electrolytes: 0.1 M Na_2HPO_4, pH 6.00 ± 0.03. Scan rate: 100 mV/s. Dashed lines indicate potentials used to monitor response to H_2O_2 in (b). (b) Background-subtracted response to H_2O_2 at nondoped, 5 and 7.5 at% N-CNTs supported on a GC electrode in saturated O_2, as measured using RDE amperometry at 1000 rpm. The potentials used for monitoring H_2O_2 response are -1.0 V (nondoped CNTs), -0.21 V (5 at% N-CNTs), and -0.18 V (7.5 at% N-CNTs), as noted in (a). Supporting electrolyte is the same as in (a).

H_2O through a 2-electron pathway through an E1 complex similar to that formed during HRP-catalyzed H_2O_2 reduction. An exception is the Fe_3O_4 nanoparticle peroxidase mimetic,[20] in which no peripheral porphyrin-like structure is present, meaning that the oxyferryl porphyrin E1 complex cannot be formed. Nevertheless, spectrophotometric assays of H_2O_2 and typical HRP electron donors in the presence of these Fe_3O_4 particles indicate that H_2O_2 has been reduced to H_2O, suggesting that Fe_3O_4 reduces H_2O through a Fenton-like reaction mechanism, though no proof of this reaction pathway is given in the report. Obviously our N-CNTs do not contain porphyrin moieties, but they do contain residual mixed $Fe^{2+/3+}$ oxide nanoparticles, as demonstrated in Chapter 2. We previously demonstrated in Chapter 2 that this residual Fe contained in our N-CNTs does not contribute to the observed electrocatalytic activity toward ORR, but we conducted additional experiments here to confirm that the observed response to H_2O_2 is not Fe-based. These experiments were based on RDE studies conducted by Gorton et al., in which the enzymatic activity of HRP immobilized at graphite electrodes is studied by analysis of Koutecky–Levich (K–L) plots.[30, 31] More specifically, the rate of H_2O_2 consumption by HRP is determined by considering the overall observed current (I) at the RDE, which consists of both a mass-transport-limited component (I_L) and a reaction-rate-limited component (I_K):

$$1/I = 1/I_L + 1/I_K \quad (4)$$

The components I_L and I_K may be expressed mathematically as follows:

$$I_L = 0.62nFAD^{2/3}\omega^{1/2}\nu^{-1/6}c^* \quad (5)$$

$$1/I_K = (1/nFA\Gamma)(1/k_1c^*+1/k_s) \quad (6)$$

In these equations, c* is the bulk concentration of H_2O_2 in solution, n is the number of electrons transferred, F is Faraday's constant (96,485 C/mol), A is the geometric area of the electrode, D is the diffusion coefficient of H_2O_2 (1.6 x 10-5 cm2/s), *v* is the kinematic viscosity of water (0.01 cm^2/s),[32] Γ is the surface coverage of the catalytic species (such as HRP or Fe), k_1 is rate of reaction between H_2O_2 and the catalytic moiety (HRP or Fe), and k_s is the turnover number of electron transfer between the catalytic moiety and the electrode.

By varying the rotation rate of the RDE, the speed at which I_L no longer contributes to I, i.e., the speed at which the transport of H_2O_2 to the surface is fast enough to maintain an electrode surface H_2O_2 concentration equivalent to the bulk H_2O_2 concentration, may be determined. This condition is reflected by a plot of 1/I vs. $\omega^{-1/2}$ (known as a Koutecky–Levich coordinates) for varying concentrations of H_2O_2, showing H_2O_2 concentrations at which 1/I does not vary with ω. The K–L plots obtained at 5 at% N-CNTs for H_2O_2 concentrations between 25 and 400 μM and rotation rates between 1500 and 3200 rpm are shown in Figure 4.4a. At lower H_2O_2 concentrations, the observed current is clearly dependent on the rotation rate, indicating that both I_L and I_K are contributing to the observed current at these concentrations. At $[H_2O_2]$ = 400 μM, however, the observed current is now independent of rotation rate, indicating that this concentration of H_2O_2 meets the criteria described above to achieve a solely rate-limited observed current. For comparision, the same type of K–L plots obtained by Gorton et al. for HRP-mediated H_2O_2 consumption begin to exhibit rotation rate independence at H_2O_2 concentrations of only 15 μM.[30, 31] The fact that our N-CNT-modified GC assembly requires a much higher H_2O_2 concentration to reach rate-limiting current conditions suggests that the consumption of H_2O_2 at our assembly is much faster than the reduction of H_2O_2 at the HRP-modified graphite electrodes used by Gorton et al.

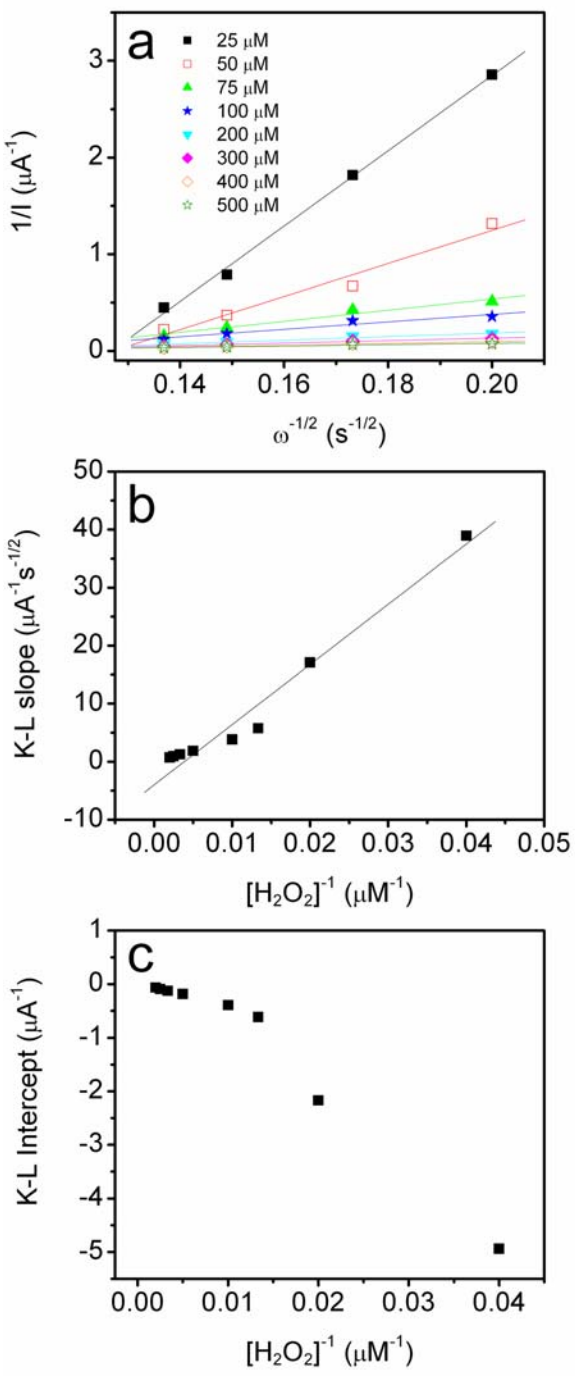

Figure 4.4. (a) Koutecky–Levich plots of H_2O_2 response at a 5 at% N-CNT-modified GC electrode assembly in O_2 saturated 0.1 M Na_2HPO_4, pH 6.00 ± 0.03. Applied potential: -0.2 V. (b) Dependence of the slopes obtained from (a) on H_2O_2 concentration. (c) Dependence of the intercepts obtained from (a) on H_2O_2 concentration.

From the K–L plot in Figure 4.4a, additional variables in Equations 5 and 6 including n and k_1 may be determined. The slopes obtained for each series of 1/I measurements collected at a given H_2O_2 concentration may be plotted as a function of $1/[H_2O_2]$, as shown in Figure 4.4b. According to Equation 5, the slope of such a plot is proportional to n, the number of electrons transferred during H_2O_2 consumption. For the HRP-catalyzed reduction of H_2O_2, Reaction 1 in Chapter 3.3, n = 2. Both the HRP-modified electrodes[30, 31] and the Fe-based peroxidase mimetics[20] mentioned above also report n = 2, i.e. H_2O_2 in these systems is reduced to H_2O by a Fe-mediated reaction. Therefore, a value of n = 2 for our system might suggest that H_2O_2 consumption follows a similar 2-electron pathway at our N-CNTs. However, the plot in Figure 4.3b does not display an obvious linear trend across all data points. The best-fit line through the entire data set gives a slope of n =1, while a fit through only the first six data points gives a slope of n = 0.4. These results indicate that the reaction between H_2O_2 and the N-CNT-modified electrode surface is not a conventional 2-electron reduction to H_2O, as would be expected for a Fe-mediated reaction.

The kinetically limited currents obtained from K–L plots may be analyzed to determine k_1 for HRP-catalyzed H_2O_2 reduction by plotting the intercepts of the K–L plots as a function of $1/[H_2O_2]$, as shown previously by Gorton et al.[30, 31] According to Equation 6, the slope of such a plot is proportional to k_1, the rate of reaction between H_2O_2 and HRP. We have constructed such a plot from the K–L data obtained at our N-CNT-modified electrodes in Figure 4.4c. This plot differs substantially from that shown by Gorton et al. for HRP-catalyzed H_2O_2 reduction at HRP-modified graphite. In the previously reported case, the intercepts are all positive numbers that increase with $1/[H_2O_2]$, resulting in a positive slope and thus a positive k_1 value. By contrast, our intercepts are all negative numbers that decrease with $1/[H_2O_2]$, resulting in a negative

(and nonsensical) k_1 value. These results indicate that our N-CNT assembly cannot be adequately described in terms of a HRP–H_2O_2 reaction scheme, and that H_2O_2 is consumed at our electrode assembly by a different mechanism than the 2-electron reduction to H_2O that is observed with HRP and other reported Fe-based peroxidase mimetics.

As additional evidence that our N-CNT-based H_2O_2 consumption mechanism differs substantially from $Fe^{2+/3+}$-based H_2O_2 reduction, it should be noted that the Fe_3O_4 "peroxidase mimetic" nanoparticles reported by Gao et al.[20] were studied through absorbance measurements of 3,3,5,5-tetramethylbenzidine (TMB), an electron donor substrate similar in its response to the HRP E1 complex as the ABTS substrate used in Chapter 3: both substrates exhibit a strong absorbance at visible wavelengths when oxidized by the HRP E1 complex. Gao's Fe_3O_4 nanoparticles did oxidize TMB upon the addition of H_2O_2, and the resulting double-reciprocal plots of absorbance v. TMB concentration produced "parallel line plots" indicative of the signature HRP "ping-pong" reaction mechanism,[33] meaning that the Fe_3O_4 nanoparticles bind and react with their first substrate (H_2O_2) before reacting with their second substrate (TMB). By contrast, we performed the ABTS assays described in Chapter 3 using our N-CNTs and found that ABTS was *not* oxidized by the N-CNTs upon the addition of H_2O_2 (see Chapter 3.3). These results suggest yet again that the H_2O_2 consumption at our N-CNTs is not Fe-mediated. Instead, we believe that H_2O_2 is decomposed to O_2 at the N-CNT surface, as described above in Reaction 3 and deduced from previous studies of our N-CNTs in the presence of H_2O_2. The O_2 thus generated at the N-CNT surface is then reduced to H_2O_2 through a 2-electron transfer from the N-CNTs (Reaction 1), resulting in the observed increase in amperometric signal at the N-CNT-modified GC electrode assembly.

4.3.3 Nonmediated Amperometric Glucose Detection at N-CNTs

Our N-CNTs' long-term stability (as demonstrated in Chapter 2), enzyme compatibility (as demonstrated in Chapter 3), and rapid, sensitive response to H_2O_2 (as demonstrated above) make them attractive composites for use in bi-enzymatic biogenic sensing schemes that typically employ peroxidases for H_2O_2-based signal transduction of oxidase-substrate interactions, as described in Chapter 3. Therefore, we constructed an electrode assembly in which 7.5 at% N-CNTs are used in lieu of HRP to detect glucose oxidation through H_2O_2 consumption in a GOx-coupled sensing scheme. This scheme is outlined in Figure 4.5, which depicts the GOx/N-CNT assembly at the GC surface. In this scheme, GOx is co-immobilized with N-CNTs at the GC surface by drop-casting a solution of both enzyme and N-CNTs in TBABr-Nafion® as described in Section 4.2. The GOx/N-CNT composite-modified GC electrode is then used in an RDE amperometry configuration similar to that shown in Figure 4.2, except that H_2O_2 is generated in the system through the oxidation of injected D-glucose by GOx at the electrode surface:

$$\text{GOx(FAD)} + \text{D-glucose} \rightarrow \text{gluconolactone} + \text{GOx(FADH}_2\text{)} \qquad (7)$$

$$\text{GOx(FADH}_2\text{)} + \text{O}_2 \rightarrow \text{GOx(FAD)} + \text{H}_2\text{O}_2 \qquad (8)$$

Here FAD and $FADH_2$ refer to the flavin adenine dinucleotide (FAD) cofactor of GOx, which is reduced upon oxidation of glucose (Equation 7) and then reoxidized by O_2, producing H_2O_2 (Equation 8), as represented schematically in Figure 4.5. Since H_2O_2 is produced in a 1:1 stoichiometric ratio with glucose consumption in this reaction, the measured amperometric signal from H_2O_2 consumption at the N-CNTs permits

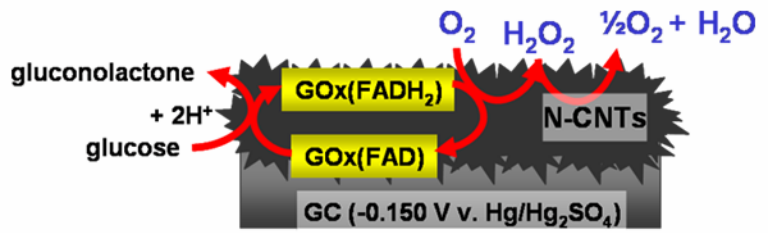

Figure 4.5. Schematic depicting the detection of H_2O_2 generated from GOx–glucose interaction at N-CNTs, resulting in glucose detection at N-CNTs. In this scheme, GOx and N-CNTs are co-immobilized at a GC electrode, and glucose is introduced into the supporting electrolyte. As GOx oxidizes glucose to gluconolactone, H_2O_2 is produced stoichiometrically. The N-CNTs then catalytically decompose this H_2O_2, leading to a local increase in O_2, which is catalytically reduced at the N-CNTs, resulting in a measurable amperometric signal at -0.15 V.

determination of the amount of glucose present in the system. Figure 4.6 shows the observed response to successive injections of D-glucose obtained at a GOx/N-CNT composite-modified GC electrode posied at -0.15 V in 0.1 M Na_2HPO_4, pH 6.00 ± 0.03. As a control study, a GC containing only GOx drop-cast in TBABr-Nafion® was also subjected to successive glucose injections, and these results are plotted in Figure 4.6 as well. The background current contributions (i.e., [glucose = 0 M]) have been subtracted from both curves. Figure 4.6 clearly shows that while only a minimal response to glucose was observed at the electrode assembly without N-CNTs, while the GOx/N-CNT assembly exhibits a linear response for 25–250 μM glucose. The amperometric sensitivity of the GOx/N-CNT assembly is 0.06 A/M*cm^2. This sensitivity surpasses that of mediated amperometric glucose detection methods reported in the literature, including GOx immobilized both in polyaniline-based redox hydrogel films (0.017 A/M*cm^2)[34] and ferrocene-containing polymer films (2 x 10^{-5} A/M vs. 0.03 A/M at our GOx/N-CNTs).[35] The limit of detection (LOD) as estimated from $3\sigma_b$, where σ_b is the standard deviation of the blank signal from 5 replicate measurements, is 3 μM glucose. Table 5.2 compares the analytical figures of merit obtained for our GOx/N-CNT glucose sensing system against other CNT-based amperometric glucose sensors reported in the literature. Though most of the other sensing schemes in Table 5.2 feature wider linear ranges than our sensing scheme, our scheme features a lower overpotential, lower or comparable LOD and better amperometric sensitivity than most of these reported methods. Furthermore, our detection limit and amperometric sensitivity could potentially be optimized, since dividing the amperometric sensitivity for glucose by the amperometric sensitivity of the 7.5 at% N-CNTs for H_2O_2 (listed above) gives a conversion efficiency of only 12%. Note also that while the glucose sensing strategy in Table 5.2 reported by Liu et al.[5] reports electrocatalytic activity of multi-walled CNTs (MWCNTs) toward

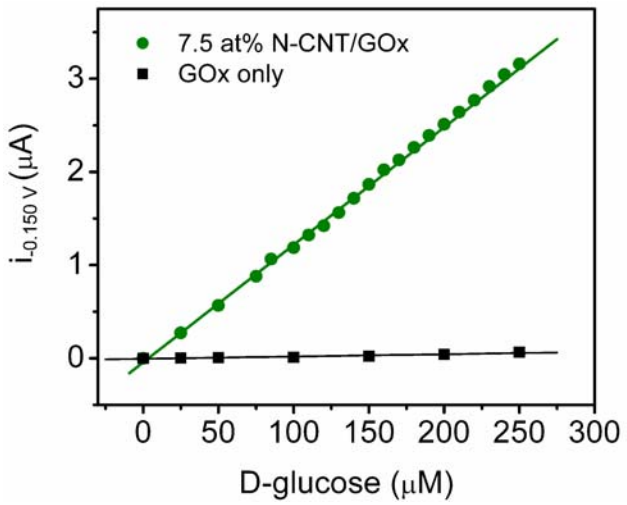

Figure 4.6. Background-subtracted response to D-glucose at 7.5 at% N-CNT/GOx composite supported on a GC electrode in saturated O_2, as measured by RDE amperometry at -0.15 V and 1000 rpm. Supporting electrolyte: 0.1 M Na_2HPO_4, pH 6.00 ± 0.03.

Table 4.2. Comparison of GOx/N-CNT electrochemical detection scheme figures of merit to those of other CNT-based amperometric glucose sensors.

CNT-based Glucose Sensing Scheme[a]	Mediator	Operating Potential (V)[b]	LOD (μM)	Linear Range (mM)	Sensitivity ($A/M*cm^2$)	Ref.
GOx/N-CNTs in TBABr-Nafion®	N-CNTs	-0.150	3	0.025 – 0.250	0.06	this work
GOx covalently linked to MWCNTs	Ferrocene monocarboxylic acid (FMCA) in solution	-0.040	30	0.5 – 40	0.0113	4
GOx/HRP linked through PAMAM dendrimers to MWCNT	HRP	-0.740	2.5	0.004 – 1.2	0.0022 A/M[c]	13
GOx/chitosan/Au NPs[d] cast on MWCNT-modified GC	none (measured via purported direct electron transfer of GOx)	-0.895	20	0.04 – 1.0	0.0024 A/M[c]	6
polyelectrolyte/ GOx/MWCNTs	MWCNTs	-0.540	7	0.015 – 6	not reported	5
irreversible glucose oxidation at MWCNTs, pH ~12	MWCNTs	-0.240	1	0.002 – 11	0.00436	22

[a]All of the assemblies reported here are supported on GC working electrodes.
[b]Potentials are reported v. Hg/Hg_2SO_4.
[c] Geometric areas of these electrode assemblies were not given in their references, but our non-normalized sensitivity of 0.03 A/M surpasses these reported sensitivities.
[d] "NPs" is an abbreviation for "nanoparticles."

enzymatically generated H_2O_2, the operating potential required to observe this response (-0.540 V) is much more negative that that needed to observe H_2O_2 decomposition (through increased O_2 reduction) at our N-CNTs. Our results demonstrate the utility of N-CNTs as a substitute for HRP in nonmediated, bi-enzymatic oxidase–substrate electrochemical detection strategies. We note that such an enzyme/N-CNT composite-modified electrode scheme can be extended to other oxidase–substrate systems, such as cholesterol oxidase–cholesterol. Future studies will investigate the sensing capabilities of N-CNTs using other oxidase–substrate systems.

4.4 CONCLUSIONS

In this chapter, we have demonstrated the intrinsic reactivity of N-CNTs toward H_2O_2 consumption. Analysis of N-CNT-modified GC electrodes in an RDE amperometry configuration indicates that the mechanism of H_2O_2 consumption is not a 2-electron reduction to H_2O, as is observed for HRP-catalyzed H_2O_2 reduction. This data also suggests that H_2O_2 consumption at N-CNTs does not involve reactive $Fe^{2+/3+}$ species, as recent studies citing Fe-based peroxidase mimetic activity report an HRP-like 2-electron reduction of H_2O_2, as well. Based on previous studies, we believe that the N-CNT reaction mechanism toward H_2O_2 occurs through the decomposition of H_2O_2 to O_2 and H_2O, resulting in an increase in current at the N-CNT electrode as the newly generated H_2O_2 is electrochemically reduced. We have exploited this intrinsic reactivity by incorporating N-CNTs as a substitute for HRP in a traditionally bi-enzymatic sensing scheme for the detection of glucose. Though the conversion efficiency between H_2O_2 and H_2O_2-mediated glucose detection at our N-CNT-based assembly is less than ideal, these studies serve as proof of concept for the use of N-CNTs as a peroxidase mimetic in unmediated biogenic analyte detection.

4.5 REFERENCES

(1) Guiseppi-Elie, A.; Lei, C.; Baughman, R. H. *Nanotechnology* **2002**, *13*, 559-564.

(2) Joshi, P. P.; Merchant, S. A.; Wang, Y.; Schmidtke, D. W. *Analytical Chemistry* **2005**, *77*, 3183-3188.

(3) Li, G.; Liao, J. M.; Hu, G. Q.; Ma, N. Z.; Wu, P. J. *Biosens. Bioelectr.* **2005**, *20*, 2140-2144.

(4) Li, J.; Wang, Y.-B.; Qiu, J.-D.; Sun, D.-c.; Xia, X.-H. *Anal. Bioanal. Chem.* **2005**, *383*, 918-922.

(5) Liu, G.; Lin, Y. *Electrochem. Comm.* **2006**, *8*, 251-256.

(6) Luo, X.; Killard, A. J.; Smyth, M. R. *Electroanalysis* **2006**, *18*, 1131-1134.

(7) Luong, J. H. T.; Hrapovic, S.; Wang, D. *Electroanalysis* **2005**, *17*, 47-53.

(8) Vamvakaki, V.; Tsagaraki, K.; Chaniotakis, N. *Analytical Chemistry* **2006**, *78*, 5538-5542.

(9) Wang, Y.; Joshi, P. P.; Hobbs, K. L.; Johnson, M. B.; Schmidtke, D. W. *Langmuir* **2006**, *22*, 9776-9783.

(10) Wen, D.; Liu, Y.; Yang, G.; Dong, S. *Electrochim. Acta* **2007**, *52*, 5312-5317.

(11) Yin, Y.; Lu, Y.; Wu, P.; Cai, C. *Sensors* **2005**, *5*, 220-234.

(12) Yu, X.; Munge, B.; Patel, V.; Jensen, G.; Bhirde, A.; Gong, J. D.; Kim, S. N.; Gillespie, J.; Gutkind, J. S.; Papadimitrakopoulos, F.; Rusling, J. F. *Journal of the American Chemical Society* **2006**, *128*, 11199-11205.

(13) Zeng, Y.-L.; Huang, Y.-F.; Jiang, J.-H.; Zhang, X.-B.; Tang, C.-R.; Shen, G.-L.; Yu, R.-Q. *Electrochemistry Communications* **2006**, *9*, 185-190.

(14) Zhao, G.-C.; Zhang, L.; Wei, X.-W. *Analytical Biochemistry* **2004**, *329*, 160-161.

(15) Ali, S. R.; Ma, Y.; Parajuli, R. R.; Balogun, Y.; Lai, W. Y. C.; He, H. *Anal. Chem.* **2007**, *79*, 2583-2587.

(16) Katz, E.; Shipway, A. N.; Willner, I. In *Electron Transfer in Chemistry*; Balzani, V., Ed.; Wiley-VCH: New York, 2001; Vol. 4, pp 127-201.

(17) Huang, X.-J.; Im, H.-S.; Lee, D.-H.; Kim, H.-S.; Choi, Y.-K. *J. Phys. Chem. C* **2007**, *111*, 1200-1206.

(18) Baldini, E.; Dall'Orto, V. C.; Danilowicz, C.; Rezzano, I.; Calvo, E. J. *Electroanalysis* **2002**, *14*, 1157-1164.

(19) Presnova, G.; Grigorenko, V.; Egorov, A.; Ruzgas, T.; Lindgren, A.; Gorton, L.; Borchers, T. *Farad. Discuss.* **2000**, *116*, 281-289.

(20) Gao, L.; Zhuang, J.; Nie, L.; Zhang, J.; Zhang, Y.; Gu, N.; Wang, T.; Feng, J.; Yang, D.; Perrett, S.; Yan, X. *Nature Nanotech.* **2007**, *2*, 577-583.

(21) Sicking, W.; Korth, H.-G.; Jansen, G.; de Groot, H.; Sustmann, R. *Chem. Eur. J.* **2007**, *13*, 4230-4245.

(22) Ye, J.-S.; Wen, Y.; Zhang, W. D.; Gan, L. M.; Xu, G. Q.; Sheu, F.-S. *Electrochem. Comm.* **2004**, *6*, 66-70.

(23) Maldonado, S.; Stevenson, K. J. *J. Phys. Chem. B* **2005**, *109*, 4707-4716.

(24) Maldonado, S.; Morin, S.; Stevenson, K. J. *Carbon* **2006**, *44*, 1429-1437.

(25) Thomas, T. J.; Ponnusamy, K. E.; Chang, N. M.; Galmore, K.; Minteer, S. D. *J. Membr. Sci.* **2003**, *213*, 55-66.

(26) Klotzbach, T.; Watt, M.; Ansari, Y.; Minteer, S. D. *J. Membr. Sci.* **2006**, *282*, 276-283.

(27) Maldonado, S.; Stevenson, K. J. *J. Phys. Chem. B* **2004**, *108*, 11375-11383.

(28) Yu, X.; Chattopadhyay, D.; Galeska, I.; Papadimitrakopoulos, F.; Rusling, J. F. *Electrochem. Comm.* **2003**, *5*, 408-411.

(29) Yang, H.-H.; Zhu, Q.-Z.; Chen, Q.-Y.; Xu, J.-G.; Li, D.-H. *Analyst* **2000**, *125*, 719-724.

(30) Lindgren, A.; Munteanu, F.-D.; Gazaryan, I. G.; Ruzgas, T.; Gorton, L. *J. Electroanal. Chem.* **1998**, *458*, 113-120.

(31) Ruzgas, T.; Gorton, L.; Emneus, J.; Marko-Varga, G. *J. Electroanal. Chem.* **1995**, *391*, 41-49.

(32) Bard, A. J.; Faulkner, L. R. In *Electrochemical Methods: Fundamentals and Applications,* 2nd ed.; John Wiley & Sons: New York, 2001, pp 334.

(33) Dunford, H. B. In *Heme Peroxidases*; Wiley-VCH: New York, 1999, pp 9-11.

(34) Mano, N.; Yoo, J. E.; Tarver, J.; Loo, Y.-L.; Heller, A. *J. Am. Chem. Soc.* **2007**, *129*, 7006-7007.

(35) Bean, L. S.; Heng, L. Y.; Yamin, B. M.; Ahmad, M. *Thin Solid Films* **2005**, *477*, 104-110.

CHAPTER 5

Future Directions*

5.1 INTRODUCTION

The CNT-based bioelectronic assemblies discussed in the previous chapters have some drawbacks. Most notably, the detection limits for H_2O_2 attained in Chapter 3 are poor compared to other reported electrochemical sensing schemes,[1-6] possibly because the HRP $Fe^{2+/3+}$ electron transfer is not as robust as that reported by other groups.[1, 4, 7, 8] Therefore, alternative strategies for creating enzyme/CNT assemblies should be explored in an effort to promote enzyme electron transfer at the GC surface. Specifically, many groups have reported the use of immobilizing films including the polyion layers,[4, 9] hydrogels,[7, 8] surfactant films,[9] and lipid bilayer membranes[10] described in Chapter 1 to promote enzyme electron transfer at electrode surfaces. Of these immobilization strategies, chitosan hydrogels are particularly promising for our applications, since their ability to permit enzymatic activity upon immobilization has been directly compared to that of the TBABr-Nafion® used in Chapter 3.[11] Therefore, we have conducted preliminary experiments incorporating both drop-cast and electrodeposited chitosan into our N-CNT-modified GC electrodes. These experiments are discussed below.

Though the H_2O_2 detection schemes described in Chapters 3 and 4 do not feature sensitivities or detection limits as promising as some biogenic analyte detection schemes that rely on the direct electrochemical oxidation of H_2O_2, such traditional H_2O_2-based sensing schemes still suffer from many drawbacks, as discussed in Chapter 1. Furthermore, because the electrochemical oxidation of H_2O_2 produces protons, a pH

* Portions of this chapter were published in Lyon, J.L.; Stevenson, K.J. *Anal. Chem.* **2006**, *78*, 8518-8525.

gradient is generated at the electrode surface, resulting in perturbation of biological samples that are sensitive in changes in pH. Moreover, quantitative measurements become complicated as the oxidation of H_2O_2 at physiological pH is mechanistically complex, involving the formation of several reactive intermediates (superoxide, hydroperoxide and hydroxyl radicals) whose stabilities are also pH dependent.[12] To circumvent the many problems associated with the direct electrochemical oxidation H_2O_2, additional redox-active mediators are often incorporated. These mediators serve to shuttle electrons between H_2O_2 and the working electrode and facilitate electrochemical regeneration following electron exchange with H_2O_2. Both soluble and immobilized mediators such as *p*-hydroquinone,[13, 14] as well as those affixed in polymeric networks on the electrode surface,[15, 16] are used to improve analytical figures of merit (detection limit, sensitivity, dynamic range, reproducibility). However, in the case when the mediator is inherently electrochemically active in both oxidized and reduced forms, care must be taken to ensure that the observed electrochemical response is an authentic result of chemical interaction with H_2O_2 and not merely induced through repeated potential cycling during analysis.

We sought to avoid the issues intrinsic with use of these redox-active mediators by utilizing an indicator or reporter molecule that is not initially electrochemically active until the reaction with H_2O_2 acts to chemically activate the mediator. As such, we chose the indicator 10-acetyl-3,7-dihydroxyphenoxazine (commercially available as Amplex Red), which has been reported to become redox-active only upon chemical oxidation by the HRP E1 complex (see Chapter 3).[16, 17] Using Amplex Red, we developed a rapid, quantitative electrochemical analysis method for the detection of hydrogen peroxide in biological matrixes at physiological pH at carbon fiber ultramicroelectrodes (UMEs), which could be slightly modified to incorporate CNTs as working electrodes. This

methodology eliminates several problems associated with traditional, direct H_2O_2 sensing. Since Amplex Red is redox-inactive until oxidized by H_2O_2, greater analytical sensitivity may be achieved compared other commonly used redox-active mediators. Additionally, the application of current sampling with microelectrodes at specified times in concert with a controlled, square potential waveform leads to S/N improvements by effectively eliminating background contributions (e.g., double layer charging current) from the amperometric signal. As such, significantly lower detection limits and greater analytical sensitivities can be achieved over other reported H_2O_2 detection methods using either electrochemical or optically-based detection schemes. Most importantly, this method offers a tremendous analytical sensing advantage as it is amenable to any detection scheme that uses enzymatically generated H_2O_2 for detection of a biogenic species, and we demonstrate this versatility by incorporating our method in the detection of cholesterol in excised mouse gonadal tissue.

5.2 EXPERIMENTAL

5.2.1 Chitosan/N-CNT Composite Films at GC Electrodes

5.2.1.1 N-CNT Synthesis

N-CNTs (5 at%) were prepared as previously described in Chapters 2-4. Again, 1.0 mL of a 20 mg/mL ferrocene-pyridine mixture was injected at 0.1 mL/min into a dual-zone quartz tube furnace. The mixture was volatilized at 150 °C in the first zone and then carried downstream to the second zone by Ar–NH_3 at a total flow rate of 575 sccm.[18] Upon reaching the second zone, the mixture was pyrolyzed at 800 °C, resulting in the base-catalyzed growth of multiwalled N-CNTs from Fe nanoparticle nucleation sites. The N-CNTs were deposited along the walls of the quartz tube and were collected after cooling the tube to room temperature under Ar. N-CNTs were stored in airtight vials

prior to electrochemical analysis.

5.2.1.2 Chitosan/N-CNT Deposition at GC

For deposition of chitosan/N-CNT films at GC, 25 mL of a pH ~4, 0.5 wt% solution of chitosan (medium molecular weight, Aldrich) was prepared by dissolving chitosan in 1% (v/v) acetic acid in ultrapure H_2O (>18 MΩ cm) with stirring at 60 °C. The resulting colorless solution was filtered through a 0.45 μm PTFE filter (Millipore) and stored at 4 °C when not in use. Chitosan/N-CNT dispersions were formed by dispersing N-CNTs in the chitosan solution at a concentration of 2 or 5 mg/mL. The chitosan/N-CNT suspensions were sonicated in ultrapure H_2O for 15 min to create an even dispersion before depositing at GC electrodes. Prior to each deposition, the GC electrode (PINE Instruments AFE2M050GC, 0.5 cm diameter) was polished successively with 0.3 and 0.05 μm almunia slurries on microcloth (Buehler) to a mirror finish and sonicated in ultrapure H_2O for 15 min. For drop-cast depositions, 5 μL of the chitosan/N-CNT dispersion was pipetted onto the surface of a GC electrode. The chitosan/N-CNT composite-modified GC assembly was covered to prevent contamination and allowed to dry for 1 h. For control studies of N-CNTs drop-cast without chitosan, N-CNTs were suspended in absolute ethanol at a concentration of 5 mg/mL, and 5 μL of this solution was drop-cast at a polished GC electrode and allowed to dry for ~15 min. Upon drying, the N-CNTs were immediately immersed into solution for use in electrochemical experiments.

For electrodeposition of chitosan/N-CNT films, the polished GC electrode was immersed into the chitosan/N-CNT dispersion, along with a Hg/Hg_2SO_4 (sat'd. K_2SO_4) reference electrode (CH Instruments, E° = +0.640 V vs. NHE) and a Pt gauze counter electrode. A potential of -2.9 V vs. Hg/Hg_2SO_4 was applied at the working electrode for 150 s, causing the dissolved chitosan to flocculate and precipitate at the GC surface and

entrapping N-CNTs at the GC surface as well.[19] The chitosan/N-CNT composite-modified GC was removed from the chitosan/N-CNT dispersion, rinsed copiously with ultrapure H_2O to remove any loosely bound precipitate, and dried in an inverted position for 1 h prior to use in electrochemical experiments.

To determine the suitability of chitosan films for HRP direct electron transfer, a 200 μM solution of HRP (EC 1.11.1.7, MW ~44 kDa, 1280 ABTS U/mg solid, Sigma Product #P-6782) was prepared in 0.1 wt% chitosan, diluted from the 0.5 wt% chitosan solution prepared above. The chitosan/HRP solution was briefly vortexed, and 5 μL was drop cast at the polished GC electrode and allowed to dry for 1 h. All composite solutions containing chitosan were stored at 4 °C when not in use.

5.2.1.3 Electrochemical Analysis

In addition to the chitosan/N-CNT composite-modified GC working electrode, a Au wire counter electrode and Hg/Hg_2SO_4 reference electrode were used in all electrochemical measurements. All electrode potentials in Section 5.3.1 (vida infra) are reported vs. Hg/Hg_2SO_4. Electrochemical measurements were performed at room temperature (23 ± 2 °C) using an Autolab™ PGSTAT30 potentiostat interfaced with Autolab™ GPES version 4.9 software. Electrodes were contained within a 125-mL volume, 5-neck glass cell containing 100 mL of 0.1 M Na_2HPO_4 at pH = 6.00 ± 0.03. The supporting electrolyte solution was prepared using ultrapure H_2O. Chitosan/N-CNT composite-modified GC and bare GC ORR evaluation experiments were conducted under flowing O_2 to maintain an O_2-saturated environment at all times. HRP electron transfer studies were conducted under flowing Ar.

5.2.2 Amplex Red-Mediated H_2O_2 Detection at Carbon UMEs

Amplex Red was purchased from Invitrogen, diluted to 0.1 M in DMSO immediately upon arrival, divided into 5 μL aliquots and stored at -20 °C until immediately before use. HRP (EC 1.11.1.7, 1280 ABTS U/mg solid) was purchased from Sigma (Product #P-6782). A stock solution of 300 U/mL HRP in 0.1 M K_2HPO_4/0.05 M citric acid buffer, pH = 5.00 ± 0.03 (referred to herein as phosphate/citric acid buffer), was stored at 4 °C and diluted to 0.2 U/mL for experiments. For experiments using immobilized HRP, glass coverslips (No. 1 thickness, Erie Scientific) were cleaned successively with methanol and isopropyl alcohol rinses and dried under N_2. After drying, 5 μL of 300 U/mL HRP stock (equivalent to the amount used in soluble HRP experiments) was pipetted onto each slide and allowed to dry in air. The slides were used in electrochemical experiments immediately after drying appeared complete. H_2O_2 (30% w/v) was purchased from Fisher Scientific and stored at 4 °C at all times. H_2O_2 standards were prepared by serial dilution of 30% H_2O_2 in the same buffer used for HRP solution preparation immediately prior to use. All other reagents were obtained from Sigma-Aldrich and used as received. All solutions were prepared using ultrapure H_2O.

Mediated amperometric peroxide detection experiments were performed at room temperature (23 ± 2 °C) using an Autolab PGSTAT30 potentiostat interfaced with Autolab GPES ver. 4.9 software. H_2O_2 standards were analyzed in a standard single-compartment, glass 3-electrode cell containing 5 mL of 0.2 U/mL HRP (either soluble or dried on a glass slide immersed in the cell) and 100 μM Amplex Red in phosphate/citric acid buffer, pH = 5.00 ± 0.03. The Amplex Red response to H_2O_2 was detected at either a 10 μm diameter GC disk-in-glass microelectrode (Cypress Systems) or a 2 mm GC-resin electrode prepared in-house, as described in Chapter 3. Working electrodes were polished successively with 0.3 and 0.05 μm alumina slurries on a polishing cloth (Buehler) to a

mirror finish, ultrasonically cleaned for 20 min in ultrapure H_2O, and used immediately in experiments. A Ag/AgCl reference electrode (3 M KCl, World Precision Instruments) and a Au wire counter electrode (Strem) were also used. A Faraday cage was used to shield the 3-electrode cell from external noise. All electrode potentials in Section 5.3.1 (vida infra) are reported vs. Ag/AgCl. These experiments were conducted in ambient air.

5.2.3 Amplex Red-Mediated Amperometric Plasma Membrane Cholesterol Detection in Mouse Gonadal Tissue

For cholesterol detection in mouse tissue experiments, HRP and cholesterol oxidase (ChOx, 100 U/mg, Wako Chemical) were co-immobilized at the surface of the 10 μm carbon fiber electrode in an electropolymerized polypyrrole film.[20, 21] The carbon fiber electrode was immersed in 1 mL of 0.1 M phosphate/citric acid buffer, pH = 5.00 ± 0.03 containing 0.4 M pyrrole (Aldrich), 30 U HRP, and 10 U ChOx. The Au wire counter and Ag/AgCl reference electrode were added to the cell, and the solution was degassed with Ar for ~20 min to prevent premature air oxidation of the pyrrole. The carbon fiber working electrode was then poised at +0.7 V vs. Ag/AgCl to induce pyrrole polymerization and deposition at the carbon surface, entrapping HRP and ChOx. When the charge had decreased to10 mC/cm^2, the PPy/enzyme electrode was removed from solution and rinsed with phosphate/citric acid buffer. The three electrodes then were immersed in a solution of phosphate/citric acid buffer, and the PPy/enzyme electrode was poised at +0.7 V vs. Ag/AgCl for 1-2 h to "overoxidize" the PPy/enzyme film, creating a stable film for further electrochemical experiments.[22]

Wild-type mouse gonadal tissue was a gift from Dr. James Burgess (Case Western Reserve University, Cleveland, OH). A 500 x 400 μm slice of tissue was immersed in a petri dish containing phosphate/citric acid buffer and 12.5 μM Amplex Red. The tissue sample was observed using a Nikon xx Microscope equipped with a 10x

objective and held in place using a flame-pulled-tip Pasteur pipet attached to a manual *xyz*-micropositioner (Newport). The PPy/enzyme electrode was attached to a separate *xyz*-micropositioner and immersed in the petri dish. A Au wire counter electrode and Ag/AgCl reference electrode were also immersed in the petri dish, out of the path of the micropositioners. The three electrodes were connected to the Autolab PGSTAT 30 potentiostat, and SWV measurements were collected with the PPy/enzyme working electrode both contacted and not contacted to the tissue sample. These experiments were conduced in ambient air, and potentials are reported vs. Ag/AgCl.

5.3 RESULTS AND DISCUSSION

5.3.1 Chitosan/N-CNT Composite Films at GC Electrodes

Chitosan, both drop-cast and electrodeposited, is often used to immobilize enzymes and other biomolecules at carbon electrodes.[7, 8, 11, 19, 23-31] Enzymes immobilized in chitosan, including HRP, have demonstrated robust voltammetry at carbon surfaces.[7, 8] Furthermore, Minteer et al. have noted that in some cases, modified chitosan membranes surpass modified Nafion membranes in promoting immobilized enzyme activity at electrode surfaces.[11] Therefore, we wish to explore the use of chitosan as an immobilizing film to possibly improve electron transfer between HRP/CNT composites and GC electrodes. Before incorporating chitosan into our enzymatic assemblies, the effect of chitosan incorporation on the N-CNTs' inherent electrochemical behavior should be investigated. Figure 5.1 shows a series of voltammograms for bare GC and at chitosan/N-CNT-modified GC electrodes in pH 6.00 phosphate supporting electrolyte, in a saturated O_2 environment. Each CV in Figure 5.1 was acquired after cycling the potential at least 50 times, both to ensure a stable ORR potential reading and to passivate the N-CNT $Fe^{2+/3+}$ redox activity that occurs in this potential window in phosphate (see

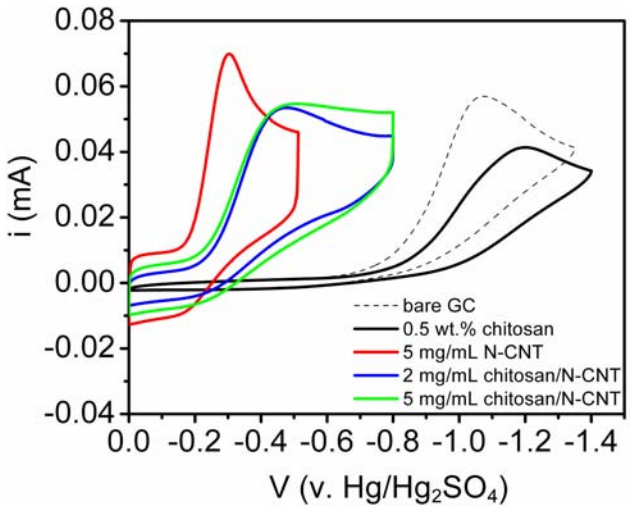

Figure 5.1. CVs of bare GC (black dashed line) and GC modified with chitosan, N-CNTs, and chitosan/N-CNT composites in saturated oxygen. Supporting electrolyte: 0.1 M Na_2HPO_4, pH = 6.00 ± 0.03. Scan rate: 20 mV/s.

Chapter 2). The oxygen reduction reaction (ORR) potential at each of these electrode assemblies is listed in Table 5.1. As a control study, a 0.5 wt% chitosan solution was drop-cast at bare GC, and the ORR at GC in 0.1 M Na_2HPO_4, pH = 6.00 ± 0.03 was evaluated with (Figure 5.1, dashed line) and without (Figure 5.1, black line) the drop-cast chitosan film present. Upon addition of the chitosan film at the GC surface, the ORR potential shifts negative by 128 mV (Table 5.1), indicating that the incorporation of chitosan at the GC surface does not result in a substantially larger overpotential being required for oxygen reduction. To determine whether chitosan induces a shift in the ORR potential at N-CNTs, 5 mg/mL dispersions of N-CNTs were drop-cast at GC in absolute ethanol, i.e., in the absence of chitosan (Figure 5.1, red line) and in a 0.5 wt% chitosan solution (green line). In the absence of chitosan, an ORR potential of -0.303 V is observed, while the same quantity of N-CNTs drop-cast in a chitosan solution displays an ORR of -0.487 V. Additionally, the peak current density of the chitosan/N-CNT-modified GC is somewhat diminished compared to that of N-CNTs drop cast in the absence of chitosan. We note that by reducing the concentration of N-CNTs to 2 mg/mL in the drop-cast chitosan/N-CNT composite, a more defined ORR peak is observed (blue line), and the ORR peak potential shifts 18 mV positive relative to the chitosan/N-CNT composite containing 5 mg/mL N-CNTs. This observed potential shift as a function of N-CNT concentration may be reflective of N-CNT occlusion in the more concentrated composite matrix at the GC surface, as a denser N-CNT matrix is present in these assemblies. These results indicate that the presence of drop-cast chitosan requires that a marginally larger overpotential be applied at our N-CNT/GC electrode assemblies to induce the ORR. However, the resulting ORR potential appears to be somewhat affected by the concentration of N-CNTs in the drop-cast composite, suggesting that further optimization

Table 5.1. Oxygen reduction reaction (ORR) potentials determined from CVs shown in Figure 5.1 of various chitosan-modified GC electrode assemblies.

Sample	ORR E_p (V vs. Hg/Hg_2SO_4)
Bare GC	-1.070
0.5 wt% chitosan	-1.198
5 mg/mL N-CNT	-0.303
2 mg/mL chitosan/N-CNT	-0.469
5 mg/mL chitosan/N-CNT	-0.487

of the chitosan/N-CNT deposition solution would be beneficial for development of chitosan-based electrode assemblies.

Several recent reports have documented the electrodeposition of chitosan films at electrode surfaces by applying reducing potentials in acidic chitosan solutions.[19, 25, 26, 28, 29] Chitosan's amino-polysaccharide backbone is protonated at pH <6, causing chitosan to be soluble in acidic solutions, including the pH 4 acetate solution used in the present studies. When the pH is increased above 6, the amino groups are deprotonated, causing chitosan to flocculate and form a hydrogel network.[32, 33] To induce a chitosan hydrogel network formation at an electrode surface, the electrode is poised at a reducing potential, thus evolving H_2 through the hydrogen evolution reaction (HER) mentioned in Chapter 2. The local pH gradient created near the electrode-solution interface by applying a reducing potential results in the precipitation of chitosan in regions where H^+ is depleted, i.e., at the electrode surface. The rate and extent of chitosan electrodeposition can be controlled by adjusting the applied potential or current density, since the extent of H^+ depletion is proportional to the HER current density.[34] When CNTs are present in the acidic chitosan deposition solution, they also become entrapped in the precipitated chitosan film at the electrode surface.[19] Therefore, we sought to compare electrodeposition to drop-cast methods for creation of chitosan/N-CNT composites. Figure 5.2 shows CVs obtained in saturated O2 at chitosan/N-CNT composite-modified GC, using either potentiostatic deposition at -2.9 V (solid line) or the drop-cast method (dashed line) to immobilize the composite film at the GC surface. Both modified electrodes were created using 2 mg/mL N-CNTs in 0.5 wt%, pH ~4 chitosan. The background current density and ORR peak current density are notably larger at the electrodeposited assembly than at the drop-cast assembly. Since the background current density at GC is not affected by the addition of a chitosan film (compare black and dashed CVs in Figure 5.1), it can be assumed that the

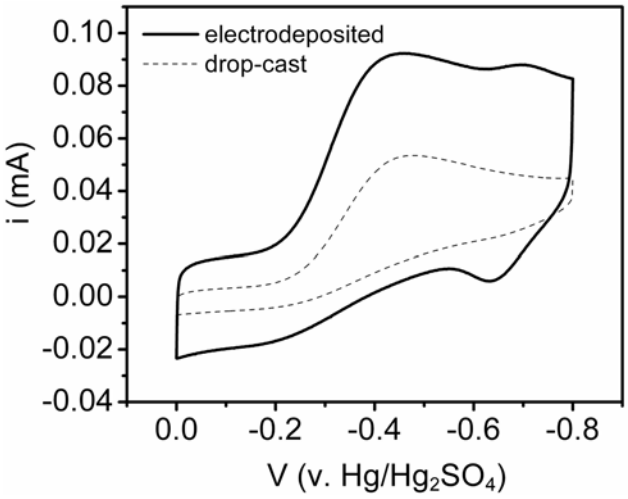

Figure 5.2. CVs in saturated O_2 of chitosan/N-CNT films, containing 2 mg/mL N-CNTs, either drop-cast (dashed line) or electrodeposited (solid line) at GC. Supporting electrolyte: 0.1 M Na_2HPO_4, pH = 6.00 ± 0.03. Scan rate: 20 mV/s.

increasing current density at the electrodeposited composite is due to a larger amount of N-CNTs being incorporated in the electrodeposited chitosan film. The ORR peak potential varies less than 5 mV between the two electrode assemblies, indicating that incorporation of N-CNTs at the electrode surface through electrodeposition of chitosan does not adversely affect the N-CNT's electrocatalytic activity toward oxygen reduction.

Both of the CVs shown in Figure 5.2 were obtained after cycling the electrodes at least 50 times, as with Figure 5.1. Nevertheless, a second redox couple centered about -0.665 V is evident in the electrodeposited chitosan/N-CNT CV. This redox couple corresponds to $Fe^{2+/3+}$ activity in the phosphate supporting electrolyte, as thoroughly discussed in Chapter 2. However, unlike the Fe redox activity discussed in Chapter 2, the $Fe^{2+/3+}$ species present in the electrodeposited chitosan/N-CNT composite is not passivated after 50 potential cycles. In fact, these peaks failed to disappear even after 500 cycles. By contrast, $Fe^{2+/3+}$ is easily passivated in the drop-cast chitosan/N-CNT composite film, as evidenced by the lack of redox peaks near -0.670 V in the dashed CV in Figure 5.2. These results suggest that phosphate anion coordination with entrapped Fe species in the N-CNTs is substantially occluded when the N-CNTs are immobilized in an electrodeposited chitosan matrix. Therefore, an alternative method for passivating Fe redox activity in our CNTs may need to be developed if the CNTs are to be entrapped using chitosan electrodeposition, particularly since HRP's $Fe^{2+/3+}$ redox couple is centered very near the N-CNT $Fe^{2+/3+}$ peak potential (see Chapter 3). As stated in Chapter 2, acid leaching is commonly used to remove residual metal catalysts from CNTs, and this method could be incorporated here to reduce the amount of Fe present in our N-CNTs. However, acid treatment could potentially alter the N-CNT structure, as such treatments been shown to introduce functional groups at CNT surfaces[35] and shorten nominal CNT lengths.[36]

Huang et al. have reported robust HRP $Fe^{2+/3+}$ redox activity at HOPG electrodes coated with drop-cast chitosan/HRP composites,[7] and Qian et al. have reported similar results obtained by glutaraldehyde-crosslinking of HRP at a drop-cast chitosan/CNT composite-modified GC electrode.[8] We have performed preliminary studies investigating $Fe^{2+/3+}$ redox activity upon immobilization in drop-cast chitosan films at GC and compared these studies to the control studies in Chapter 3, in which HRP was drop-cast in a TBABr-Nafion film at GC. The HRP Fe CV in saturated Ar from Figure 3.5a is reproduced in Figure 5.3, along with a CV obtained at a drop-cast chitosan/HRP composite-modified GC electrode (dashed line). Though both electrode assemblies contain similar quantities of HRP (±10%), the Fe^{3+} reduction observed at the chitosan/HRP electrode is much more pronounced than that observed at the TBABr-Nafion/HRP electrode. Therefore, chitosan appears promising as an immobilizing film for use with our HRP/N-CNT composites drop-cast at GC, though we have yet to drop-cast HRP/N-CNT composites simultaneously with chitosan at GC. The preliminary results presented here suggest that utilizing chitosan/HRP/N-CNT composites at GC might result in improved HRP electron transfer relative to the results presented in Chapter 3, permitting better sensitivity and lower detection limits to be attained in peroxidase-based sensing schemes.

5.3.2 Amplex Red-Mediated H_2O_2 Detection at Carbon UMEs

As stated above in the Introduction, the redox mediator Amplex Red is a unique reported molecule in that it becomes redox-active only upon chemical oxidation by the HRP E1 complex produced from H_2O_2 consumption. Figure 5.4 outlines the signal transduction approach for electrochemical detection of enzymatically generated H_2O_2 using Amplex Red in a schematic depiction. In this scheme, horseradish peroxidase (HRP) that is either soluble in solution or immobilized on a solid support catalyzes the

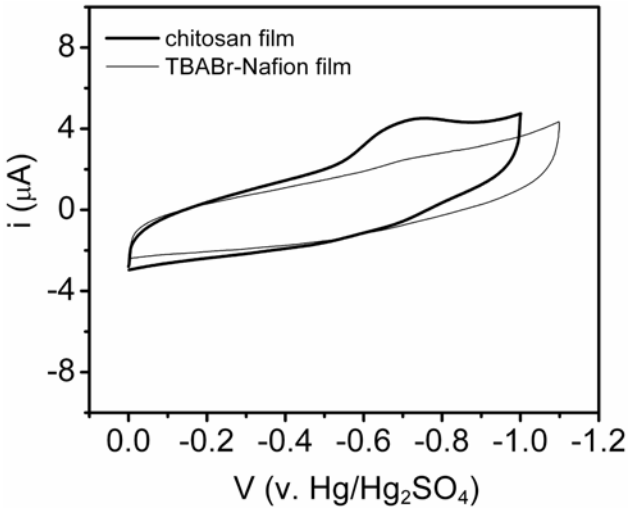

Figure 5.3. CVs (saturated Ar) of HRP drop-cast with chitosan (heavy trace) and with TBABr-Nafion (light trace) at GC. Supporting electrolyte: 0.1 M Na_2HPO_4, pH = 6.00 ± 0.03. Scan rate: 100 mV/s.

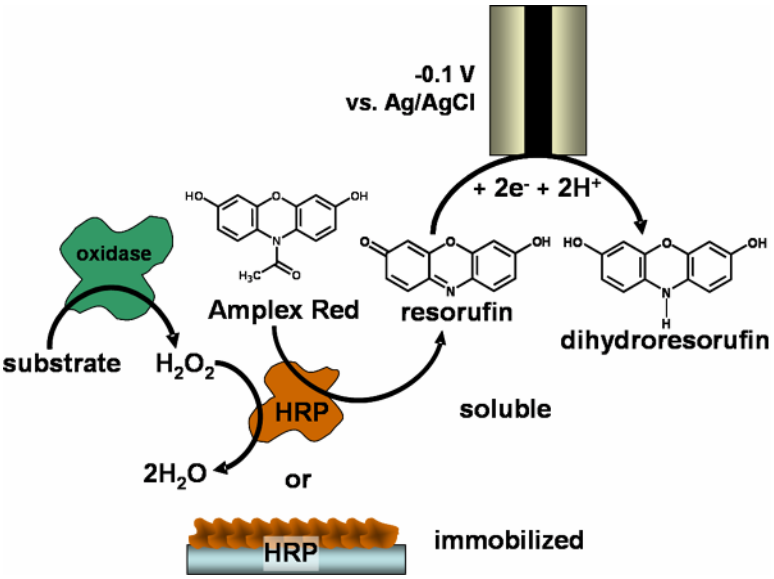

Figure 5.4. Depiction of enzymatically generated H_2O_2 detection using the Amplex Red redox mediator. In this scheme, H_2O_2 produced as a byproduct of oxidase-substrate is reduced to H_2O by either soluble or immobilized HRP(Fe^{3+}), forming the HRP E1 complex noted in Chapter 3. The solvated Amplex Red mediator is rendered electroactive via a chemically irreversible oxidation to resorufin through its reduction of E1 to HRP(Fe^{3+}). Resorufin is subsequently reduced to dihydroresorufin at -0.1 V vs. Ag/AgCl on a carbon electrode, elucidating the amount of H_2O_2 present.

reduction of H_2O_2 generated from oxidase-substrate interactions to H_2O. Through this process, HRP is oxidized from its native Fe^{3+} state to the oxyferryl/porphyrin cation radical state E1 (see Chapter 3, Reaction 1). E1 is reduced to native HRP via an irreversible chemical oxidation of Amplex Red to its redox-active form, resorufin. Resorufin is then detected electrochemically at a GC electrode through a reversible, two-electron reduction step to generate dihydroresorufin[37] at approximately -100 mV vs. Ag/AgCl.[17] Because Amplex Red is activated in a 1:1 ratio with H_2O_2 consumption, the amount of free H_2O_2 can be quantified at a lower reduction potential than that typically used for direct electrochemical oxidation of H_2O_2. This methodology effectively reduces the electrochemical background, eliminates interferences from other electroactive species with higher oxidation potentials, lessens the chances for electrode fouling, and diminishes electrochemically-induced pH changes due to oxidation or reduction of the aqueous solution (water) known to occur at large overpotentials.

While Amplex Red has been preliminarily explored as an electrochemical assay for H_2O_2 in exhaled breath condensates,[17] we sought to evaluate its use in more generally applicable enzyme based biosensing schemes that employ electrochemical detection protocols with microelectrodes, built-in background reduction, faster time response, and higher diagnostic value. We note that while a 10 μm disk-in-glass carbon UME is used in the studies presented here, this sensing assembly could easily be extended to our CNTs, as they may be synthesized directly at a variety of electrode geometries, including those of UME dimensions.[38] However, the fact that Amplex Red oxidation is dependent on HRP–H_2O_2 interaction means that N-CNTs should not be used in this particular sensing scheme, as the H_2O_2 decomposition rate at N-CNTs appears to exceed the H_2O_2 reduction rate at HRP, as mentioned in Chapter 3. Instead, N-CNTs are better suited to be explored as peroxidase mimetics, similar to the method described in Chapter 4.

As stated above, resorufin is converted to dihydroresorufin via a reversible two-electron reduction at ~ -0.1 V vs. Ag/AgCl. Upon addition of H_2O_2 to the supporting electrolyte solution described above, reversible voltammetric behavior for resorufin was observed, Figure 5.5 (light trace). CVs of H_2O_2 and HRP in the absence of Amplex Red showed no electrochemical behavior in this potential range (data not shown). The half-wave potential, $E_{1/2}$, for the resorufin-dihydroresorufin couple was -96 mV, consistent with values reported in the literature.[17] The peak-to-peak separation, ΔE_p, of 28 mV agrees with the expected result where 59/n mV and n = 2, the number of electrons transferred in the redox reaction[39] for a reversible process. The maximum current response for all concentrations of H_2O_2 was determined to occur at t = 5 min following introduction of H_2O_2 to the buffered Amplex Red solution, suggesting that adsorption of the resorufin/dihydroresorufin couple to the working electrode surface is a controlling factor in the observed current response. All measurements reported herein were thus collected after thoroughly stirring the sample solution and allowing a 5 min equilibration period.

Clearly, a minimal amount of sample perturbation is desired when performing experiments *in vivo*; ultra-sensitive electrochemical measurements can help achieve this goal by minimizing the amount of necessary contact time between the biological system and the sensor (working electrode) in order to generate a substantial current response. Traditionally, real-time electrochemical signals obtained from H_2O_2 oxidation in biological samples have employed chronoamperometric methods in which the working electrode is poised at a H_2O_2 oxidation potential and the current response is measured on a timescale of tens of seconds to several minutes.[40-42] We sought to decrease the amount of time required to collect an amperometric signal from H_2O_2 by employing square wave voltammetry (SWV) in our sensing scheme. In addition to the wide range of time scales

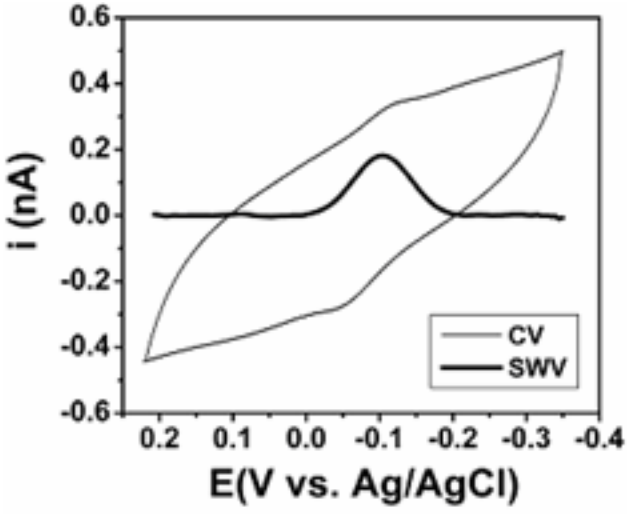

Figure 5.5. Comparison of SWV (heavy trace) and CV (light trace) for a 300 nM H_2O_2 standard, demonstrating improved S/N attainable with SWV. SWV parameters: amplitude = 25 mV, step height = 5 mV, frequency = 25 Hz. CV scan rate = 125 mV/s. Experimental conditions: 10 μm diameter carbon fiber working electrode, Ag/AgCl reference electrode, Au wire counter electrode, 0.1 M K_2HPO_4/0.05 M citric acid buffer, pH = 5.00 ± 0.03, 0.2 U/mL HRP, 10 μM Amplex Red.

available, SWV was chosen as an experimental method due to its many promising features, including background suppression and diagnostic value.[43-46]

The SWV waveform consists of a square wave modulation superimposed on a staircase potential ramp. SWV traditionally utilize parameters that adhere to the quantities in the range for nE_{step} = 10 mV and nE_{sw} = 50 mV, where E_{step} and E_{sw} are the step height and amplitude of the imposed square waveform, respectively.[44, 45, 47] For ease of comparison between experimental data and theoretical calculations, the SWV parameters E_{step} = 5 mV and E_{sw} = 25 mV were used unless otherwise noted. The resulting current is sampled on both the forward (i_f) and reverse (i_r) pulse of each waveform, and the net difference current ($i_{net} = i_f - i_r$) is plotted in real time as a function of potential. To illustrate the enhanced sensing capabilities of SWV, Figure 5.5 compares a SWV voltammogram to a CV obtained for a 300 nM H_2O_2 sample. Both the SWV and CV shown in Figure 5.5 were obtained using a scan rate of 125 mV/s. (The effective scan rate for SWV is obtained using the formula $v = f(E_s)$, where v is the effective scan rate and f and E_s are the frequency and step height of the applied square waveform, respectively.[43]) The features of the CV shown in Figure 5.5 are convoluted due to large non-Faradaic current contributions, necessitating background correction in order to accurately extract numerical values for peak-to-peak separation, ΔE_p, and peak potential, $E_{1/2}$. By contrast, the SWV exhibits an improvement in signal-to-noise (S/N) over the CV by roughly a factor of five. Additionally, the enhanced S/N inherent in SWV permits peak parameters to be readily analyzed in "raw data" format, without further manipulation or filtering or curve fitting. This also allows for faster detection and data analysis. It should also be noted that while our mediated SWV sensing scheme is actually capable of detecting H_2O_2 concentrations more than four orders of magnitude below the 300 nM standard shown in Figure 5.5 (vida infra), no such detection limit can be

achieved using CV since the voltammograms appear nearly featureless even at very fast or slow scan rates, as the background charging currents and other non-Faradaic processes dominate the current-potential response.

Using the peak heights, i_p, obtained from SWV measurements for H_2O_2 standards of varying concentration, calibration curves for the mediated H_2O_2 sensing scheme were constructed. Calibration curves for both soluble and immobilized HRP are shown in Figure 5.6. For each sensing scheme, two distinct linear regions exist. The first linear region, observed at H_2O_2 concentrations < 300 pM or 50 nM when using soluble or immobilized HRP, respectively, is shown in Figures 5.6a and b. The amperometric sensitivity for soluble HRP in this region is $4.0 \pm 0.1 \times 10^3$ $\mu A/\mu M*mm^2$. Upon immobilization of HRP to a glass support (Figure 5.6b), a decrease in amperometric sensitivity occurs ($2.1 \pm 0.3 \times 10^1$ $\mu A/\mu M*mm^2$). By dividing $3\sigma_b$ by the amperometric sensitivity, where σ_b is the standard deviation of the blank signal (i.e., $[H_2O_2] = 0$ M), the limits of detection were calculated as 8 pM and 2 nM for soluble and immobilized HRP, respectively. Such decreases in analytical response upon enzyme immobilization are abundant in the literature,[48-50] and are attributed to hindrance of enzyme–substrate interaction, since HRP is no longer free to orient its heme cofactor most efficiently for H_2O_2 turnover. Though below the statistically determined detection limit, clearly resolved peaks have been observed for as little as 3 pM H_2O_2 (Figure 5.6a) and 200 pM H_2O_2 (Figure 5.6b).

A second, much broader linear range is observed between the upper limit of the regions described in the preceding paragraph and low μM H_2O_2 concentrations (Figure 5.6c). For soluble HRP in this range, an amperometric sensitivity of 1.22 ± 0.04 $\mu A/\mu M*mm^2$ is obtained. Again as in Figure 5.6b, immobilization of HRP effects a decrease in amperometric sensitivity ($2.1 \pm 0.6 \times 10^{-1}$ $\mu A/\mu M*mm^2$). For both sensing

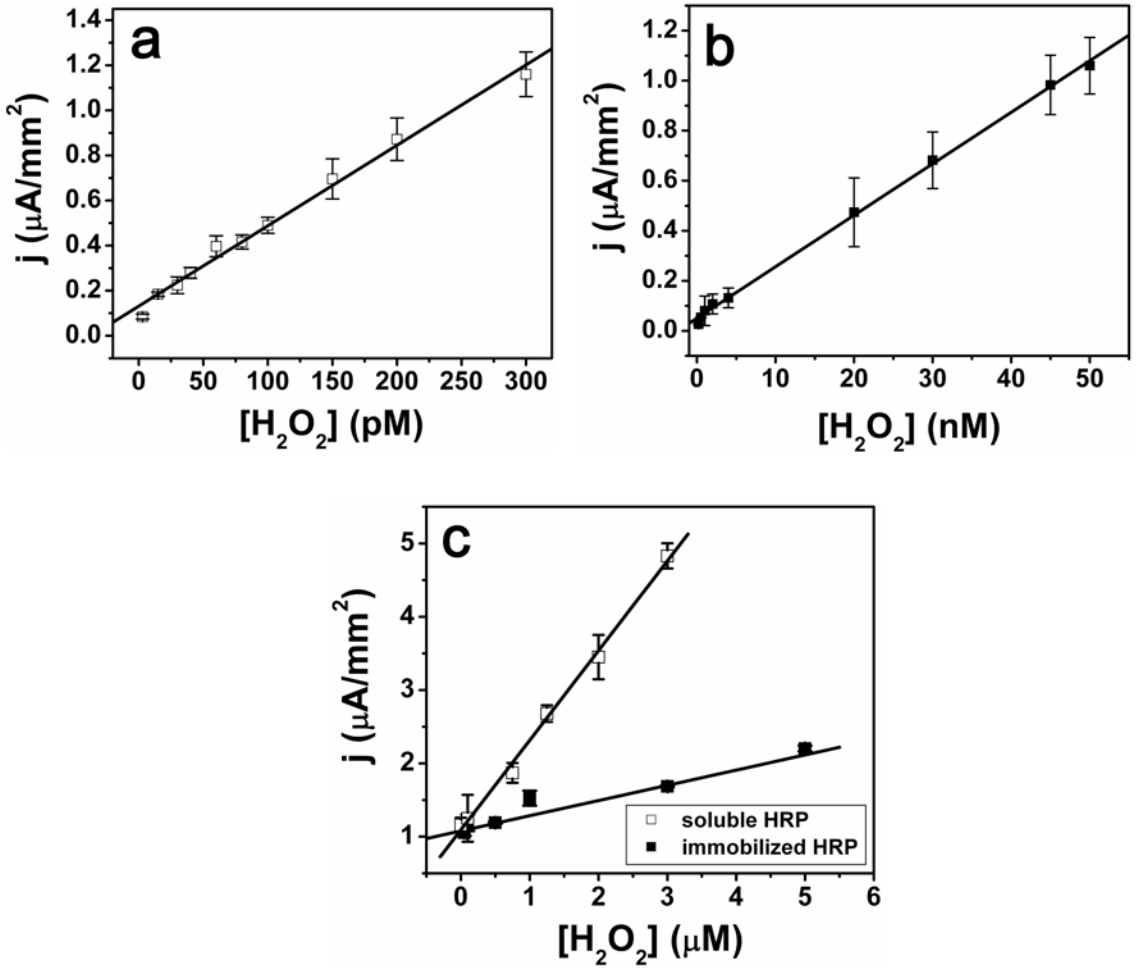

Figure 5.6. Calibration curves for H_2O_2 standards detected via Amplex Red-mediated electrochemical sensing, utilizing either soluble (open squares) or immobilized (closed squares) HRP. Peak currents were obtained using SWV experiments outlined in the text and normalized to the working electrode area. SWV parameters: amplitude = 25 mV, step height = 5 mV, frequency = 25 Hz. Experimental conditions: 10 μM diameter carbon fiber working electrode, Ag/AgCl reference electrode, Au wire counter electrode, 0.1 M K_2HPO_4/0.05 M citric acid buffer, pH = 5.00 ± 0.03, 10 μM Amplex Red. For soluble HRP, [HRP] = 0.2 U/mL. For immobilized HRP, an equivalent amount of HRP was adsorbed to a glass slide placed in the electrochemical cell. (a) Linear current response in the pM H_2O_2 range for soluble HRP. (b) Linear current response in the pM–nM range for immobilized HRP. (c) Wide-range linear responses for both soluble and immobilized HRP observed between 300 pM and low μM H_2O_2 concentrations. Sensitivities of these calibration curves are ~3 orders of magnitude less those in (a) and (b).

schemes, these respective decreases in sensitivity relative to the plots shown in Figures 5.6a and b are most likely a result of substrate inhibition effects brought about by the increasing ratio of substrate to enzyme.[48, 51] Additionally, the linear range of the immobilized HRP data (50 nM to 5 μM) is reduced compared to soluble HRP. Through optimization of the HRP immobilization strategy, we plan to decrease this limit to match that of the soluble HRP scheme. Our calculated sensitivities and detection limits demonstrate a marked improvement over other reported schemes for direct H_2O_2 detection and Amplex Red-mediated H_2O_2 detection via chronoamperometric methods.[17, 40, 42] For comparison, detection limits and dynamic linear ranges are listed for competing methods of analysis in Table 5.2. Quite clearly, by combining a chemically activated redox mediator scheme in conjunction with microelectrodes and SWV, we have extended the H_2O_2 detection limit by at least ~3 orders of magnitude below other known reported values.

We note that in addition to being redox active, resorufin is also fluorescent (ex. 563 nm, em. 587 nm[52]), and its use in optically based biological sensing schemes is well-documented.[52-54] However, such sensing strategies are inherently insensitive due to the high fluorescence background produced as resorufin diffuses through the sample solution. To control the fluorescence background, as well as utilize Amplex Red fluorescence for localized sensing, a flow cell must be implemented to control resorufin diffusion. Even with use of a flow cell detection limits still remain in the low nM range and analytical sensitivity is poor. Some reported analytical figures of merit for various optical detection schemes are also presented in Table 5.2. Comparison of our sensitivity and detection limit for both soluble and immobilized HRP to those reported in the table undoubtedly shows significant improvement over other established protocols for H_2O_2 detection using either electrochemical or optical methods.

Table 5.2. Comparison of Amplex Red-mediated SWV electrochemical detection scheme figures of merit to current protocols for H_2O_2-based sensing.

H_2O_2 Detection Scheme	Limit of Detection (nM)	Linear Range (nM)	Amperometric Sensitivity ($\mu A/\mu M*mm^2$)	Reference
Amplex Red-mediated SWV; soluble HRP	0.008 0.3	$8 \times 10^{-3} - 3 \times 10^{-1}$ $3 \times 10^{-1} - 3 \times 10^{3}$	$4.0 \pm 0.1 \times 10^{3}$ 1.22 ± 0.04	present work
Amplex Red-mediated SWV; immob. HRP	2 50	$2 - 50$ $50 - 5 \times 10^{3}$	$2.1 \pm 0.3 \times 10^{1}$ $2.1 \pm 0.6 \times 10^{-1}$	present work
Amplex Red-mediated chronoamperometry	100	$10^{2} - 10^{3}$	2.86×10^{-3}	17
Resorufin fluorescence	18	$20 - 2 \times 10^{4}$	n/a	51
Unmediated H_2O_2 oxidation	500	$10^{4} - 2 \times 10^{5}$	not reported	38
Flow-injection chemiluminescence	1	$10 - 2 \times 10^{2}$	n/a	54
Hydroquinone-mediated CV	60	$60 - 2 \times 10^{4}$	not reported	14
Prussian Blue-mediated CV	10	$10^{1} - 10^{7}$	2.00×10^{-3}	16

Many conventional biogenic sensors that employ direct H_2O_2 oxidation for detection experience severe interference from other redox-active species such as ascorbic and uric acids, which are present in μM levels in human serum.[55] Because our sensing scheme is based upon the reduction of the resorufin-dihydroresorufin couple, the detection scheme does not require the working electrode to be poised at an extreme oxidative potential where other interfering species are electroactive (e.g., E° = +0.1 V and + 0.35 V vs. Ag/AgCl for ascorbic and uric acids, respectively). As shown in Figure 5.7, the peak potential and peak currents for detection of 300 pM H_2O_2 remains unaffected in the presence of uric and ascorbic acid even at concentrations twice as high as those normally present in human serum.

5.3.3. Amplex Red-Mediated Amperometric Plasma Membrane Cholesterol Detection in Mouse Gonadal Tissue

In an effort to develop miniature biosensors for localized, in vitro and in vivo based detection of important bioanalytes in tissue and cellular matrixes, we have modified our Amplex Red-based sensing strategy to detect cholesterol in the plasma membrane (PM) of excised mouse gonadal tissue samples. The reaction mechanism for cholesterol detection using our sensing scheme is as follows:

$$\text{Cholesterol} + \text{ChOx} + O_2 \rightarrow \text{cholestenone} + H_2O_2 \quad (1)$$

$$\text{HRP}(Fe^{3+}) + H_2O_2 \rightarrow \text{E1}(Fe^{4+}{=}O,\ P^{\bullet+}) + H_2O \quad (2)$$

$$\text{E1}(Fe^{4+}{=}O,\ P^{\bullet+}) + \text{Amplex Red} \rightarrow \text{HRP}(Fe^{3+}) + \text{Resorufin} \quad (3)$$

$$\text{Resorufin} + 2H^+ + 2e^- \rightarrow \text{Dihydroresorufin} \quad (4)$$

For real-time detection of PM cholesterol content in excised tissues, we have confined the enzymatic components of our sensing scheme to the surface of the GC

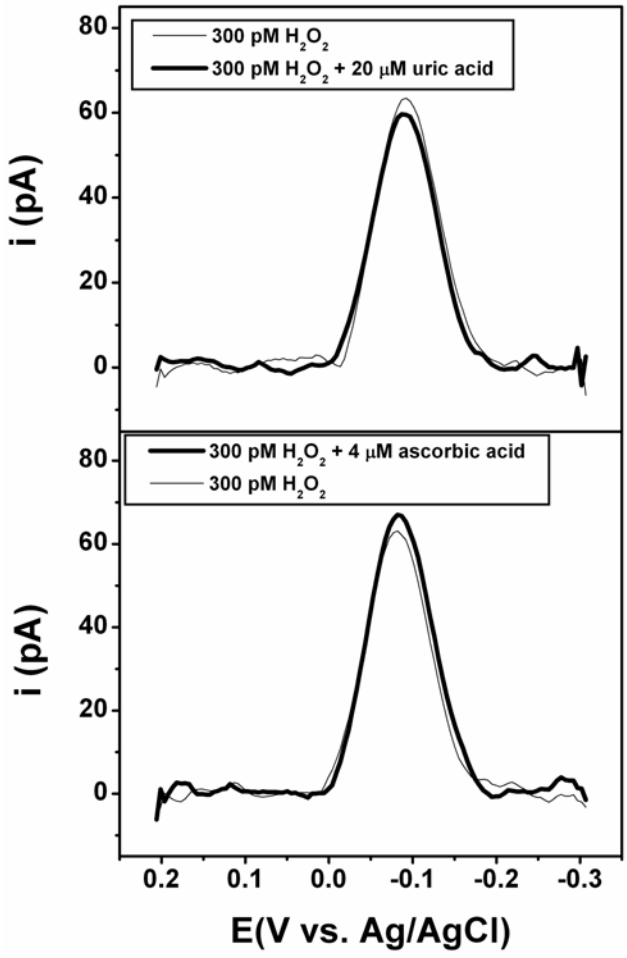

Figure 5.7. SWV detection of 300 pM H_2O_2 in the presence of 20 μM uric acid (top) and 4 μM ascorbic acid (bottom). Experimental conditions: 10 μm carbon fiber working electrode, Ag/AgCl reference electrode, Au wire counter electrode; 0.1 M K_2HPO_4/0.05 M citric acid buffer, pH = 5.00 ± 0.03, 0.2 U/mL HRP, 10 μM Amplex Red. SWV parameters: amplitude = 25 mV, step height = 5 mV, f = 25 Hz.

working electrode through electrochemical co-immobilization of ChOx and HRP in an "over-oxidized" polypyrrole (PPy) film. This immobilization is achieved through chronoamperometric deposition from a solution containing both enzymes and pyrrole monomer. Pyrrole polymerizes upon oxidation (+0.7 V v. Ag/AgCl), entrapping the enzymes at the surface of the GC electrode.[20, 21] Following immobilization, the PPy-enzyme electrode is poised at an oxidizing potential for 1-2 h in pure buffer solution to ensure that the PPy is completely oxidized and thus unable to participate in electron transfer reactions at the GC surface. This over-oxidation of PPy effectively creates an electrochemically inactive network for the entrapment of the active enzymes while still permitting diffusion of generated H_2O_2 and Amplex Red to the GC surface.[22] Future experiments will explore the use of the aforementioned chitosan immobilization strategies to co-immobilize HRP and ChOx for real-time sensing applications.

For excised tissue experiments, a PPy/enzyme-modified GC electrode is placed in direct contact with the tissue sample while both are immersed in the phosphate/citric acid buffer solution containing Amplex Red. The current response is then immediately obtained using square wave voltammetry, with no preconditioning time necessary. Figure 5.8 (red line) shows representative data obtained from cholesterol measurements in WT mouse tissue. For comparison, a control experiment in which the PPy/enzyme-modified GC electrode is placed ~100 μm from the tissue was performed in addition to the experiment described above (Figure 5.8, black line). As can be seen in Figure 5.8, a dramatic increase in current at the potential for Amplex Red reduction is observed upon contact of the electrode with the tissue, indicating the presence of PM cholesterol. Thus, the mediated electrochemical detection scheme presented here provides proof-of-concept for fast, quantitative analysis of cholesterol in mouse tissue samples. Future experiments will involve analysis of peak current intensities from such measurements to calibrate and

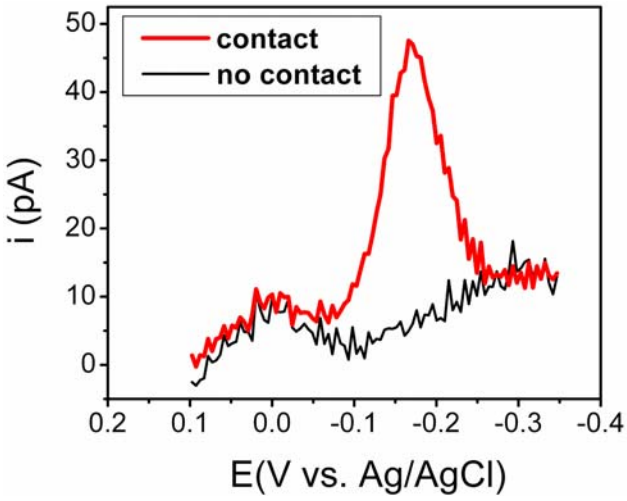

Figure 5.8. Cholesterol response from excised mouse gonadal tissue at 10 μm diameter PPy/enzyme-modified carbon fiber electrode using Amplex Red-mediated SWV. Sample: 500 x 400 μm mouse gonadal tissue (wild-type, untreated). Experimental conditions: Ag/AgCl reference electrode, Au counter electrode. Buffer: 0.05 M citric acid/0.1 M K_2HPO_4.

quantify the local concentration of cholesterol contained within the "footprint" of the PPy/enzyme-modified GC electrode.

5.4 CONCLUSIONS

In this chapter, we have discussed preliminary experiments conducted in efforts to improve the electrochemical response at our CNTs, both for enzymatic redox chemistry and for biogenic analyte detection. The immobilization of N-CNTs and HRP at GC surfaces using chitosan films was explored in attempts to improve HRP $Fe^{2+/3+}$ electron transfer. We have also described Amplex Red-mediated sensing strategies to detect H_2O_2 at carbon fiber UMEs using both soluble HRP and HRP immobilized on glass supports in aqueous assay formats. Detection limits and analytical sensitivities obtained using both variations of this sensing scheme demonstrate significant improvements over previously published electrochemical and optical based detection methods for peroxide. Future studies will detect H_2O_2 that is enzymatically generated from oxidase–substrate interactions in efforts to directly compare our sensing scheme with current protocols for substrate analysis that rely upon direct H_2O_2 oxidation. We also hope to develop strategies for chitosan-based immobilization of our sensing components directly on the electrode surface for applications in the in vivo detection of biogenic analytes such as cholesterol and glucose.

5.5 REFERENCES

(1) Yu, X.; Chattopadhyay, D.; Galeska, I.; Papadimitrakopoulos, F.; Rusling, J. F. *Electrochem. Comm.* **2003**, *5*, 408-411.

(2) Yu, X.; Kim, S. N.; Papadimitrakopoulos, F.; Rusling, J. F. *Mol. BioSys.* **2005**, *1*, 70-78.

(3) Yu, X.; Munge, B.; Patel, V.; Jensen, G.; Bhirde, A.; Gong, J. D.; Kim, S. N.; Gillespie, J.; Gutkind, J. S.; Papadimitrakopoulos, F.; Rusling, J. F. *J. Am. Chem. Soc.* **2006**, *128*, 11199-11205.

(4) Yu, X.; Sotzing, G. A.; Papadimitrakopoulos, F.; Rusling, J. F. *Anal. Chem.* **2003**, *75*, 4565-4571.

(5) Zhang, Z.; Chouchane, S.; Magliozzo, R. S.; Rusling, J. F. *Anal. Chem.* **2002**, *74*, 163-170.

(6) Zhao, G.-C.; Zhang, L.; Wei, X.-W. *Anal. Biochem.* **2004**, *329*, 160-161.

(7) Huang, H.; Hu, N.; Zeng, Y.; Zhou, G. *Anal. Biochem.* **2002**, *308*, 141-151.

(8) Qian, L.; Yang, X. *Talanta* **2006**, *68*, 721-727.

(9) Rusling, J. F.; Zhang, Z. In *Electroanalytical Methods for Biological Materials*; Brajter-Toth, A., Chambers, J. Q., Eds.; Marcel Dekker, Inc.: New York, 2002, pp 195-231.

(10) Burgess, J. D.; Hawkridge, F. M. In *Electroanalytical Methods for Biological Materials*; Brajter-Toth, A., Chambers, J. Q., Eds.; Marcel Dekker, Inc.: New York, 2002, pp 109-142.

(11) Klotzbach, T.; Watt, M.; Ansari, Y.; Minteer, S. D. *J. Membr. Sci.* **2006**, *282*, 276-283.

(12) Maldonado, S.; Stevenson, K. J. *J. Phys. Chem. B* **2005**, *109*, 4707-4716.

(13) Kalab, T.; Skladal, P. *Anal. Chim. Acta* **1995**, *304*, 361-368.

(14) Stiene, M.; Bilitewski, U. *Anal. Bioanal. Chem.* **2002**, *372*, 240-247.

(15) Mulchandani, A.; Pan, S. *Anal. Biochem.* **1999**, *267*, 141-147.

(16) Puganova, E. A.; Karyakin, A. A. *Sens. Act. B* **2005**, *B109*, 167-170.

(17) Gajovic-Eichelmann, N.; Bier, F. F. *Electroanalysis* **2005**, *17*, 1043-1050.

(18) Maldonado, S.; Morin, S.; Stevenson, K. J. *Carbon* **2006**, *44*, 1429-1437.

(19) Hao, C.; Ding, L.; Zhang, X.; Ju, H. *Anal. Chem.* **2007**, *79*, 4442-4447.

(20) Vidal, J. C.; Garcia-Ruiz, E.; Espuelas, J.; Aramendia, T.; Castillo, J. R. *Anal. Bioana. Chem.* **2003**, *377*, 273-280.

(21) Vidal, J.-C.; Garcia-Ruiz, E.; Castillo, J.-R. *Electroanalysis* **2001**, *13*, 229-235.

(22) Vidal, J. C.; Garcia, E.; Castillo, J. R. *Anal. Chim. Acta* **1999**, *385*, 213-222.

(23) Chakraborty, S.; Retna Raj, C. *Electrochem. Comm.* **2007**, *9*, 1323-1330.

(24) Chenite, A.; Chaput, C.; Wang, D.; Combes, C.; Buschmann, M. D.; Hoemann, C. D.; Leroux, J. C.; Atkinson, B. L.; Binette, F.; Selmani, A. *Biomaterials* **2000**, *21*, 2155-2161.

(25) Fernandes, R.; Wu, L.-Q.; Chen, T.; Yi, H.; Rubloff, G. W.; Ghodssi, R.; Bentley, W. E.; Payne, G. F. *Langmuir* **2003**, *19*, 4058-4062.

(26) Fernandes, R.; Yi, H.; Wu, L.-Q.; Rubloff, G. W.; Ghodssi, R.; Bentley, W. E.; Payne, G. F. *Langmuir* **2004**, *20*, 906-913.

(27) Rinaudo, M. *Prog. Polym. Sci.* **2006**, *31*, 603-632.

(28) Yi, H.; Wu, L.-Q.; Ghodssi, R.; Rubloff, G. W.; Payne, G. F.; Bentley, W. E. *Anal. Chem.* **2004**, *76*, 365-372.

(29) Zangmeister, R. A.; Park, J. J.; Rubloff, G. W.; Tarlov, M. J. *Electrochim. Acta* **2006**, *51*, 5324-5333.

(30) Zhang, M.; Mullens, C.; Gorski, W. *Anal. Chem.* **2007**, *79*, 2446-2450.

(31) Zhang, M.; Smith, A.; Gorski, W. *Anal. Chem.* **2004**, *76*, 5045-5050.

(32) Sorlier, P.; Denuziere, A.; Viton, C.; Domard, A. *Biomacromol.* **2001**, *2*, 765-772.

(33) Varum, K. M.; Ottoy, M. H.; Smidsrod, O. *Carbohyd. Polym.* **1994**, *25*, 65-70.

(34) Harinipriya, S.; Sangaranarayanan, M. V. *Langmuir* **2002**, *18*, 5572-5578.

(35) McCreery, R. L. In *Electroanalytical Chemistry*; Bard, A. J., Ed.; Marcel Dekker, Inc.: New York; Vol. 17, pp 221-292.

(36) Liu, J.; Rinzler, A. G.; Dai, H.; Hafner, J. H.; Bradley, R. K.; Boul, P. J.; Lu, A.; Iverson, T.; Shelimov, K.; Huffman, C. B.; Rodriguez-Macias, F.; Shon, Y.-S.; Lee, T. R.; Colbert, D. T.; Smalley, R. E. *Science* **1998**, *280*, 1253-1256.

(37) Twigg, R. S. *Nature* **1945**, *155*, 401-402.

(38) Maldonado, S.; Stevenson, K. J. *J. Phys. Chem. B* **2004**, *108*, 11375-11383.

(39) Bard, A. J.; Faulkner, L. R. In *Electrochemical Methods: Fundamentals and Applications,* 2nd ed.; John Wiley & Sons: Hoboken, NJ, 2001, pp 168-178.

(40) Bokoch, M. P.; Devadoss, A.; Palencsar, M. S.; Burgess, J. D. *Anal. Chim. Acta* **2004**, *519*, 47-55.

(41) Devadoss, A.; Burgess, J. D. *J. Am. Chem. Soc.* **2004**, *126*, 10214-10215.

(42) Garcia-Ruiz, E.; Vidal, J. C.; Aramendia, M. T.; Castillo, J. R. *Electroanalysis* **2004**, *16*, 497-504.

(43) Bard, A. J.; Faulkner, L. R. In *Electrochemical Methods: Fundamentals and Applications,* 2nd ed.; John Wiley & Sons: Hoboken, NJ, 2001, pp 293-301.

(44) Osteryoung, J.; O'Dea, J. J. In *Electroanalytical Chemistry*; Bard, A. J., Ed.; Marcel Dekker: New York, 1986; Vol. 14, pp 209-308.

(45) Osteryoung, J. G.; Osteryoung, R. A. *Anal. Chem.* **1985**, *57*, 101A-110A.

(46) Ramaley, L.; Krause, M. S., Jr. *Anal. Chem.* **1969**, *41*, 1362-1365.

(47) Whelan, D. P.; O'Dea, J. J.; Osteryoung, J.; Aoki, K. *J. Electroanal. Chem.* **1986**, *202*, 23-36.

(48) Rao, S. V.; Anderson, K. W.; Bachas, L. G. *Biotech. Bioeng.* **1999**, *65*, 389-396.

(49) Rauf, S.; Zhou, D.; Abell, C.; Klenerman, D.; Kang, D.-J. *Chem. Comm.* **2006**, 1721-1723.

(50) Vianello, F.; Zennaro, L.; Di Paolo, M. L.; Rigo, A.; Malacarne, C.; Scarpa, M. *Biotech. Bioeng.* **2000**, *68*, 488-495.

(51) Andrieux, C. P.; Liomges, B.; Saveant, J.-M.; Yazidi, D. *Langmuir* **2006**, ACS ASAP.

(52) Zhou, M.; Diwu, Z.; Panchuk-Voloshina, N.; Haugland, R. P. *Anal. Biochem.* **1997**, *253*, 162-168.

(53) Mohanty, J. G.; Jaffe, J. S.; Schulman, E. S.; Raible, D. G. *J. Immun. Meth.* **1997**, *202*, 133-141.

(54) Reszka, K. J.; Wagner, B. A.; Burns, C. P.; Britigan, B. E. *Anal. Biochem.* **2005**, *342*, 327-337.

(55) Li, J.; Peng, T.; Peng, Y. *Electroanalysis* **2003**, *15*, 1031-1037.

(56) Greenway, G. M.; Leelasattarathkul, T.; Liawruangrath, S.; Wheatley, R. A.; Youngvises, N. *Analyst* **2006**, *131*, 501-508.

Bibliography

Ali, S. R.; Ma, Y.; Parajuli, R. R.; Balogun, Y.; Lai, W. Y. C.; He, H. *Anal. Chem.* **2007**, *79*, 2583-2587.

Alliata, D.; Haring, P.; Haas, O.; Kotz, R.; Siegenthaler, H. *Electrochem. Comm.* **1999**, *1*, 5-9.

Allred, C. D.; McCreery, R. L. *Anal. Chem.* **1992**, *64*, 444-448.

Andrieux, C. P.; Liomges, B.; Saveant, J.-M.; Yazidi, D. *Langmuir* **2006**, ACS ASAP.

Armstrong, F. A.; Bond, A. M.; Hill, H. A. O.; Oliver, B. N.; Psalti, I. S. M. *J. Am. Chem. Soc.* **1989**, *111*, 9185-9189.

Azambuja, D. S.; Holzle, L. R.; Muller, I. L.; Piatnicki, C. M. S. *Corr. Sci.* **1999**, *41*, 2083-2097.

Azambuja, D. S.; Mueller, I. L. *Corr. Sci.* **1994**, *36*, 1835-1845.

Azambuja, D. S.; Muller, I. L.; Feris, L. A.; Ladeira, F.; Ries, L. S. *Corr. Sci.* **1996**, *38*, 1235-1244.

Azamian, B. R.; Davis, J. J.; Coleman, K. S.; Bagshaw, C. B.; Green, M. L. H. *J. Am. Chem. Soc.* **2002**, *124*, 12664-12665.

Baker, S. E.; Colavita, P. E.; Tse, K.-Y.; Hamers, R. J. *Chem. Mater.* **2006**, *18*, 4415-4422.

Baldini, E.; Dall'Orto, V. C.; Danilowicz, C.; Rezzano, I.; Calvo, E. J. *Electroanalysis* **2002**, *14*, 1157-1164.

Banks, C. E.; Crossley, A.; Salter, C.; Wilkins, S. J.; Compton, R. G. *Angew. Chem.* **2006**, *45*, 2533-2537.

Bard, A. J.; Faulkner, L. R. *Electrochemical Methods: Fundamentals and Applications*, 2nd ed.; John Wiley & Sons: Hoboken, NJ, 2001.

Bean, L. S.; Heng, L. Y.; Yamin, B. M.; Ahmad, M. *Thin Solid Films* **2005**, *477*, 104-110.

Bennett, J. A.; Wang, J.; Show, Y.; Swain, G. M. *J. Electrochem. Soc.* **2004**, *151*, E306-E313.

Benzakour, J.; Derja, A. *Electrochim. Acta* **1993**, *38*, 2547-2550.

Blanford, C. F.; Armstrong, F. A. *J. Solid State Electrochem.* **2006**, *10*, 826-832.

Blase, X.; Charlier, J. C.; De Vita, A.; Car, R.; Redlich, P.; Terrones, M.; Hsu, W. K.; Terrones, H.; Carroll, D. L.; Ajayan, P. M. *Phys. Rev. Lett.* **1999**, *83*, 5078-5081.

Bokoch, M. P.; Devadoss, A.; Palencsar, M. S.; Burgess, J. D. *Anal. Chim. Acta* **2004**, *519*, 47-55.

Bongiovanni, C.; Ferri, T.; Poscia, A.; Varalli, M.; Santucci, R.; Desideri, A. *Bioelectrochem.* **2001**, *54*, 17-22.

Borras, C. A.; Romagnoli, R.; Lezna, R. O. *Electrochim. Acta* **2000**, *45*, 1717-1725.

Bowling, R. J.; Packard, R. T.; McCreery, R. L. *J. Am. Chem. Soc.* **1989**, *111*, 1217-1223.

Brusova, Z.; Ferapontova, E. E.; Sakharov, I. Y.; Magner, E.; Gorton, L. *Electroanalysis* **2005**, *17*, 460-468.

Burgess, J. D.; Hawkridge, F. M. In *Electroanalytical Methods for Biological Materials*; Brajter-Toth, A., Chambers, J. Q., Eds.; Marcel Dekker, Inc.: New York, 2002, pp 109-142.

Castro, P. A.; Vago, E. R.; Calvo, E. J. *J. Chem. Soc. Farad. Trans.* **1996**, *92*, 3371-3379.

Chakraborty, S.; Retna Raj, C. *Electrochem. Comm.* **2007**, *9*, 1323-1330.

Chastain, J.; King, R. C., Eds. *Handbook of X-Ray Photoelectron Spectroscopy*; Physical Electronics, Inc.: Eden Prairie, 1995.

Chen, P.; Fryling, M. A.; McCreery, R. L. *Anal. Chem.* **1995**, *67*, 3115-3122.

Chenite, A.; Chaput, C.; Wang, D.; Combes, C.; Buschmann, M. D.; Hoemann, C. D.; Leroux, J. C.; Atkinson, B. L.; Binette, F.; Selmani, A. *Biomaterials* **2000**, *21*, 2155-2161.

Choudhury, T.; Saied, S. O.; Sullivan, J. L.; Abbot, A. M. *J. Phys. D* **1989**, *22*, 1185-1195.

Christie, A. B. In *Methods of Surface Analysis*; Walls, J. M., Ed.; Cambridge University Press: Cambridge, 1989, pp 136.

Conway, B. E. In *Electrochemical Supercapacitors: Scientific Fundamentals and Technological Applications*; Kluwer Academic/Plenum: New York, 1999, pp 218.

Csoeregi, E.; Joensson-Pettersson, G.; Gorton, L. *J. Biotech.* **1993**, *30*, 315-337.

Dai, X.; Wildgoose, G. G.; Compton, R. G. *Analyst* **2006**, *131*, 901-906.

Danilov, F. I.; Protsenko, V. S.; Ubiikon, A. V. *Russ. J. Electrochem.* **2005**, *41*, 1282-1289.

Delincee, H.; Radola, B. J. *Eur. J. Biochem.* **1975**, *52*, 321-330.

Devadoss, A.; Burgess, J. D. *J. Am. Chem. Soc.* **2004**, *126*, 10214-10215.

Diez-Perez, I.; Gorostiza, P.; Sanz, F.; Muller, C. *J. Electrochem. Soc.* **2001**, *148*, B307-B313.

Domenech-Carbo, A.; Sanchez-Ramosa, S.; Domenech-Carbo, M. T.; Gimeno-Adelantado, J. V.; Bosch-Reig, F.; Yusa-Marco, D. J.; Sauri-Peris, M. C. *Electroanal.* **2002**, *14*, 685-696.

Downard, A. J.; Roddick, A. D. *Electroanalysis* **1994**, *6*, 409-414.

Droppa, R.; Hammer, P.; Carvalho, A. C. M.; dos Santos, M. C.; Alvarez, F. *J. Non-Cryst. Sol.* **2002**, *299-302*, 874-879.

Dunford, H. B. In *Peroxidases in Chemistry and Biology*; Everse, J., Everse, K. E., Grisham, M. B., Eds.; CRC Press: Boca Raton, FL, 1991; Vol. 2.

Dunford, H. B. *Heme Peroxidases*; Wiley-VCH: New York, 1999.

DuVall, S. H.; McCreery, R. L. *Anal. Chem.* **1999**, *71*, 4594-4602.

Fang, H.-T.; Liu, C.-G.; Liu, C.; Li, F.; Liu, M.; Cheng, H.-M. *Chem. Mater.* **2004**, *16*, 5744-5750.

Farrell, J.; Kason, M.; Melitas, N.; Li, T. *Environ. Sci. Tech.* **2000**, *34*, 514-521.

Feldman, B.; McGarraugh, G.; Heller, A.; Bohannon, N.; Skyler, J.; DeLeeuw, E.; Clarke, D. *Diabetes Tech. Ther.* **2000**, *2*, 221-229.

Ferapontova, E.; Dominguez, E. *Bioelectrochem.* **2002**, *55*, 127-130.

Ferapontova, E.; Gorton, L. *Bioelectrochem.* **2002**, *55*, 83-87.

Ferapontova, E.; Puganova, E. *J. Electroanal. Chem.* **2002**, *518*, 20-26.

Ferapontova, E. E. *Electroanalysis* **2004**, *16*, 1101-1112.

Fernandes, R.; Wu, L.-Q.; Chen, T.; Yi, H.; Rubloff, G. W.; Ghodssi, R.; Bentley, W. E.; Payne, G. F. *Langmuir* **2003**, *19*, 4058-4062.

Fernandes, R.; Yi, H.; Wu, L.-Q.; Rubloff, G. W.; Ghodssi, R.; Bentley, W. E.; Payne, G. F. *Langmuir* **2004**, *20*, 906-913.

Fischer, A. E.; Show, Y.; Swain Greg, M. *Anal. Chem.* **2004**, *76*, 2553-2560.

Frew, J. E.; Hill, H. A. O. *Eur. J. Biochem.* **1988**, *172*, 261-269.

Gajovic-Eichelmann, N.; Bier, F. F. *Electroanalysis* **2005**, *17*, 1043-1050.

Gao, L.; Zhuang, J.; Nie, L.; Zhang, J.; Zhang, Y.; Gu, N.; Wang, T.; Feng, J.; Yang, D.; Perrett, S.; Yan, X. *Nature Nanotech.* **2007**, *2*, 577-583.

Garcia-Ruiz, E.; Vidal, J. C.; Aramendia, M. T.; Castillo, J. R. *Electroanalysis* **2004**, *16*, 497-504.

Gnanaraj, J. S.; Levi, M. D.; Levi, E.; Salitra, G.; Aurbach, D.; Fischer, J. E.; Claye, A. *J. Electrochem. Soc.* **2001**, *148*, A525-A536.

Gojkovic, S. L.; Gupta, S.; Savinell, R. F. *J. Electrochem. Soc.* **1998**, *145*, 3493-3499.

Gooding, J. J. *Electrochim. Acta* **2005**, *50*, 3049-3060.

Goss, C. A.; Brumfield, J. C.; Irene, E. A.; Murray, R. W. *Anal. Chem.* **1993**, *65*, 1378-1389.

Greenway, G. M.; Leelasattarathkul, T.; Liawruangrath, S.; Wheatley, R. A.; Youngvises, N. *Analyst* **2006**, *131*, 501-508.

Groat, K. A.; Creager, S. E. *Langmuir* **1993**, *9*, 3668-3675.

Guiseppi-Elie, A.; Lei, C.; Baughman, R. H. *Nanotech.* **2002**, *13*, 559-564.

Guo, Y.; Guadalupe, A. R. *Chem. Comm.* **1997**, 1437-1438.

Hang, B. T.; Watanabe, T.; Eashira, M.; Watanabe, I.; Okada, S.; Yamaki, J.-i. *Electrochem. Sol.-St. Lett.* **2005**, *8*, A476-A480.

Hao, C.; Ding, L.; Zhang, X.; Ju, H. *Anal. Chem.* **2007**, *79*, 4442-4447.

Harinipriya, S.; Sangaranarayanan, M. V. *Langmuir* **2002**, *18*, 5572-5578.

Heller, A. *Annu. Rev. Biomed. Eng.* **1999**, *1*, 153-175.

Heng, L. Y.; Chou, A.; Yu, J.; Chen, Y.; Gooding, J. J. *Electrochem. Comm.* **2005**, *7*, 1457-1462.

Huang, H.; Hu, N.; Zeng, Y.; Zhou, G. *Anal. Biochem.* **2002**, *308*, 141-151.

Huang, X.-J.; Im, H.-S.; Lee, D.-H.; Kim, H.-S.; Choi, Y.-K. *J. Phys. Chem. C* **2007**, *111*, 1200-1206.

Huang, Y. H.; Zhang, T. C. *Water Res.* **2005**, *39*, 1751-1760.

Jia, N.; Wang, L.; Liu, L.; Zhou, Q.; Jiang, Z. *Electrochem. Comm.* **2005**, *7*, 349-354.

Jiang, D.; Devadoss, A.; Palencsar, M. S.; Fang, D.; White, N. M.; Kelley, T. J.; Smith, J. D.; Burgess, J. D. *J. Am. Chem. Soc.* **2007**, *129*, 11352-11353.

Joshi, P. P.; Merchant, S. A.; Wang, Y.; Schmidtke, D. W. *Anal. Chem.* **2005**, *77*, 3183-3188.

Jovanovic, V. M.; Hackerman, N. *J. Phys. Chem. B* **1998**, *102*, 9855-9860.

Jurkschat, K.; Ji, X.; Crossley, A.; Compton, R. G.; Banks, C. E. *Analyst* **2007**, *132*, 21-23.

Kalab, T.; Skladal, P. *Anal. Chim. Acta* **1995**, *304*, 361-368.

(Katz, E.; Shipway, A. N.; Willner, I. In *Electron Transfer in Chemistry*; Balzani, V., Ed.; Wiley-VCH: New York, 2001; Vol. 4, pp 127-201.

Kim, N. S.; Lee, Y. T.; Park, J.; Han, J. B.; Choi, Y. S.; Choi, S. Y.; Choo, J.; Lee, G. H. *J. Phys. Chem. B* **2003**, *107*, 9249-9255.

King, B. C.; Hawkridge, F. M.; Hoffman, B. M. *J. Am. Chem. Soc.* **1992**, *114*, 10603-10608.

Kinoshita, K. *Carbon: Electrochemical and Physicochemical Properties*; John Wiley and Sons, Inc.: New York, 1988.

Kladekova, D.; Galova, M.; Pikna, L. u. *Part. Sci. Tech.* **2005**, *23*, 189-199.

Klotzbach, T.; Watt, M.; Ansari, Y.; Minteer, S. D. *J. Membr. Sci.* **2006**, *282*, 276-283.

Kurusu, F.; Tsunoda, H.; Saito, A.; Tomita, A.; Kadota, A.; Kayahara, N.; Karube, I.; Gotoh, M. *Analyst* **2006**, *131*, 1292-1298.

Laviron, E. *J. Electroanal. Chem.* **1979**, *101*, 19-28.

Li, G.; Liao, J. M.; Hu, G. Q.; Ma, N. Z.; Wu, P. J. *Biosens. Bioelectr.* **2005**, *20*, 2140-2144.

Li, J.; Peng, T.; Peng, Y. *Electroanalysis* **2003**, *15*, 1031-1037.

Li, J.; Wang, Y.-B.; Qiu, J.-D.; Sun, D.-c.; Xia, X.-H. *Anal. Bioanal. Chem.* **2005**, *383*, 918-922.

Li, L.; Xing, Y. *J. Electrochem. Soc.* **2006**, *153*, A1823-A1828.

Li, W.; Liang, C.; Qiu, J.; Zhou, W.; Han, H.; Wei, Z.; Sun, G.; Xin, Q. *Carbon* **2002**, *40*, 791-794.

Lide, D. R., Ed. *CRC Handbook of Chemistry and Physics*, 86th ed.; Taylor & Francis: Boca Raton, 2005.

Lindgren, A.; Munteanu, F.-D.; Gazaryan, I. G.; Ruzgas, T.; Gorton, L. *J. Electroanal. Chem.* **1998**, *458*, 113-120.

Lindgren, A.; Tanaka, M.; Ruzgas, T.; Gorton, L.; Gazaryan, I.; Ishimori, K.; Morishima, I. *Electrochem. Comm.* **1999**, *1*, 171-175.

Liu, G.; Lin, Y. *Electrochem. Comm.* **2006**, *8*, 251-256.

Liu, J.; Rinzler, A. G.; Dai, H.; Hafner, J. H.; Bradley, R. K.; Boul, P. J.; Lu, A.; Iverson, T.; Shelimov, K.; Huffman, C. B.; Rodriguez-Macias, F.; Shon, Y.-S.; Lee, T. R.; Colbert, D. T.; Smalley, R. E. *Science* **1998**, *280*, 1253-1256.

Lozzi, I.; Calamai, L.; Fusi, P.; Bosetto, M.; Stotzky, G. *Soil Bio. Biochem.* **2001**, *33*, 1021-1028.

Luo, X.; Killard, A. J.; Smyth, M. R. *Electroanalysis* **2006**, *18*, 1131-1134.

Luong, J. H. T.; Hrapovic, S.; Wang, D. *Electroanalysis* **2005**, *17*, 47-53.

Lyon, J. L.; Stevenson, K. J. *Langmuir* **2007**, *23*, 11311-11318.

Maldonado, S.; Morin, S.; Stevenson Keith, J. *Analyst* **2006**, *131*, 262-267.

Maldonado, S.; Morin, S.; Stevenson, K. J. *Carbon* **2006**, *44*, 1429-1437.

Maldonado, S.; Stevenson, K. J. *J. Phys. Chem. B* **2004**, *108*, 11375-11383.

Maldonado, S.; Stevenson, K. J. *J. Phys. Chem. B* **2005**, *109*, 4707-4716.

Mano, N.; Yoo, J. E.; Tarver, J.; Loo, Y.-L.; Heller, A. *J. Am. Chem. Soc.* **2007**, *129*, 7006-7007.

Martinez, L.; Leinen, D.; Martin, F.; Gabas, M.; Ramos-Barrado, J. R.; Quagliata, E.; Dalchiele, E. A. *J. Electrochem. Soc.* **2007**, *154*, D126-D133.

Masek, J.; Mesickova, E. *J. Electroanal. Chem.* **1971**, *33*, 219-223.

Matter, P. H.; Ozkan, U. S. *Catal. Lett.* **2006**, *109*, 115-123.

Matter, P. H.; Wang, E.; Arias, M.; Biddinger, E. J.; Ozkan, U. S. *J. Phys. Chem. B* **2006**, *110*, 18374-18384.

Matter, P. H.; Wang, E.; Arias, M.; Biddinger, E. J.; Ozkan, U. S. *J. Mol. Catal. A* **2007**, *264*, 73-81.

Matter, P. H.; Wang, E.; Millet, J.-M. M.; Ozkan, U. S. *J. Phys. Chem. C* **2007**, *111*, 1444-1450.

Matter, P. H.; Wang, E.; Ozkan, U. S. *J. Catal.* **2006**, *243*, 395-403.

McCreery, R.; Cline, K. K. In *Laboratory Techniques in Electroanalytical Chemistry*, 2nd ed.; Kissinger, P. T., Heineman, W. R., Eds.; Marcel Dekker: New York, 1996, pp 293-332.

McCreery, R. L. In *Electroanalytical Chemistry*; Bard, A. J., Ed.; Marcel Dekker, Inc.: New York; Vol. 17, pp 221-292.

McMahon, C. P.; Rocchitta, G.; Serra, P. A.; Kirwan, S. M.; Lowry, J. P.; O'Neill, R. D. *Anal. Chem.* **2006**, *78*, 2352-2359.

Merkoci, A.; Pumera, M.; Llopis, X.; Perez, B.; del Valle, M.; Alegret, S. *Trend. Anal. Chem.* **2005**, *24*, 826-838.

Merkofer, M.; Kissner, R.; Hider, R. C.; Brunk, U. T.; Koppenol, W. H. *Chem. Res. Toxic.* **2006**, *19*, 1263-1269.

Miranda, M. V.; Magri, M. L.; Cabrera, R. B.; Fernandez Lahore, H. M.; Cascone, O. *Lat. Am. App. Res.* **2003**, *33*, 67-71.

Mishra, D.; Farrell, J. *Environ. Sci. and Tech.* **2005**, *39*, 645-650.

Moatti-Sirat, D.; Velho, G.; Reach, G. *Biosens. Bioelectr.* **1992**, *7*, 345-352.

Mohanty, J. G.; Jaffe, J. S.; Schulman, E. S.; Raible, D. G. *J. Immun. Meth.* **1997**, *202*, 133-141.

Moore, R. R.; Banks, C. E.; Compton, R. G. *Anal. Chem.* **2004**, *76*, 2677-2682.

Morcos, I.; Yeager, E. *Electrochim. Acta* **1970**, *15*, 953-975.

Moura, F. C. C.; Araujo, M. H.; Costa, R. C. C.; Fabris, J. D.; Ardisson, J. D.; Macedo, W. A. A.; Lago, R. M. *Chemosphere* **2005**, *60*, 1118-1123.

Moura, F. C. C.; Oliveira, G. C.; Araujo, M. H.; Ardisson, J. D.; Macedo, W. A. A.; Lago, R. M. *App. Catal. A* **2006**, *307*, 195-204.

Mulchandani, A.; Pan, S. *Anal. Biochem.* **1999**, *267*, 141-147.

Musameh, M.; Lawrence, N. S.; Wang, J. *Electrochem. Comm.* **2005**, *7*, 14-18.

Musameh, M.; Wang, J.; Merkoci, A.; Lin, Y. *Electrochem. Comm.* **2002**, *4*, 743-746.

Nassar, A.-E. F.; Rusling, J. F.; Tominaga, M.; Yanagimoto, J.; Nakashima, N. *J. Electroanal. Chem.* **1996**, *416*, 183-185.

Niculescu, M.; Ruzgas, T.; Nistor, C.; Frebort, I.; Sebela, M.; Pec, P.; Csoeregi, E. *Anal. Chem.* **2000**, *72*, 5988-5993.

Nurmi, J. T.; Tratnyek, P. G.; Sarathy, V.; Baer, D. R.; Amonette, J. E.; Pecher, K.; Wang, C.; Linehan, J. C.; Matson, D. W.; Penn, R. L.; Driessen, M. D. *Environ. Sci. Tech.* **2005**, *39*, 1221-1230.

Oblonsky, L. J.; Ryan, M. P.; Isaacs, H. S. *Corr. Sci.* **2000**, *42*, 229-241.

O'Connor, M.; Kim Sang, N.; Killard Anthony, J.; Forster Robert, J.; Smyth Malcolm, R.; Papadimitrakopoulos, F.; Rusling James, F. *Analyst* **2004**, *129*, 1176-1180.

Osteryoung, J.; O'Dea, J. J. In *Electroanalytical Chemistry*; Bard, A. J., Ed.; Marcel Dekker: New York, 1986; Vol. 14, pp 209-308.

Osteryoung, J. G.; Osteryoung, R. A. *Anal. Chem.* **1985**, *57*, 101A-110A.

Pera, M. *The Ambiguous Frog: The Galvani-Volta Controversy on Animal Electricity*; Princeton University Press: Princeton, NJ, 1992.

Pourbaix, M. *Atlas of Electrochemical Equilibria in Aqueous Solutions*; Pergamon Press: Oxford, 1966.

Presnova, G.; Grigorenko, V.; Egorov, A.; Ruzgas, T.; Lindgren, A.; Gorton, L.; Borchers, T. *Farad. Discuss.* **2000**, *116*, 281-289.

Puganova, E. A.; Karyakin, A. A. *Sens. Act. B* **2005**, *B109*, 167-170.

Pumera, M. *Langmuir* **2007**, *23*, 6453-6458.

Pupkevich, V.; Glibin, V.; Karamanev, D. *Electrochem. Comm.* **2007**, *9*, 1924-1930.

Qian, L.; Yang, X. *Talanta* **2006**, *68*, 721-727.

Ramaley, L.; Krause, M. S., Jr. *Anal. Chem.* **1969**, *41*, 1362-1365.

Ranganathan, S.; Kuo, T.-C.; McCreery, R. L. *Anal. Chem.* **1999**, *71*, 3574-3580.

Rao, C. N. R.; Govindaraj, A. *Accounts of Chemical Research* **2002**, *35*, 998-1007.

Rao, S. V.; Anderson, K. W.; Bachas, L. G. *Biotech. Bioeng.* **1999**, *65*, 389-396.

Rauf, S.; Zhou, D.; Abell, C.; Klenerman, D.; Kang, D.-J. *Chem. Comm.* **2006**, 1721-1723.

Redlich, P.; Loeffler, J.; Ajayan, P. M.; Bill, J.; Aldinger, F.; Ruehle, M. *Chem. Phys. Lett.* **1996**, *260*, 465-470.

Reed, D. E.; Hawkridge, F. M. *Anal. Chem.* **1987**, *59*, 2334-2339.

Reszka, K. J.; Wagner, B. A.; Burns, C. P.; Britigan, B. E. *Anal. Biochem.* **2005**, *342*, 327-337.

Rinaudo, M. *Prog. Polym. Sci.* **2006**, *31*, 603-632.

Ritter, K.; Odziemkowski, M. S.; Simpgraga, R.; Gillham, R. W.; Irish, D. E. *J. Contam. Hydr.* **2003**, *65*, 121-136.

Rochette, J. F.; Sacher, E.; Meunier, M.; Luong, J. H. T. *Anal. Biochem.* **2005**, *336*, 305-311.

Rusling, J. F.; Zhang, Z. In *Electroanalytical Methods for Biological Materials*; Brajter-Toth, A., Chambers, J. Q., Eds.; Marcel Dekker, Inc.: New York, 2002, pp 195-231.

Ruzgas, T.; Csoeregi, E.; Emmneus, J.; Gorton, L.; Marko-Varga, G. *Anal. Chim. Acta* **1996**, *330*, 123-138.

Ruzgas, T.; Gorton, L.; Emneus, J.; Marko-Varga, G. *J. Electroanal. Chem.* **1995**, *391*, 41-49.

Ruzgas, T.; Lindgren, A.; Gorton, L.; Hecht, H.-J.; Reichelt, J.; Bilitewski, U. In *Electroanalytical Methods for Biological Materials*; Brajter-Toth, A., Chambers, J. Q., Eds.; Marcel Dekker, Inc.: New York, 2002, pp 233-254.

Salinas, E.; Rivero, V.; Torriero, A. A. J.; Benuzzi, D.; Sanz, M. I.; Raba, J. *Talanta* **2006**, *70*, 244-250.

Sen, R.; Satishkumar, B. C.; Govindaraj, A.; Harikumar, K. R.; Renganathan, M. K.; Rao, C. N. R. *J. Mater. Chem.* **1997**, *7*, 2335-2337.

Sethuraman, A. R.; Stencel, J. M.; Rubel, A. M.; Cavin, B.; Hubbard, C. R. *J. Vac. Sci. Tech. A* **1994**, *12*, 443-451.

Shao, Y.; Yin, G.; Gao, Y.; Shi, P. *J. Electrochem. Soc.* **2006**, *153*, A1093-A1097.

Sicking, W.; Korth, H.-G.; Jansen, G.; de Groot, H.; Sustmann, R. *Chem. Eur. J.* **2007**, *13*, 4230-4245.

Sljukic, B.; Banks, C. E.; Compton, R. G. *Nano Lett.* **2006**, *6*, 1556-1558.

Sorlier, P.; Denuziere, A.; Viton, C.; Domard, A. *Biomacromol.* **2001**, *2*, 765-772.

Stevens, D. A.; Hicks, M. T.; Haugen, G. M.; Dahn, J. R. *J. Electrochem. Soc.* **2005**, *152*, A2309-A2315.

Stiene, M.; Bilitewski, U. *Anal. Bioanal. Chem.* **2002**, *372*, 240-247.

Surmann, P.; Peter, B. *Electroanalysis* **1996**, *8*, 692-697.

Szucs, A.; Novak, M. *J. Electroanal. Chem.* **1995**, *384*, 47-55.

Takahashi, K.; Bardwell, J. A.; MacDougall, B.; Graham, M. J. *Electrochim. Acta* **1992**, *37*, 477-487.

Takahashi, K.; Bardwell, J. A.; MacDougall, B.; Graham, M. J. *Electrochim. Acta* **1992**, *37*, 489-494.

Terrones, M.; Jorio, A.; Endo, M.; Rao, A. M.; Kim, Y. A.; Hayashi, T.; Terrones, H.; Charlier, J. C.; Dresselhaus, G.; Dresselhaus, M. S. *Mater. Today* **2004**, *7*, 30-45.

Terrones, M.; Terrones, H.; Grobert, N.; Hsu, W. K.; Zhu, Y. Q.; Hare, J. P.; Kroto, H. W.; Walton, D. R. M.; Kohler-Redlich, P.; Ruhle, M.; Zhang, J. P.; Cheetham, A. K. *Appl. Phys. Lett.* **1999**, *75*, 3932-3934.

Thomas, J. G. N.; Nurse, T. J. *Brit. Corr. J.* **1967**, *2*, 13-20.

Thomas, T. J.; Ponnusamy, K. E.; Chang, N. M.; Galmore, K.; Minteer, S. D. *J. Membr. Sci.* **2003**, *213*, 55-66.

Twigg, R. S. *Nature* **1945**, *155*, 401-402.

Vago, E.; Calvo, E. J. *J. Chem. Soc. Farad. Trans.* **1995**, *91*, 2323-2329.

Vago, E. R.; Calvo, E. J. *J. Electroanal. Chem.* **1992**, *339*, 41-67.

Vago, E. R.; Calvo, E. J.; Stratmann, M. *Electrochim. Acta* **1994**, *39*, 1655-1659.

Vamvakaki, V.; Tsagaraki, K.; Chaniotakis, N. *Anal. Chem.* **2006**, *78*, 5538-5542.

Varum, K. M.; Ottoy, M. H.; Smidsrod, O. *Carbohyd. Polym.* **1994**, *25*, 65-70.

Vianello, F.; Zennaro, L.; Di Paolo, M. L.; Rigo, A.; Malacarne, C.; Scarpa, M. *Biotech. Bioeng.* **2000**, *68*, 488-495.

Vidal, J. C.; Garcia, E.; Castillo, J. R. *Anal. Chim. Acta* **1999**, *385*, 213-222.

Vidal, J. C.; Garcia-Ruiz, E.; Espuelas, J.; Aramendia, T.; Castillo, J. R. *Anal. Bioana. Chem.* **2003**, *377*, 273-280.

Vidal, J.-C.; Garcia-Ruiz, E.; Castillo, J.-R. *Electroanalysis* **2001**, *13*, 229-235.

Vijayaraghavan, G.; Stevenson, K. J. *Langmuir* **2007**, *23*, 5279-5282.

Wagner, J. G.; Schmidtke, D. W.; Quinn, C. P.; Fleming, T. F.; Bernacky, B.; Heller, A. *Proc. Nat. Acad. Sci.* **1998**, *95*, 6379-6382.

Wang, G.; Thai, N. M.; Yau, S.-T. *Electrochem. Comm.* **2006**, *8*, 987-992.

Wang, X.; Hu, W.; Liu, Y. Q.; Long, C.; Xu, Y.; Zhou, S.; Zhu, D.; Dai, L. *Carbon* **2001**, *39*, 1533-1536.

Wang, X.; Li, W.; Chen, Z.; Waje, M.; Yan, Y. *J. Pow. Sour.* **2006**, *158*, 154-159.

Wang, Y.; Joshi, P. P.; Hobbs, K. L.; Johnson, M. B.; Schmidtke, D. W. *Langmuir* **2006**, *22*, 9776-9783.

Wen, D.; Liu, Y.; Yang, G.; Dong, S. *Electrochim. Acta* **2007**, *52*, 5312-5317.

Whelan, D. P.; O'Dea, J. J.; Osteryoung, J.; Aoki, K. *J. Electroanal. Chem.* **1986**, *202*, 23-36.

Wightman, R. M.; Wipf, D. O. In *Electroanalytical Chemistry*; Bard, A. J., Ed.; Marcel Dekker: New York, 1989; Vol. 15, pp 343.

Willner, I.; Katz, E. *Angew. Chem.* **2000**, *39*, 1181-1218.

Wilson, G. S.; Hu, Y. *Chem. Rev.* **2000**, *100*, 2693-2704.

Yang, H.-H.; Zhu, Q.-Z.; Chen, Q.-Y.; Xu, J.-G.; Li, D.-H. *Analyst* **2000**, *125*, 719-724.

Ye, J.-S.; Wen, Y.; Zhang, W. D.; Gan, L. M.; Xu, G. Q.; Sheu, F.-S. *Electrochem. Comm.* **2004**, *6*, 66-70.

Yi, H.; Wu, L.-Q.; Ghodssi, R.; Rubloff, G. W.; Payne, G. F.; Bentley, W. E. *Anal. Chem.* **2004**, *76*, 365-372.

Yin, Y.; Lu, Y.; Wu, P.; Cai, C. *Sensors* **2005**, *5*, 220-234.

Yu, X.; Chattopadhyay, D.; Galeska, I.; Papadimitrakopoulos, F.; Rusling, J. F. *Electrochem. Comm.* **2003**, *5*, 408-411.

Yu, X.; Kim, S. N.; Papadimitrakopoulos, F.; Rusling, J. F. *Mol. BioSys.* **2005**, *1*, 70-78.

Yu, X.; Munge, B.; Patel, V.; Jensen, G.; Bhirde, A.; Gong, J. D.; Kim, S. N.; Gillespie, J.; Gutkind, J. S.; Papadimitrakopoulos, F.; Rusling, J. F. *J Am Chem Soc* **2006**, *128*, 11199-11205.

Yu, X.; Sotzing, G. A.; Papadimitrakopoulos, F.; Rusling, J. F. *Anal. Chem.* **2003**, *75*, 4565-4571.

Yudasaka, M.; Kikuchi, R.; Ohki, Y.; Yoshimura, S. *Carbon* **1997**, *35*, 195-201.

Zangmeister, R. A.; Park, J. J.; Rubloff, G. W.; Tarlov, M. J. *Electrochim. Acta* **2006**, *51*, 5324-5333.

Zeng, Y.-L.; Huang, Y.-F.; Jiang, J.-H.; Zhang, X.-B.; Tang, C.-R.; Shen, G.-L.; Yu, R.-Q. *Electrochem. Comm.* **2006**, *9*, 185-190.

Zhang, M.; Mullens, C.; Gorski, W. *Anal. Chem.* **2007**, *79*, 2446-2450.

Zhang, M.; Smith, A.; Gorski, W. *Anal. Chem.* **2004**, *76*, 5045-5050.

Zhang, T. C.; Huang, Y. H. *J. Environ. Eng.* **2005**, *131*, 461-470.

Zhang, T. C.; Huang, Y. H. *Water Res* **2006**, *40*, 2311-2320.

Zhang, T. C.; Huang, Y. H. *J. Environ. Eng.* **2006**, *132*, 527-536.

Zhang, Z.; Chouchane, S.; Magliozzo, R. S.; Rusling, J. F. *Anal. Chem.* **2002**, *74*, 163-170.

Zhao, G.-C.; Zhang, L.; Wei, X.-W. *Anal. Biochem.* **2004**, *329*, 160-161.

Zhou, M.; Diwu, Z.; Panchuk-Voloshina, N.; Haugland, R. P. *Anal. Biochem.* **1997**, *253*, 162-168.

Vita

Jennifer Lee Lyon, the daughter of Timothy F. and Leda V. Lyon, was born on the bayou in Shreveport, Louisiana on July 28, 1981. After graduating from Smethport Area Jr.–Sr. High School in Smethport, Pennsylvania in 1999, she enrolled at the Pennsylvania State University in University Park, Pennsylvania. She graduated with a Bachelor of Science in Chemistry and English minor from Penn State in May 2003. She entered the University of Texas at Austin in August 2003 to begin her graduate studies under the guidance of Prof. Keith J. Stevenson.

Permanent address: 301 E Main Street, Smethport, PA 16749-1323

This dissertation was typed by the author.